ABSTRACT

Title of Dissertation: WAVE INTERACTION WITH INJECTOR FLOWFIELD IN ROTATING DETONATION ENGINE

Minwook Chang,
Doctor of Philosophy, 2024

Dissertation directed by: Professor Kenneth H. Yu,
Department of Aerospace

Rotating Detonation Engines (RDE) utilize detonative combustion processes for heat release instead of deflagration, which is more commonly used in conventional combustors. Potential benefits of RDE include pressure gain combustion, efficient energy conversion, and simpler designs that avoid combustion instability problems due to their cyclic nature of operation. It has been observed, however, that RDE operation can become unsteady due to the onset of counter-rotating detonation waves. In addition, the random presence of residual liquid fuel droplets and their unexpected breakup could also affect the periodic operation of RDE. This study aims to better understand the physical mechanisms that destabilize the RDE's periodic processes and lead to unsteady operation. Specifically, the investigation focuses on understanding physical mechanisms associated with two key off-design scenarios: (i) the onset of counter-rotating detonation waves and their impact on next cycle fuel injection, and (ii) the breakup of liquid fuel droplets by detonation wave and decoupled detonation wave which consists of shock and flame fronts. Experiments using either hydrogen-oxygen or ethylene-oxygen detonation in linear channel

simulate an unwrapped RDE combustor process. For the counter-rotating wave study, detonation waves are initiated from both ends of the channel, and complex recovery behavior associated with colliding detonation waves is examined providing insights into RDE slapping mode operation. For the fuel droplet breakup study, 2-mm diameter ethanol and JP-8 droplets are placed on the downstream path of detonation waves and decoupled shock-flame fronts, which propagate at average wave speeds of Mach 7.3, 3.6, and 2.6, respectively. Liquid droplets break up faster when exposed to slower decoupled shock-flame waves compared to faster detonation waves. This unexpected difference is attributed to the initial slip flow Mach number around the droplet, which is subsonic for detonation waves but supersonic for decoupled waves. Research findings suggest that the slip flow Mach number, along with the Weber number, plays a crucial role in RDE fuel droplet breakup.

WAVE INTERACTION WITH INJECTOR FLOWFIELD IN ROTATING DETONATION ENGINE

by

Minwook Chang

Dissertation submitted to the Faculty of the Graduate School of the
University of Maryland, College Park, in partial fulfillment
of the requirements for the degree of
Doctor of Philosophy
2024

Advisory Committee:
Professor Kenneth H. Yu, Chair/Advisor
Professor James Baeder
Professor Christopher Cadou
Professor Stuart J. Laurence
Professor Bao Yang, Dean's Representative

Acknowledgements

I would like to express my gratitude to my advisor, Dr. Kenneth H. Yu, whose unwavering guidance, support, and patience have been invaluable in shaping me into a better researcher over the years. Without his support, this work would not have been possible. I have appreciated and grown from our numerous meetings as well as his commitment.

I would also like to extend my thanks to all my committee members, Dr. James Baeder, Dr. Christopher Cadou, Dr. Stuart Laurence, and Dr. Bao Yang, for their invaluable support. I greatly appreciate the time and effort they have spent. I had a great learning experience working with the committee inside and outside the class. I must also acknowledge the Air Force Office of Scientific Research (AFOSR), whose financial support made this work possible. Their funding has been crucial in providing me with the resources and tools needed to carry out this research.

To my dear friends and colleagues at the Advanced Propulsion Research Laboratory, specifically Dr. Jason Burr, Dr. Kyung-Hoon Shin, Dr. Shikha Redhal, and Dr. Mithuun Kanapathipillai, I am extremely grateful for their support throughout these years. Without their help and support, none of my achievements would have been possible. I also want to extend my gratitude to all the friends who have played a significant role in making my life more enjoyable.

Last but not least, I would like to express my heartfelt gratitude to my loving family, who have been a constant source of support and inspiration. My parents' unyielding encouragement and guidance have been the driving force behind my success.

My sister's presence has been a great source of comfort and support. They have been my pillars of strength, helping me overcome every obstacle that came my way. Lastly, I would like to thank Mino for always being there for me.

Table of Contents

List of Tables

List of Figures

List of Abbreviations

RDE	Rotating Detonation Engine
CJ	Chapmann-Jouguet
eLMDE	Extended Linear Model Detonation Engine
AFRL	U.S. Air Force Research Laboratory
NRL	U.S. Naval Research Laboratory
RR	Right Running
LR	Left Running
RRR	Re-ignited Right Running
DDT	Deflagration to Detonation Transition
M_{slip}	Induced Mach Number
We	Weber Number
Re_D	Reynolds number of the liquid droplet
FLDI	Focused Laser Differential Interferometry

Chapter 1: Introduction

1.1 Overview and Motivation

Increased interest in developing efficient combustor is demanded due to serious global warming issue. Conventional systems which use deflagration-based heat release could be outperformed by detonation-based heat release systems such as a Rotating Detonation Engine (RDE). Although it is in development stage, effective and efficient energy conversion are expected. In addition, a simple design and compact size of combustor provide potential usage on various applications such as supersonic combustor, launch vehicle and power generation. An RDE combustor is composed of an annular channel, and inside the channel, detonation waves propagate circumferentially, continuously following the channel at a supersonic speed with respect to the fresh reactants injected into the channel shown as Figure 1.1.1.

(1) Injection of reactants from the closed end

(3) Azimuthal propagation of traverse detonation waves

(4) Material interface or deflagration zone

(5) Oblique shock waves in the products

(6) Products exit from the open end

In typical RDE it consists of two stages of operation cycle as shown in the Figure 1.1.2. First stage starts with the arrival of a lead detonation wave front, followed by associated compression, heat release and expansion processes. Next, injection

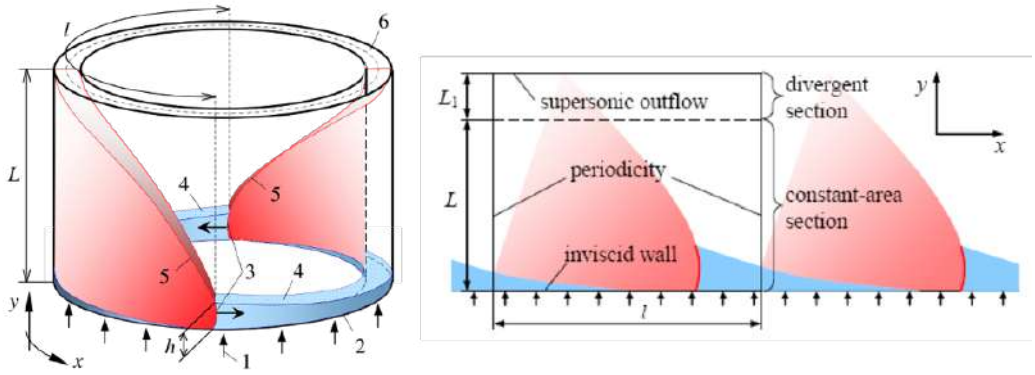

Figure 1.1.1 Schematic of typical rotating detonation engine (RDE) operation [1]

refresh phase starts. Continuously injected fresh reactants in axial direction are suppressed from the pressure jump from the detonation wave which propagates

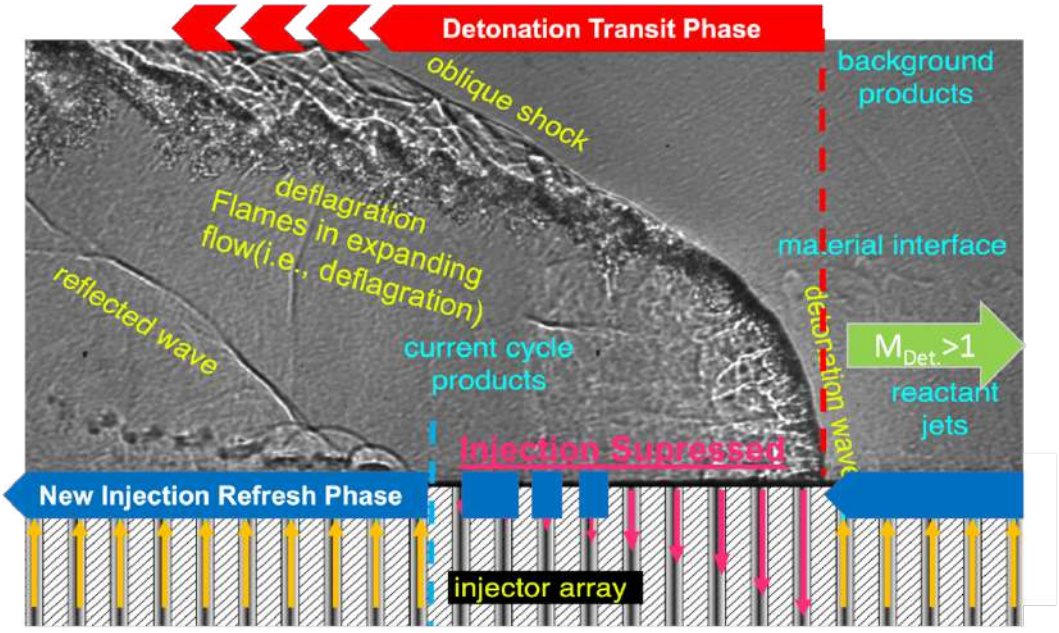

(a)

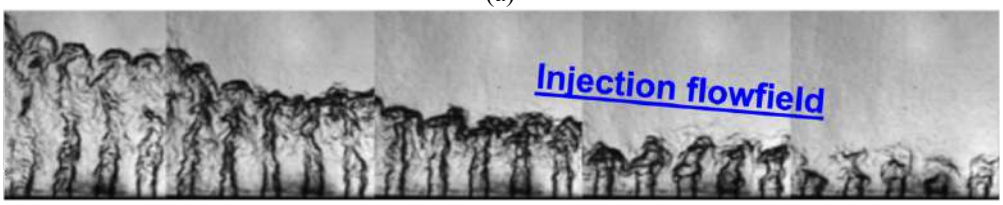

(b)

Figure 1.1.2 Illustration of operation cycle of RDE

orthogonal direction to the flow axis. In certain cases, an underdamped response of the injector is expected. Therefore, it is essential to consider the injection refresh behavior and quantify the refresh delay time when designing the RDE combustor.

Furthermore, additional challenge using liquid propellant needs to be addressed prior to practical implementation. Liquid fuels have its advantage of high energy density, which leads to performance improvement. However, liquid reactant must go through breakup, atomization, and vaporization processes before getting mixed with oxidizer. Additional processes require additional time to become a detonable reactant, which leads to another difficulty to sustain the detonation wave inside the RDE combustor.

Various physical processes occurring inside the RDE combustor are not only complex but also highly coupled, thus not very well understood yet. Various studies have been conducted both experimentally and numerically. However, limitation from both methods exists, such as restriction in measurement due to its of geometry, extreme condition inside the combustor and expensive computational expense. Hence, simplified configuration model combustor could help understand the fundamental physics of flowfield inside the RDE combustor and provide framework for the numerical studies.

1.2 Technical Objective

This research aims to better understand the flowfield inside the RDE and analyze pertinent physical mechanisms by providing detailed experimental data on crucial physical processes that are poorly understood. A linear model setup was used to experimentally explore the physics of gaseous fuel injection inside the RDE combustor. In addition, dynamic interaction between the detonation wave and liquid fuel droplet was studied experimentally using linear combustor model. The linear combustor model setup allows experimentally simulates an unwrapped RDE with controllable wave conditions such as strength and various reactant composition. The specific of the two different unit-physics problems were:

1. Understand the physics of RDE fuel injection dynamic interaction between the detonation wave and gaseous injector flowfield.
    a. Study the transient response of injectors in RDE, that are impulsively blocked by detonation wave passage ad recover after a characteristic delay producing refresh jets.
    b. Better understand the refresh jet behavior, including the effects of wave dynamics and injector characteristics on the refresh delay time.
    c. Quantify the characteristic delay time associated with the injector refresh jets as a function of injector flow rate and wave strength.
2. Investigate the interaction between the liquid fuel droplet and waves inside the RDE.
    a. Study the behavior of fuel droplets exposed to detonation waves propagating in a narrow open channel, unwrapped RDE combustor.

b. Compare the breakup and vaporization of liquid fuel droplet caused by different types of detonation waves; detonation wave, weakly-coupled detonation wave, and decoupled shock-deflagration wave.

1.3 Scope

This work includes utilizing the linearized RDE combustor channel. The facility does not consider the curvature effect on the detonation wave propagation. Also, it has limitation of operation that it could not work in a steady state (wave propagating continuously as in the RDE). However, it simplifies the problem to focus on the jet refresh behavior/liquid fuel droplet breakup after the controlled wave(s) pass by.

Also, surrogate gaseous reactant was injected for jet refresh behavior investigation. This was to inject the reactant that does not react from the detonation wave which could have advantage in visualizing the refresh jet after the wave passes.

Another part of this work includes the investigation of interaction between several liquid fuel droplet and three different wave strength. The scope of this work is limited to the case when the droplet size is relatively large and suspended through dispenser needle. This is because of the specific situation that the study is assuming. When liquid fuel is injected to the RDE, it should go through atomization/vaporization before injecting into the combustor. However, not all liquid fuel successfully gets atomized/vaporized and some portion of liquid fuel should enter the combustor in form of relatively large size droplet. In terms of energy density per volume, these droplets could hold high energy and change the condition for the current/consequent cycle. Thus,

despite the limitation, it has advantage of focusing the observation of the liquid droplet breakup with controlled wave.

Both scopes will require to observe the features in high-speed visualization techniques due to rapidness of physics of detonation wave. Therefore, shadowgraph, schlieren, chemiluminescence, and luminescence using high-speed camera will be required.

Chapter 2: Background

2.1 Theory of Detonation Wave

The rapid form of combustion is what differs detonation from deflagration which are two main processes of combustion. In case of deflagration, flame propagates at subsonic speed and causes reduce of pressure and density. On the other hand, detonation is a shock wave followed by flame propagating in supersonic speed. This strong shock wave compresses the material which heats up and triggers the chemical reaction and supports the shock to be sustained. This mechanism leads product from detonation to achieve higher pressure and density. Propagation velocity of the detonation front is most easily measured characteristic property. Simplest one-dimensional theory was brought from Chapman (1899) and Jouguet (1905, 1917) which referred as Chapman-Jouguet (CJ) theory [2].

CJ theory assumes the entire flow to be one-dimensional and the detonation front will be considered as discontinuity. This discontinuity is modeled as a sudden

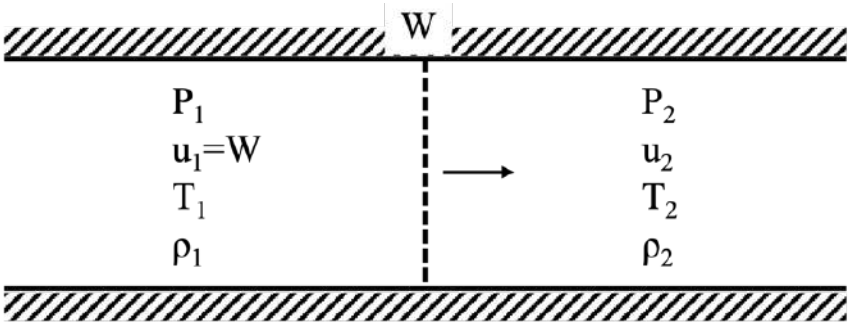

Figure 2.1.1 Framework of Chapman-Jouguet (CJ) theory detonation model

jump with a chemical reaction occurring within a short distance, instantaneously. The framework of the CJ theory is shown in the Figure 2.1.

Here, the detonation wave propagates into a quietly sitting reactant and both the reactant and product are assumed to be calorically perfect gases with constant heat capacity. The conservation of mass, momentum, and energy equations are

$$\rho_1 u_1 = \rho_2 u_2 \tag{2.1}$$

$$P_1 + \rho_1 u_1^2 = P_2 + \rho_2 u_2^2 \tag{2.2}$$

$$c_p T_1 + \frac{1}{2} u_1^2 + q_{in} = c_p T_2 + \frac{1}{2} u_2^2 \tag{2.3}$$

Assuming ideal gas, the equation of state is

$$P = \rho R T \tag{2.4}$$

From Eqn.2.1 and 2.2, equation for the Rayleigh line could be obtained as shown in Eqn. 2.5.

$$\frac{P_2}{P_1} = \left[-\frac{W^2}{P_1 \nu_1}\right]\left(\frac{\nu_2}{\nu_1}\right) + \left[1 + \frac{W^2}{P_1 \nu_1}\right] \tag{2.5}$$

Eqn. 2.5 shows that the slope of the Rayleigh line in P-ν space depends on the incident wave speed W. Combining Eqn. 2.5, energy equation, in addition to the equation of state would yield the Hugoniot curve:

$$\frac{P_2}{P_1} = \frac{\frac{2\gamma}{\gamma - 1}\left[\frac{q_{in}}{c_p T_1}\right] + \frac{\gamma + 1}{\gamma - 1} - \frac{\nu_2}{\nu_1}}{\left[\frac{\gamma + 1}{\gamma - 1}\right]\frac{\nu_2}{\nu_1} - 1} \tag{2.6}$$

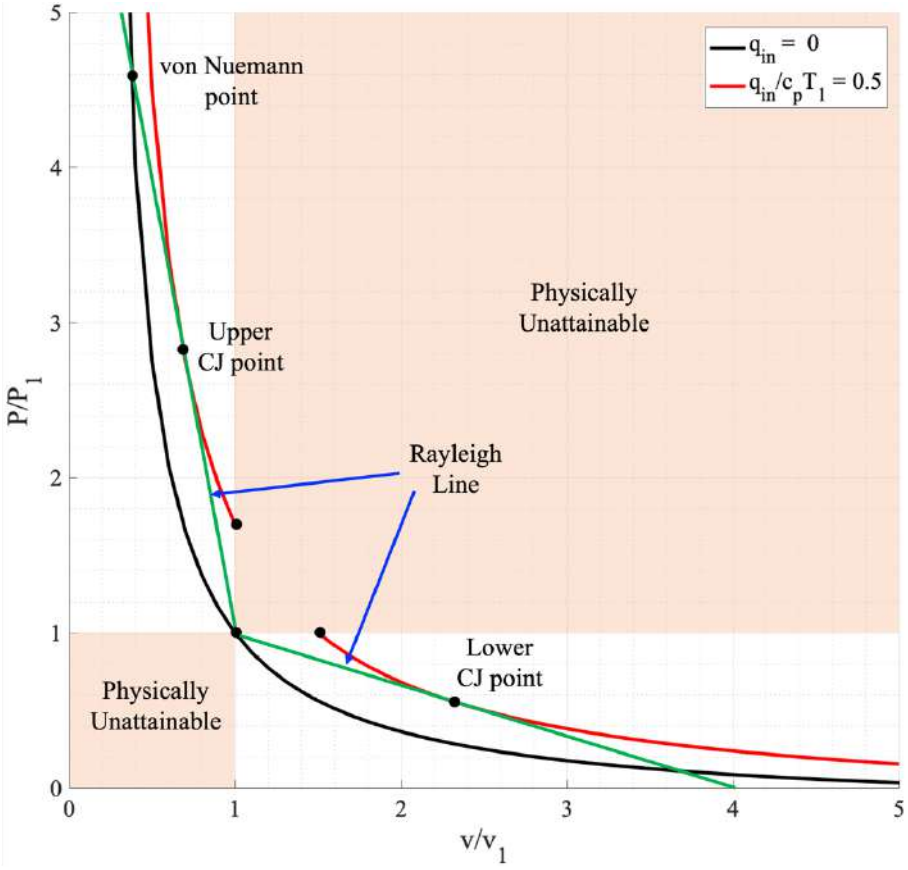

Figure 2.1.2 Hugoniot curves with and without heat release in P-v

As shown in the Figure 2.1.2, when there is no heat addition (q_{in}=0) the Hugoniot curve, Shock-Hugoniot, represents the locus of all states that satisfy the mass, momentum, and energy equation. Another curve corresponds to the locus of all states after the heat is added. Hugoniot curve with heat addition has two branches, detonation (upper branch) and deflagration (lower branch) solution. When pressure increases and specific volume decreases it is detonation branch and on the deflagration branch pressure decreases and specific volume increases. Wave speed along the detonation branch is supersonic and subsonic along the deflagration branch.

Each branch has a possible solution that Rayleigh line is tangent to the heat added Hugoniot curve. These two points are referred as upper and lower Chapman-Jouguet points and are shown in the Figure 2.1.2 as upper and lower CJ point. When reactant gas is shocked along the Shock-Hugoniot curve and reach where it intersects with the Rayleigh line, this point is called von Nuemann point as indicated in Figure 2.1.2. It would follow along the Rayleigh line as heat is added to the flow until it reaches upper CJ point (CJ detonation point). Detonation corresponds to this point is called CJ detonation. CJ detonation have minimum entropy, sonic flow downstream of the wave, and minimum wave speed along the detonation branch. The equation for wave speed of CJ detonation could be derived from Eqn. 2.5 and 2.6 and is shown as:

$$\frac{V_{cj}^2}{a_1^2} = [(\gamma + 1)\hat{q} + 1 + \sqrt{[(\gamma + 1)\hat{q} + 1]^2 - 1} \tag{2.7}$$

where a_1 is reactant sound speed and $\hat{q} = \frac{q_{in}}{c_p T_1}$. While this approach yields the detonation velocity, it assumes calorically perfect gas, which cannot be applied due to the unknown changes in species from significantly high pressure and temperature in the detonation. For better estimate of one-dimensional CJ detonation speed, it is suggested to use various tools that could calculate the composition for real gas such as NASA Chemical Equilibrium with Applications (CEA), CHEMKIN, and Cantera.

2.2 Studies of Rotating Detonation Engine

Conventional propulsion systems based on Brayton-cycle, depends on pressure ratio for its combustion performance, which has potential constraints from mechanical

issues. However, until 1990's, studies of engines using detonation was limited due to more interest in gas turbine and rocket engines. Bussing et al. [3] presented the demonstration of pulse detonation engine (PDE), which induced various research to investigate the fundamental phenomena related to PDE [4–7]. PDE was the first attempt to utilize the detonation-based heat addition in modern era. Nonetheless, there were several issues for practical PDE. Operate cycle of PDE includes filling the reactant, ignition, detonation propagation, exhaust product, and purge. Due to its nature of operation, PDE have limited the operation frequency to 10-100 Hz [6,7].

For further potential performance gain from utilizing detonation in heat addition process, interest have been moved from pulse to continuous mode of operation. This led an increased interest in RDE research in the past two decades. Due to the potential benefits, such as increased thermodynamic efficiency and simpler configuration over the existing engines that use the Brayton cycle various research have been conducted [8–18]. To be specific, stemming from potential increase in propulsion performance and flexible geometry these could accommodate both air-breathing[19–21] and rocket applications [22–24]. Many studies used oxygen-based propellants targeting applications such as rocket engines to potentially increase specific impulse [11,25–31].

Inside a rotating detonation engine (RDE) combustor, detonation waves propagate continuously around an annular channel when freshly reactants are injected. Its operation frequency is restrained by number of detonation waves propagating, speed of detonation wave, and annulus circumference. It could operate in the range of 1-10 kHz frequency[13]. It is known that the RDE flowfield is highly complex and coupled. Characteristics of detonation waves changes by the pressure, mass flow rate of reactants

supplied to the RDE combustor [32]. Thus, fundamental understanding of features of this flowfield is required.

2.3 Operation Mode of RDE

Various research observed from both experimentally and numerically that number of detonation waves present inside the combustor is depended on the operation condition. Inside a rotating detonation engine combustor, fuel and oxidizer is supplied into from one end and detonation wave propagates tangentially consuming the fed reactant. In order to operate the RDE stably, sufficient amount of detonable mixture must be supplied so that detonation wave could sustain. Detonation wave require critical number of cells that allows to propagate stably and this involves sufficient amount of mixture in height (volume). To be specific, if sufficient height (volume) of mixture is not filled, detonation fails to propagate due to insufficient number of cells. On the other hand, when there is too much of reactant supplied, multiple number of detonation waves are observed which could lead to "slapping mode" [33]. One attempt to describe the propagation condition was suggested from Wolanski proposing non-dimensional number "W", detonation wave number [34]. It compares times of detonation revolution inside the RDE combustor chamber with the time of new mixture generated that would be consumed from detonation wave. When W is one or higher, stable propagation of one or more detonation waves is observed inside the combustor and when it is under one, unstable operation is observed.

Furthermore, depending on the level of fuel-oxidizer mixing and the amount of heat release directly coupled to the wave front, detonation waves of various amplitudes

and velocities are observed in RDE combustors. Previous experimental observations have shown that RDEs operate in several modes, such as running one or multiple co-rotating waves (n-wave mode) and ones with counter-rotating waves (slapping mode) [33,35–42].

RDEs can also operate in different instabilities [43,44] near their lean operability limits. These studies suggest that instabilities might be due to an underdamped response of the injector. The injector exit pressure is at a maximum value immediately after the wave passage and decreases with time. As long as the exit pressure exceeds the stagnation pressure of the reactant jets, it will result in flow blockage or flow reversal. After a certain characteristic delay time, as the exit pressure becomes sufficiently low, the reactant jets would refresh, and the detonation cycle can be repeated [14]. Thus, it may be essential to consider the injection refresh behavior and quantify the refresh delay time under carefully controlled experimental conditions.

2.4 Studies of Liquid Fueled RDE

While many previous studies have focused on gaseous propellants, much of the practical usage would require high-density liquid fuel. Using liquid propellants would increase higher energy density, leading to improved performance. Some investigations have used liquid fuels for practical reasons and feasibility testing purposes[11,45]. Heating the mixture, pre-vaporize and inject the liquid fuel of small droplet helps the detonation process. Thus, liquid fuel must undergo a breakup, vaporization, and atomization processes before entering the combustor. Also, very short time to mix with the oxidizer to create detonable reactant and evaporation of the liquid fuel led to

additional challenges creating localized inhomogeneity of the mixture which is additional challenge for sustaining detonation wave[45]. In addition, some liquid-fueled RDE experiments were conducted to understand the effects of different types of liquid fuels, total temperature, and equivalence ratio on detonation wave propagation characteristics [11,45–49]. Bykovskii et al.[11,47] have done various work on two-phase rotating detonation using Kerosene/liquid oxygen, kerosene/oxygen-rich air, kerosene/oxygen, diesel/oxygen-rich air, or gasoline/oxygen-rich air and performed successful rotating detonation. Kindracki et al.[45] conducted experiments on initiation of rotating detonation for liquid kerosene-gaseous air with the addition of hydrogen and/or isopropyl nitrate. Ma et al.[46] assessed the applying rotating detonation engine to turbine engine using liquid gasoline-high temperature air. Zheng et al. [48] studied instability of propagation characteristics of room temperature liquid kerosene and different total temperature of oxygen-rich air inside the rotating detonation engine. Frolov et al. [49] injected liquid propane into the rotating detonation combustor when a sustained continuous-detonation combustion of hydrogen-air mixture was attained and obtained detonation combustion of liquid propane.

Various studies proved feasibility of liquid propellent fueled rotating detonation engine. Most likely liquid fuels are sprayed or pre-vaporized before injected into the rotating detonation engine combustor. This could lead to possible off-design case when the liquid fuel is injected into the rotating detonation combustor relatively large droplet size. These large droplets could enter the combustor due to the size distribution from the pre-vaporization process. However, little is known about the physical mechanisms

associated with off-design scenario of interaction between the liquid fuel droplets and complex detonation waves, those found inside RDEs.

2.5 Studies of Liquid Droplet Breakup from Shock Wave and Detonation Wave

Previous studies have investigated the interaction between liquid droplet and detonation wave [50–57] or shock wave. Early works studied the ignition of hydrocarbon fuels in detonation waves or shock waves in relation to industrial explosion safety, advanced engines, etc. Dabora et al.[50,54] conducted experiments of propagation of detonations with sprays of liquid diethyl cyclohexane in gaseous oxygen inside the detonation tube. It investigated the effect of the droplet size on the development time of detonation and effect of mixture ratio. Raland et al. [51] showed that the liquid fuel would cause larger reaction zone thickness than that of a gaseous detonation due to deformation, stripping, vaporization and diffusion of liquid fuel. Cramer [52] showed that the small liquid fuel droplets under 10μm could sustain a detonation wave in premixed gas and in the heterogeneous spray in shock tube device. Bowen et al. [53] supported this idea by showing that 2μm droplet fog could reach the ideal gas/gas Chapman-Jouguet velocity.

Some of early works studied the interaction between the water droplet and shock wave for different purposes, the rain erosion on high-speed vehicles [58–61]. Engel et al. [58] investigated the water droplets exposed to shock waves in the air. Nicholson and Hill[59] extended the work to higher range of Mach number and reduced the pressure for simulated altitude. Reinecke et al. [60,61] again increased the Mach number range and studied the breakup of 1mm water droplet.

The first comprehensive review was provided by Pilch and Erdman [62]. Pilch and Erdman used the Weber number to distinct different mechanisms of droplet breakup, illustrated in Figure 2.5.1. The Weber number is used as the independent

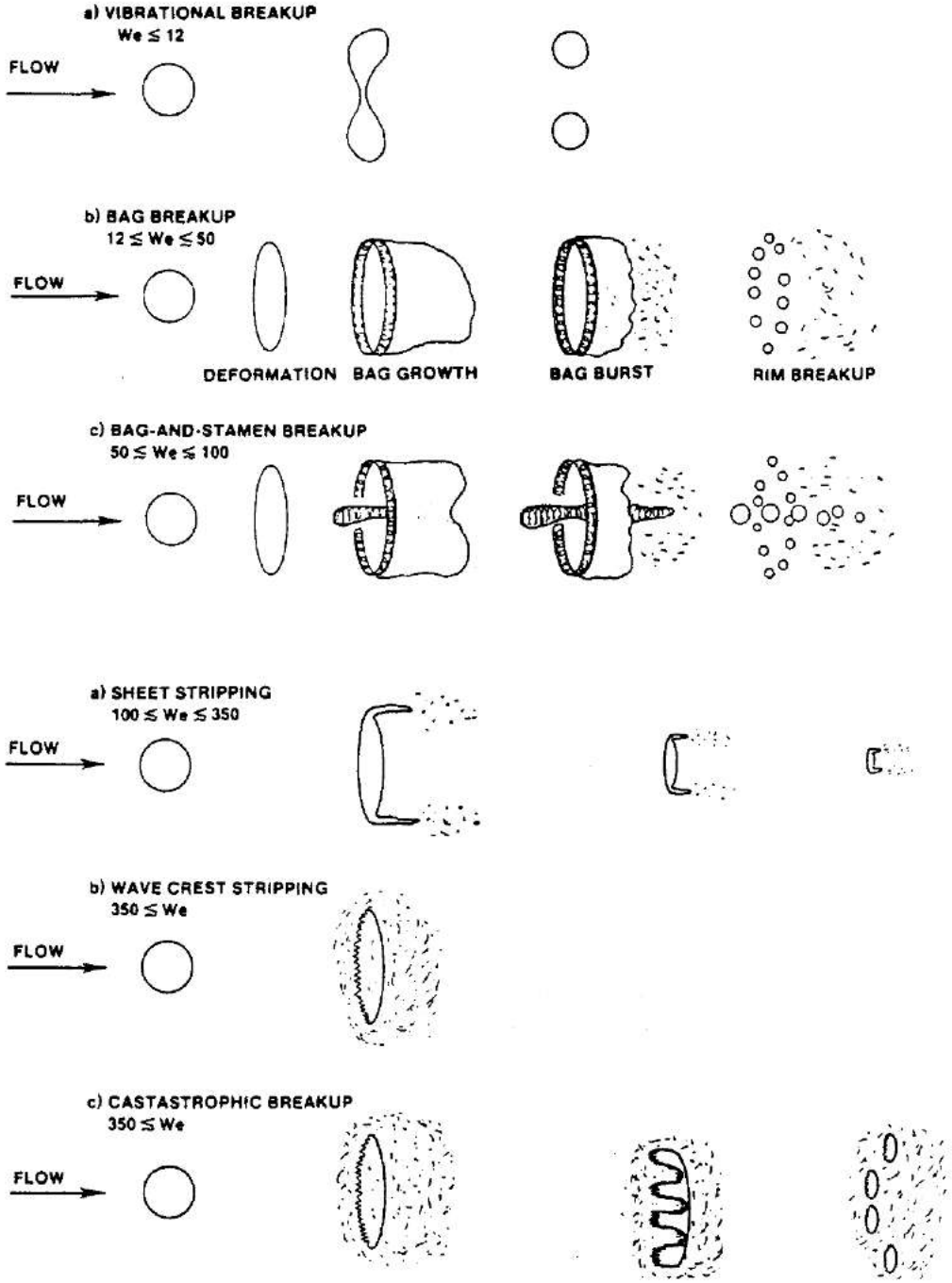

Figure 2.5.1 Breakup mechanisms [62]

variable, which represents the ratio of disruptive hydrodynamic forces to the stabilizing surface tension force.

Recent studies explain the deformation and breakup of liquid droplet suddenly exposed to a gas flow is strongly dependent on the Weber number [63–66]. Various breakup regimes follow the Pilch and Erdman's review as shown in the Figure 2.5.1. The reason why the past research explained their results in terms of Weber number is because the deformation and breakup is caused by the aerodynamic forces and surface tension resists this deformation. As a result, the Weber number is defined as the ratio of the disrupting aerodynamic forces to the restorative surface tension forces. In addition, many authors use of Ohnesorge number, which represents the ratio of droplet viscous forces to surface tension forces. When Ohnesorge number is high, this means that the liquid droplet is less likely to fragment. Other dimensionless parameters could be Reynolds number, which is ratio of aerodynamics forces to the viscous forces.

In recent year, some works attempts to compare the experiments results from previous studies using numerical simulations [65–67]. Martinez and Heister [67] suggests a simple model to investigate the behavior of a droplet in a heterogeneous detonation flowfield. They identified that the initial droplet diameter and the dynamic pressure behind the leading shock front are the important factors that influence the liquid droplet breakup process.

However, these studies were not conducted in multi-dimensional boundary conditions those found in RDE combustors. Unlike the fully confined conditions that were used in the previous studies, boundary condition is partially confined in the RDE combustor. This causes detonation waves to propagate are more complex way, such as

transient change of pressure and velocity drop rapidly after the wave passage. In addition, often single, multiple, counter-propagating waves are observed when operating the rotating detonation engine, which requires more tailored geometry to study the interaction between various waves and liquid fuel sprays.

Chapter 3: Experimental Methodology and Diagnostics

3.1 Description of Linear Model Detonation Engine (eLMDE)

The linear model detonation engine (eLMDE) [68–76] is designed to simulate an RDE combustor section that is unwrapped in a linear direction. eLMDE could be connected with either one or two pre-detonators. When one pre-detonator is connected, it could simulate a single detonation wave propagating in the combustor. On the other hand, when it is connected to two pre-detonators in the opposite side, it could create counter propagating detonation wave inside the combustor, so called slapping mode. Also, it could inject partially premixed gas from bottom of the combustor so that propagating detonation wave from the pre-detonator could survive from the transition and propagate. Although it factors out of accounting the curvature effect of a detonation wave propagation and could only produce single cycle, it benefits to have direct visual access inside the RDE combustor.

3.1.1 Description of Utilizing eLMDE for Detonation wave-Injector Refresh Interaction Experiment

As illustrated in the Figure 3.1.1.1, two pre-detonators are connected to the eLMDE at each end. It is capable of testing single detonation wave and counter propagating detonation wave interacting with the injector refresh jet. In order to generate detonation wave from the pre-detonator, stoichiometric mixture of gaseous fuel and oxidizer are fed from both end and a spark plug located at the center could detonate. Shchelkin spiral is installed inside the tube, located downstream of the spark

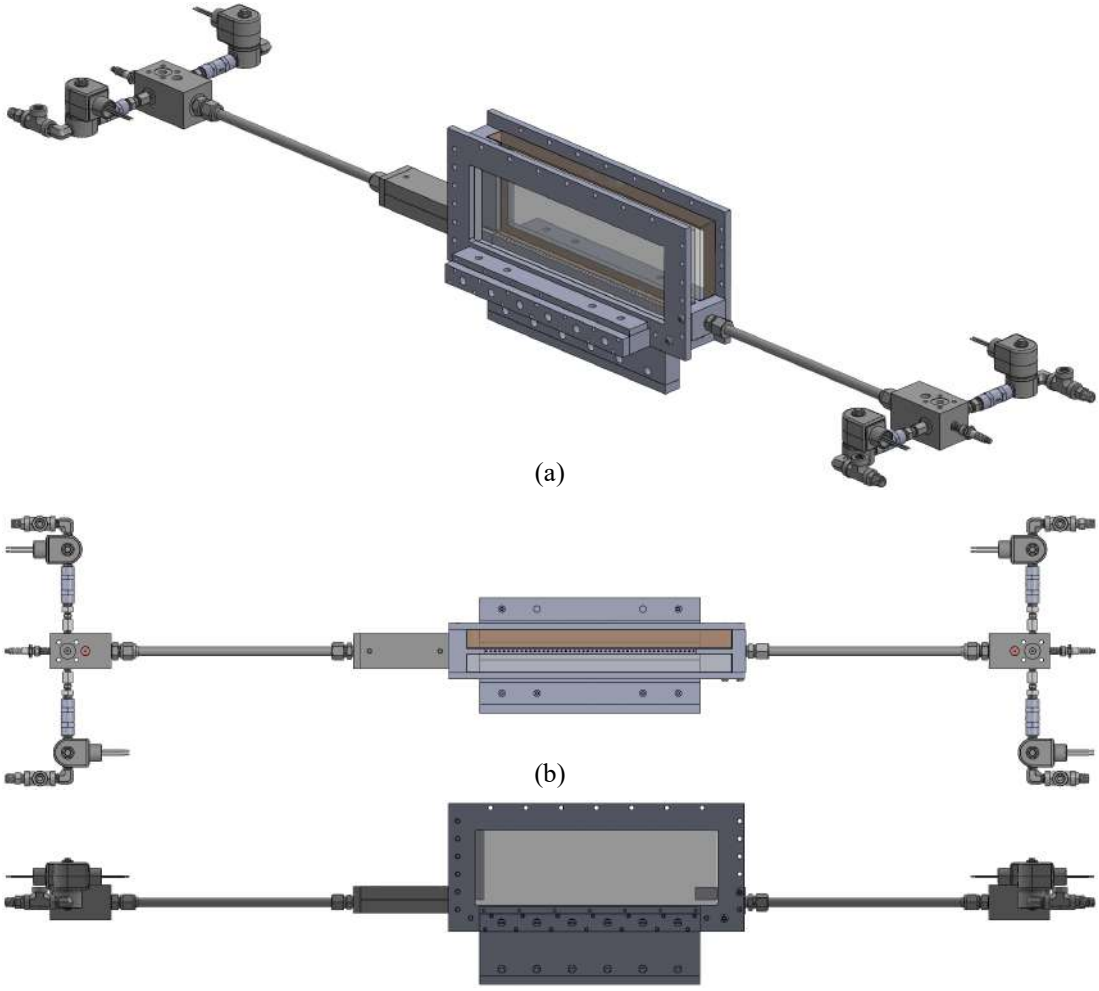

Figure 3.1.1 (a) Isoview, (b) topview, and (c) sideview of eLMDE

plug, to assist the transition from deflagration to detonation. Detonation wave, generated from a pre-detonator propagates inside the tube, passes the transition component, and enters the eLMDE.

eLMDE's injector arrangement and the aspect ratio were modeled after the elements of the AFRL's 6-inch RDE design [15] and the NRL's premixed microinjection system [77]. As shown in Figure 3.1.1.2, each injector has an internal diameter(d) of 2.54mm. Dimensions in subsequent figures are normalized by the tube diameter, d. The combustor section contains 48 injectors, each spaced 2.5d apart.

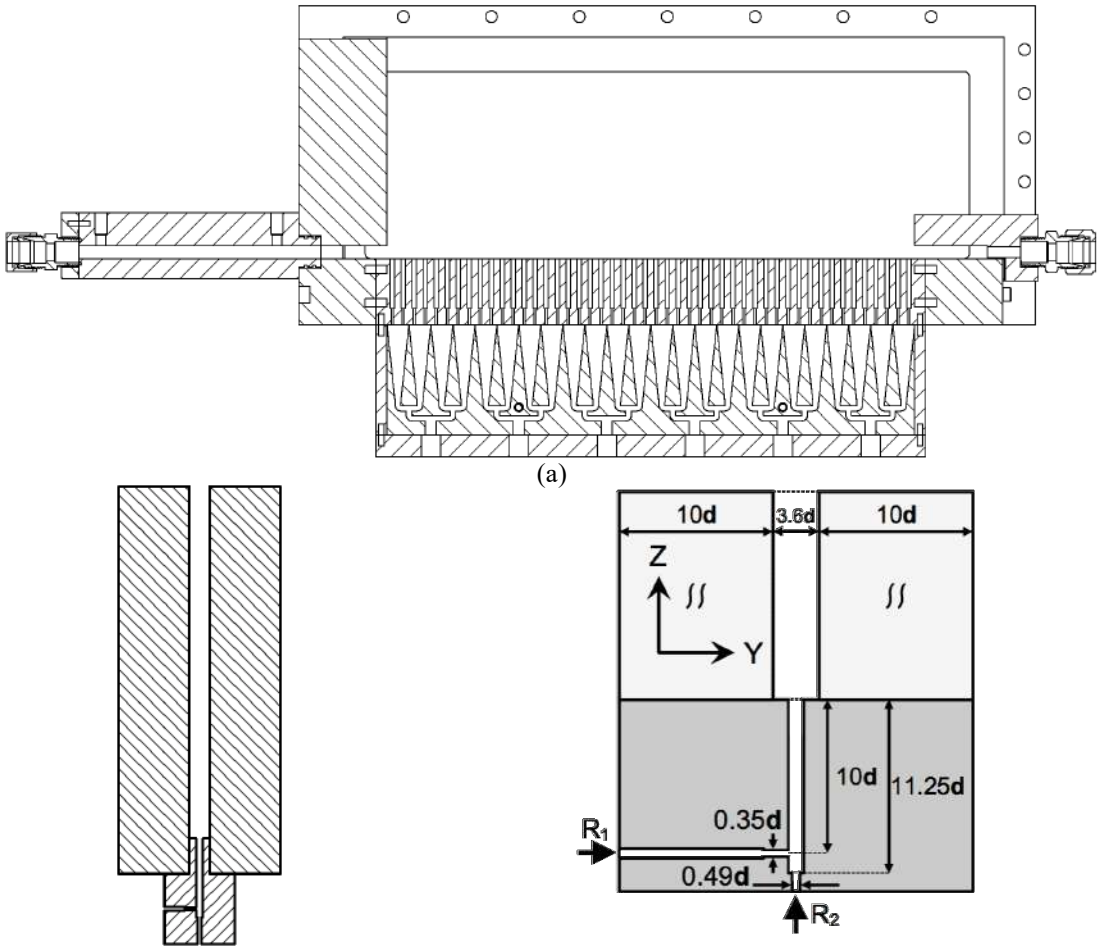

Figure 3.1.2 (a) Center cross section view of eLMDE, (b) side cross section view of eLMDE, and (c) schematic drawing of one injector

The injector is a recessed tube with a depth-to-diameter ratio of 11.25. Each injector is connected to both fuel and oxidizer. Fuel is injected from the side and oxidizer is injected from the bottom. Both fuel and oxidizer are expected to get choked from the orifice before entering the recessed tube and meets perpendicular. Reactants have 10d to partially mix before entering the combustor. 8 injectors are paired to one reservoir of fuel and oxidizer. Total of six reservoirs are connected to each fuel and oxidizer source tanks.

Injector was designed as a rail, in order to be replaced with different design for various purpose of tests. For the liquid droplet breakup test, it was replaced by smooth surface rail without the injectors, which will be explained later of this chapter. The width of the eLMDE channel is 3.6d and is created from two optically accessible quartz windows installed on each side, which will create partially confined boundary condition similar to the RDE combustor. One quartz window could be replaced to a metal window to install dynamic pressure measurement when needed.

3.1.2 Description of Utilizing eLMDE for Detonation Wave-Liquid Droplet Interaction Experiment

As noted previously, eLMDE is capable of modifying the injector rail component. In order to isolate the test condition so that it is mainly considering the propagating detonation wave interacting with the liquid droplet, 48 injector rail is replaced with a smooth surface rail. Therefore, there is no reactant injected from bottom of the combustor as shown in the Figure 3.1.2.1. However, to sustain the detonation to propagate inside the eLMDE combustor, timing of the reactant injected from the pre-detonator is varied. One pre-detonator connected to the combustor feeds extra amount of stoichiometric mixture of gaseous fuel and oxidizer, which will create a premixed reactant spilled inside the combustor. Different amount of premixed reactant spillage controls the strength of the detonation wave. When there is enough reactant, detonation wave survives and propagate as detonation wave along the eLMDE. And when there is not sufficient reactant, detonation wave starts to decouple which would create decoupled detonation wave propagating. If the reactant is sufficiently low, detonation

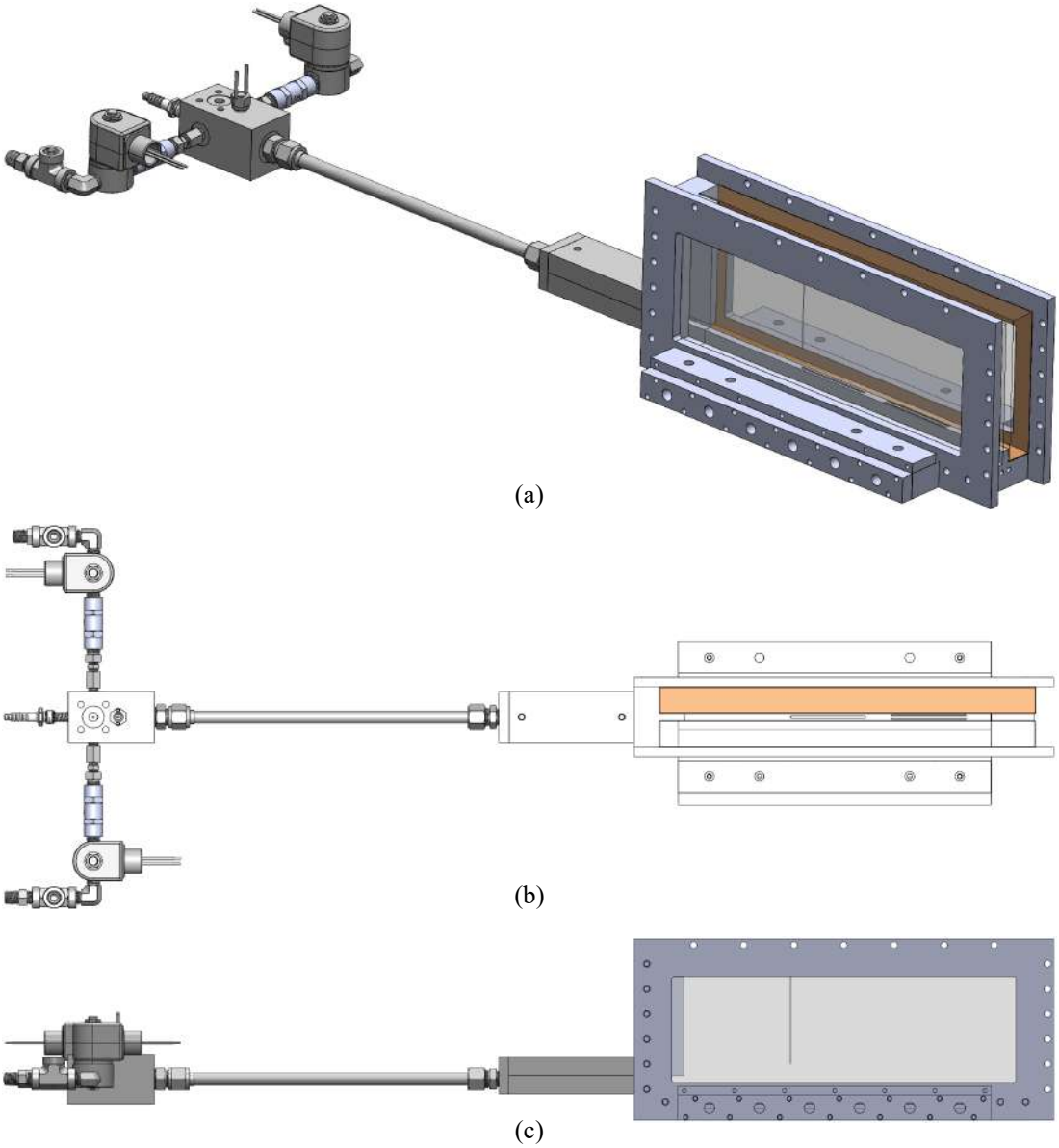

Figure 3.1.3 (a) Isoview, (b) top view, and (c) sideview of eLMDE

wave would not survive and generate decoupled shock-flame wave. Detail of these conditions will be described in later chapter 5.

Additional modification was made to test the liquid droplet interaction with detonation wave. As shown in Figure 3.1.2.2, dispensing needle is placed inside the eLMDE combustor. This needle is connected to the 1ml syringe outside the combustor.

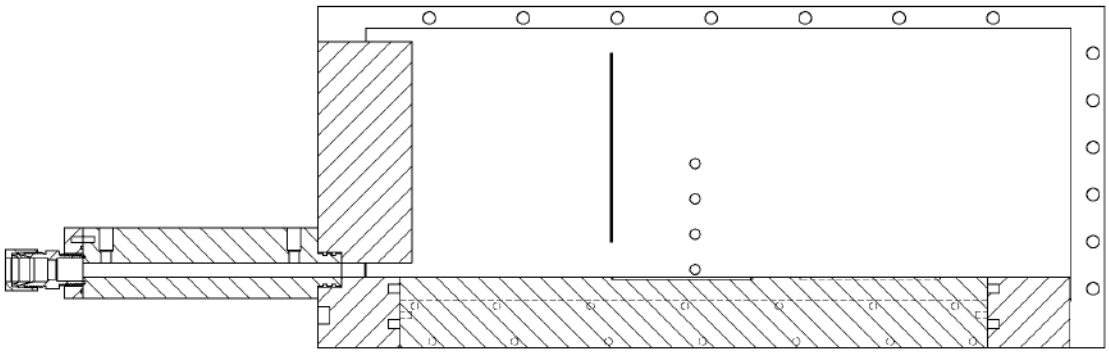

Figure 3.1.4 Section view of eLMDE for detonation wave-liquid droplet interaction experiment

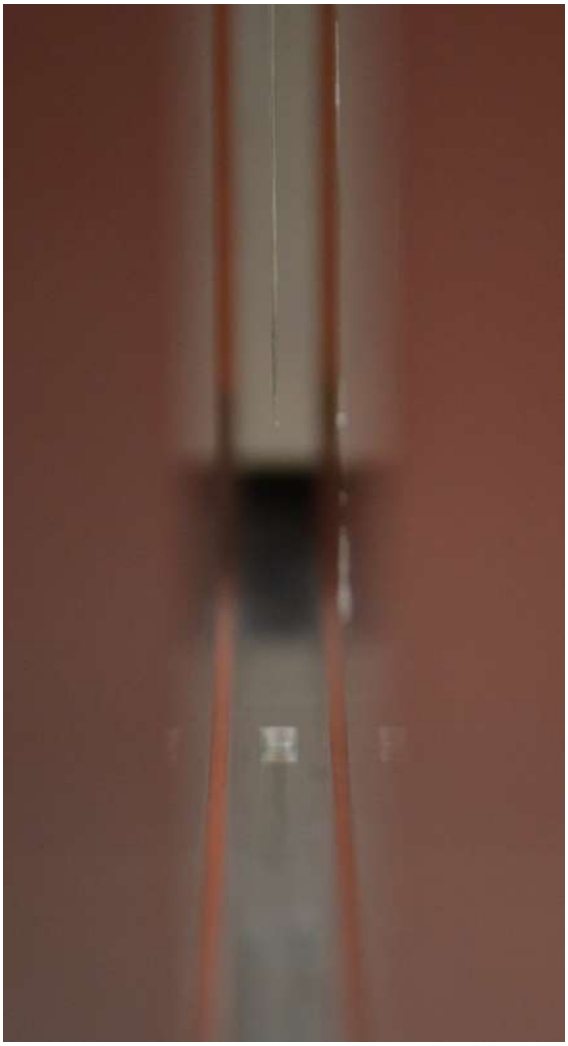

Figure 3.1.5 Dispensing needle sitting inside the eLMDE combustor

Varying the outer diameter of dispensing needle allowed to change the diameter of the liquid droplet. Dispensing needle was specifically located between 17^{th} and 18^{th} injector counted from the entrance of the combustor. This was sufficiently apart from the entrance so that the quenched detonation wave entering the eLMDE combustor would have enough length/time to recover.

3.2 Description of Liquid Droplet

Liquid fuel droplet was suspended inside the eLMDE combustor for droplet breakup tests. As shown in the Figure 3.2.1, thin stainless steel dispensing needle is located inside the eLMDE combustor. It is connected to 1 ml syringe and the syringe is connected to the frame of the eLMDE outside the combustor. Liquid droplet is located 0.75" above the bottom surface of the eLMDE. And it is placed 4.25" downstream of the entrance which is chosen far downstream of the combustor's inlet in order to collide the liquid droplet to the recovered detonation wave quenched from entering the combustor. Various size of needle was used to control the size of the droplet. Here, only the data from the blunt needle which has ID of 0.006" and OD of 0.012" will be presented. Liquid droplet was suspended manually just before the test sequence starts. Due to its uncertainty control of the liquid droplet size, calibrated image was used to measure the diameter of the liquid droplet for every test just before it collides with the detonation wave. As shown in the Figure3.2.2, calibrated length/pixel scale conversion the dark area pixel showing liquid droplet to the diameter of the droplet.

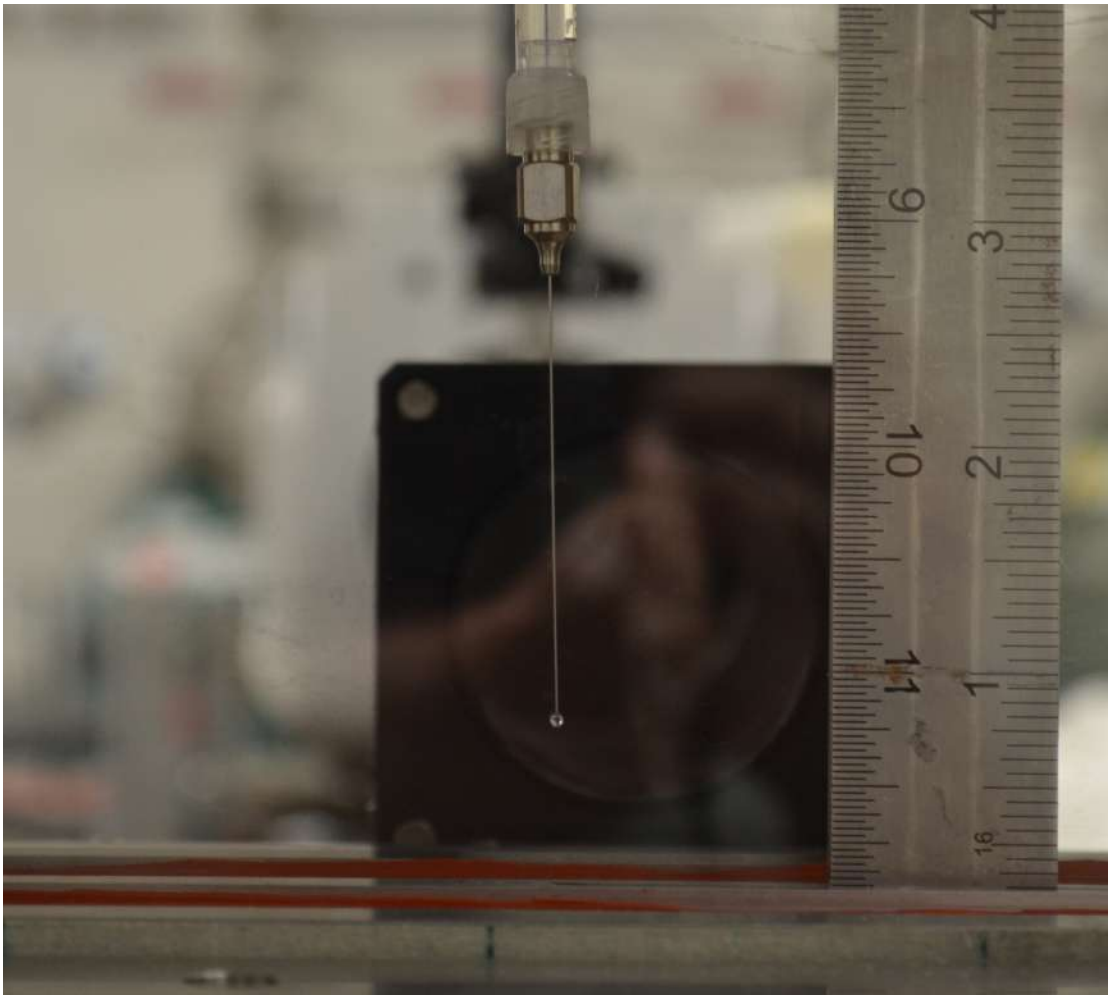

(a)

(b)

Figure 3.2.1 Liquid droplet suspended inside the eLMDE combustor

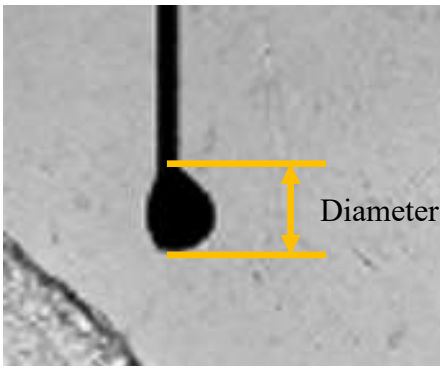

Figure 3.2.2 Description of how liquid fuel diameter is defined

3.3 Diagnostics

Various diagnostics were used to analyze the result. Dynamic pressure measurements were used to verify the detonation waves propagating inside the eLMDE combustor. Especially for analyzing the counter propagating detonation waves, dynamic pressure measurements provided valuable data, showing clear difference between a single and counter propagating wave.

Schlieren and shadowgraph imaging was mainly used for investigating both detonation wave-injector refresh and detonation wave-liquid fuel droplet interactions. Both imaging technique was able to provide valuable qualitative data which also provided useful data after post-processing.

In addition, to verify additional combustion from either counter propagating detonation waves or detonation wave interaction with liquid fuel droplet chemiluminescence imaging was conducted. High-speed camera was used to view a large field of view and photomultiplier was used to at small local area.

3.3.1 Pressure Measurements

Measurement of dynamic pressure was conducted on one side of the eLMDE by replacing the quartz window to metal window. Four dynamic pressure transducers (PCB Piezotronics model 113B24) were installed either horizontal or vertical array. Horizontal array was installed for the injector refresh experiments to capture the detonation wave propagation and collision of the counter propagation detonation wave. In addition, vertical array was installed for the liquid fuel breakup experiments in order to understand the dynamic pressure field before and after the liquid fuel collides the detonation wave. Pressure measurements were done at 500 kHz.

3.3.2 Schlieren and shadowgraph Imaging

Both schlieren and shadowgraph techniques are non-intrusive method to visualize the disturbance in the flowfield by relying on the refraction of light rays when passing a transparent medium [78,79]. Two different type of optical arrangement was used to obtain the detailed flowfield information as shown in the Figure 3.3.1. Z-type arrangement was used to visualize wider view to consider the large-scale movement and Toepler's lens-type schlieren/shadowgraph system was used to capture detailed small-scale information. Table 3.3.1 shows the specification of the equipment used.

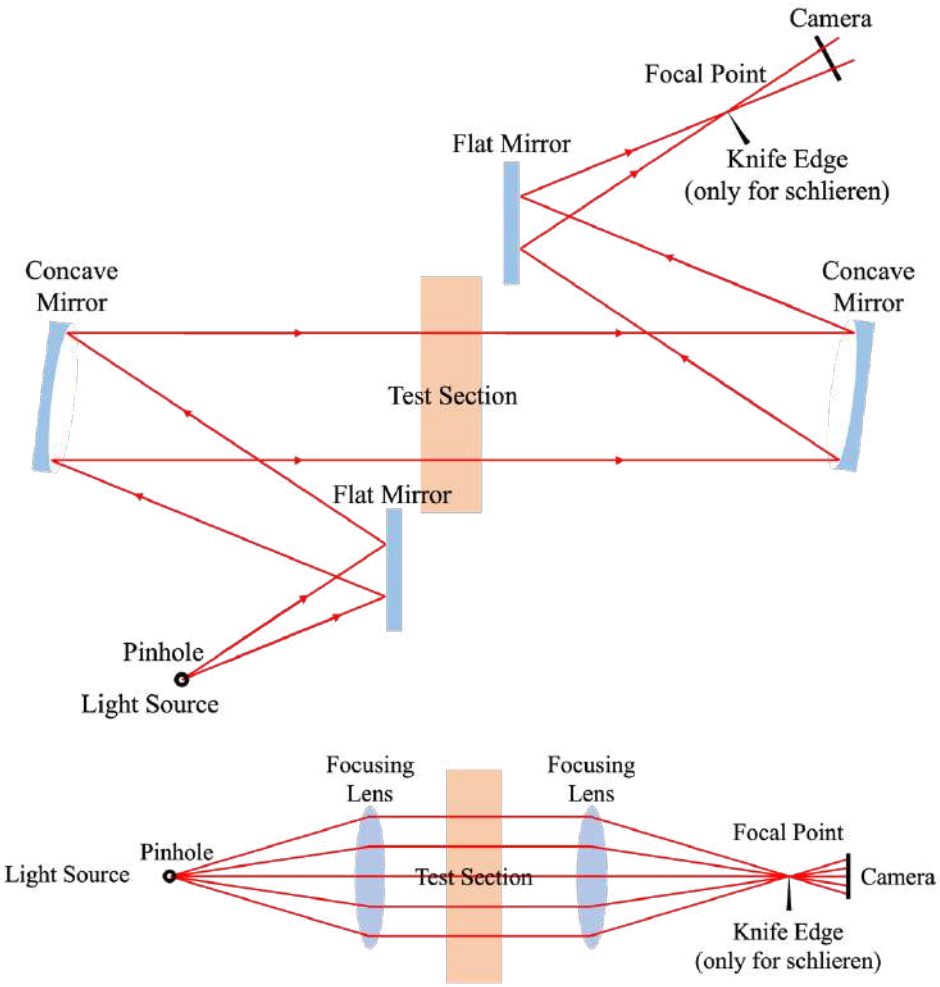

Figure 3.3.1 Schematic of (a) z-type arrangement and (b) Toepler's lens-type arrangement for schlieren/shadowgraph

Table 3.3.1 Information of schlieren/shadowgraph visualization equipment

Equipment	Schlieren Setup	Shadowgraph
Light Source	CAVILUX Smart pulsing diode laser	
Parabolic mirror	d=6", f/10	
Focusing Lens	d=2", f/10	
Knife Edge	Circular/Horizontal /Vertical direction	-
Camera	Phantom v2512	

3.3.3 Chemiluminescence Imaging

3.3.3.1 High-speed Camera

Chemiluminescence is often attractive in combustion analysis due to its simplicity compared to laser-based diagnostics. Chemiluminescence is non-intrusive method to detect spontaneous emission of light, which is chemical reaction excites species and radiate light when excitation is discharge. This could indicate the reaction zone in the combustion experiments. Common species in combustion reaction of hydrocarbon are CH*, OH*, C2*, and CO2* [80,81]. Here, CH* chemiluminescence using high-speed camera (Phantom v2512) was used to identify the reaction zone in the detonation wave and additionally determine the combustion of the liquid fuel reaction. Images were collected with 430±5 nm optical band pass filter at 250 and 500 kHz.

3.3.3.2 Photomultiplier Measurement

Photomultiplier tube could be preferrable method to detect chemiluminescence because it amplifies the signal(light) especially when quantifying a weak/short-lived light. Also, simultaneous measurement using dynamic pressure transducer (PCB) and a CH* chemiluminescence associated with photomultiplier tube with 430 nm band pass filter could enhance the understanding of the coupling of the detonation wave by observing the correlation between the pressure and chemiluminescence signal [82]. For instance, when the detonation wave is not coupled, the rise of the chemiluminescence signal would lag the rise of the pressure, which implies the heat release is occurring behind the detonation wave front. Here, photomultiplier tube and dynamic pressure transducer was used to determine the reaction of the liquid fuel after the detonation

wave passes by. Dynamic pressure transducer was installed on one side where the metal window is placed, and photomultiplier tube (Hamamatsu) was aligned where possible reaction of liquid fuel could occur on the other side where the quartz window is installed. Both data was collected at the same frequency of 500 kHz.

3.3.4 Measurement of Detonation Wave Propagation Velocity

High-speed schlieren/shadowgraph images could be utilized to estimate the velocity and the propagation of local wave direction. During the liquid droplet experiment using the schlieren/shadowgraph visualization technique, direct measurement of the detonation wave propagation speed was hard to achieve. Thus, post-processing of the schlieren/shadowgraph images could quantify the data efficiently and accurately. Based on the new functions and image processing algorithms on MATLAB propagation velocity of the detonation and collision angle to the liquid droplet could be achieve. As shown in the Figure 3.3.2, both edges of the liquid droplet and the detonation wave was captured using MATLAB. Consecutive images were used to track the edge of the detonation wave front. From measuring the shortest distance between the liquid droplet and the detonation wave, wave propagation speed could be estimated. However, closest distance did not always agree with the wave propagation direction. Thus, wave front data was plotted and fitted to estimate the angle of the propagation as shown in the Figure 3.3.3. Next, from the obtained perpendicular direction, shortest distances that follow the obtained perpendicular direction was chosen to be the actual distance between the edges of liquid fuel and the detonation wave for every image, as shown in the Figure 3.3.4. Hence, the velocity of the detonation wave is obtained for every test.

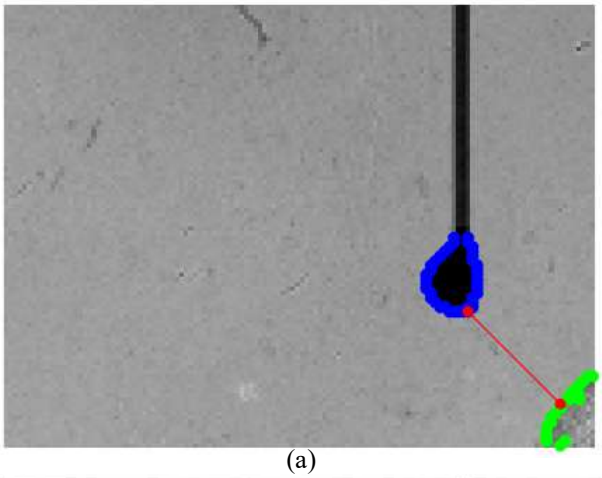

(a)

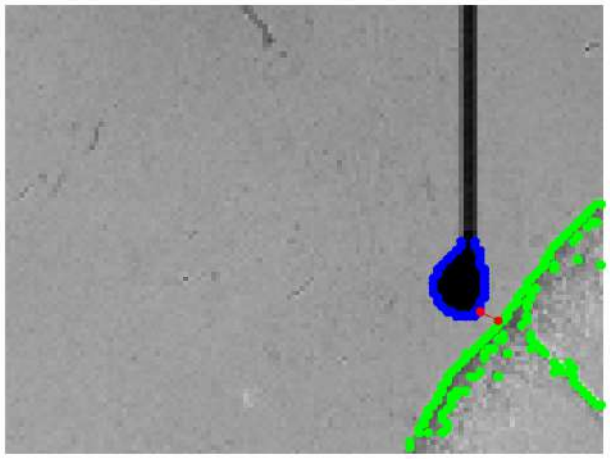

(b)

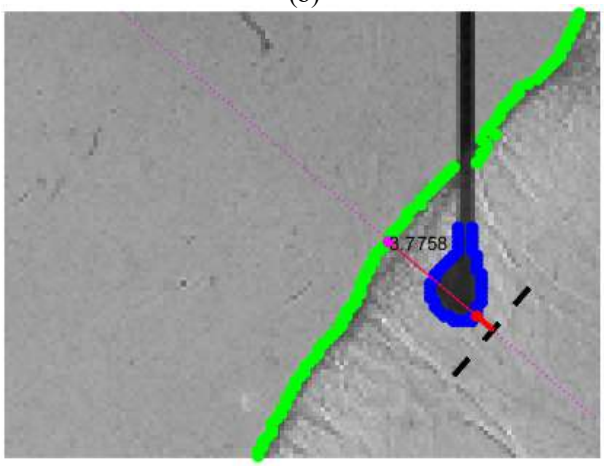

(c)

Figure 3.3.2 Consecutive images to calculate the detonation wave speed using (a) before (b) collision and (c) after the collision to the liquid droplet

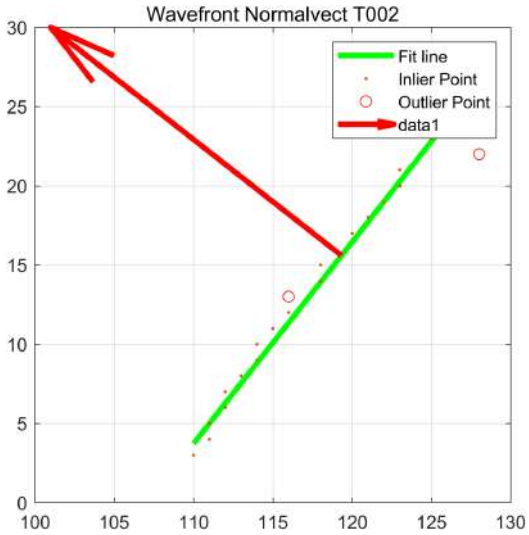

Figure 3.3.3 Fitted data of wave front and perpendicular direction

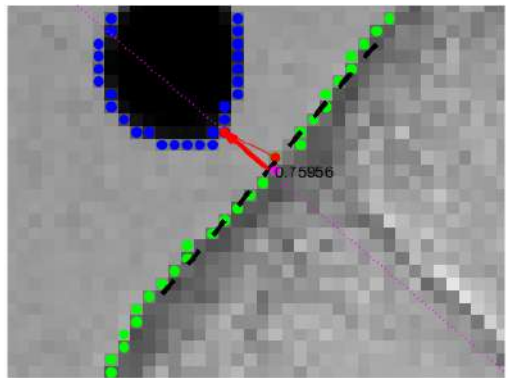

(a)

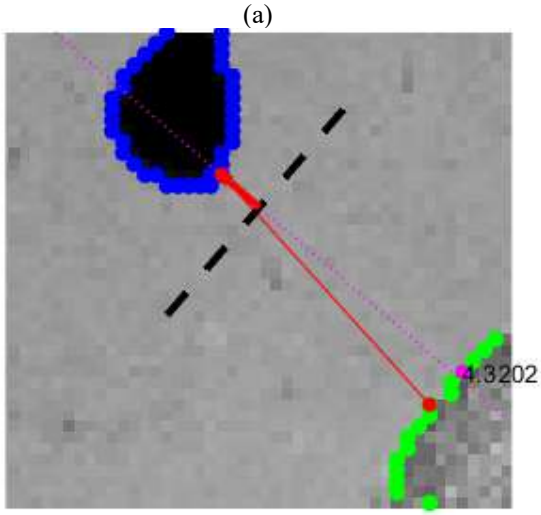

(b)

Figure 3.3.4 Example of estimating the distance between liquid droplet and wave front (a) using perpendicular direction from the wave front at closest (b) following the perpendicular direction obtained from (a)

3.4 Sequence of the Experiment

Complex control system was used to inject precise amount and timing of reacting gas for the experiment. A NI-cRIO-9024 was used through a LabView software to send trigger signal, which would open the solenoid valves for the pre-detonator and inside the eLMDE combustor when necessary. It was controlled in a way to manage the duration of the valve opening and follow the sequence timing for each test. The trigger signal also activates the data acquisition system (Ni-cDAQ-9188),

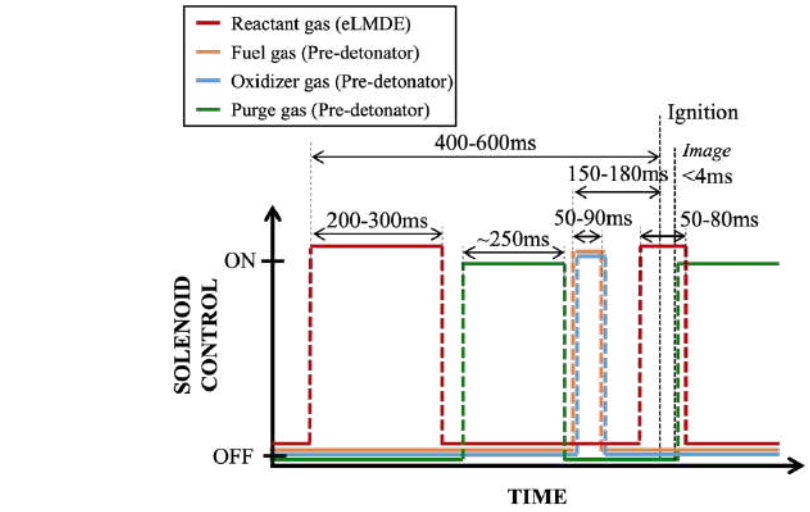

(a)

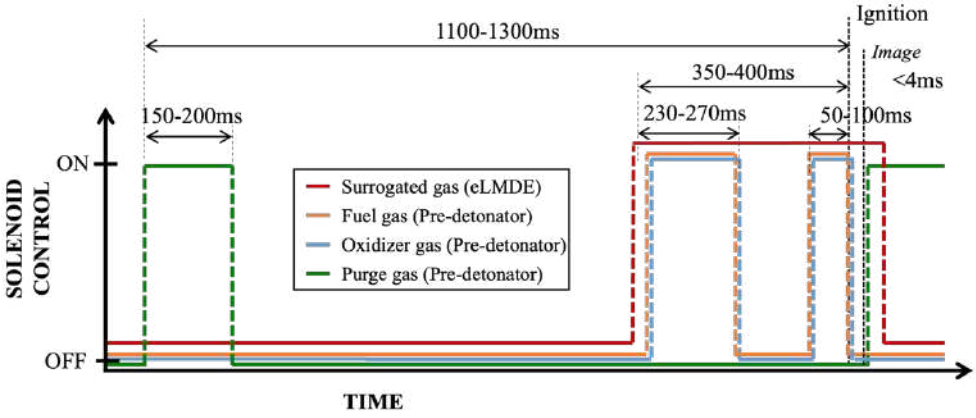

(b)

Figure 3.4.1 Sequence of injected gas for injector refresh experiment (a) detonation wave and (b) decoupled detonation wave

high-speed camera, and CAVILUX Smart pulsing diode laser synchronously. Figure 3.4.1 and Figure 3.4.2 shows examples of injection timing of both pre-detonator and eLMDE and signals to trigger the spark plug and camera for the injector refresh test and liquid fuel droplet breakup test, respectively.

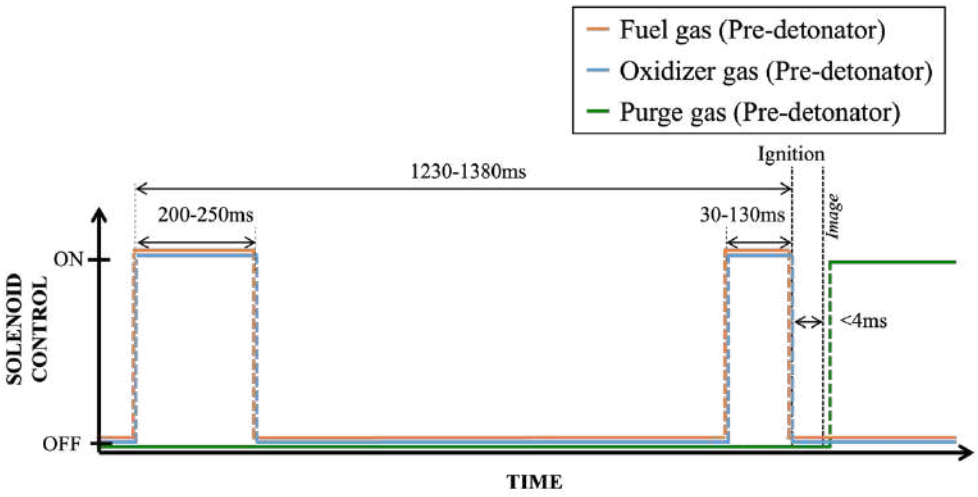

Figure 3.4.2 Sequence of injected gas for liquid droplet breakup experiment

Chapter 4: Detonation Wave-Refresh Jet Interaction in Unwrapped RDE Combustor

4.1 Test Conditions

In this study, the linear model detonation engine (eLMDE) was modified to operate at two different modes. One mode is to operate at a single wave propagation, assuming to simulate one or more waves are propagating inside the RDE combustor. Another mode is counter wave propagation mode, simulating multiple wave counter propagate and collide inside the RDE, so called slapping mode. As shown in the Figure 4.1.1, additional detonation inlet is attached from the right end to generate the wave collision. Specific details of the facility's dimension are described in the previous chapter.

In the experiments, non-reactant nitrogen gas is injected from the oxidizer supply tube to simulate the RDE inflow. Among the 48 injectors placed inside the linear channel, eight adjacent injectors in the middle, that are connected to the same plenum, are utilized. Those injectors are referred in this paper as injector number one through eight, starting from right to left.

Two different boundary conditions are used in this paper to obtain data. They are illustrated in Figure4.1.2(a) and 4.1.2(b). Figure 4.1.2(a) represents a normal operating condition with a single wave propagating over the injectors. On the other hand, Figure 4.1.2(b) corresponds to an experiment with counter-rotating waves similar to the slapping-mode operation. At each end of the channel, a PDE tube or a pre-detonator generates a detonation wave that propagates into the pre-established injector

jets. The pre-detonators used various combinations of hydrogen-oxygen mixture and timing-controlled ignition to obtain different wave velocities. The initial and background conditions are summarized in Table 4.1.1 for those experiments, where conditions for (i) a single wave running from right to left, or (ii) two counter-propagating waves running in both directions are simulated.

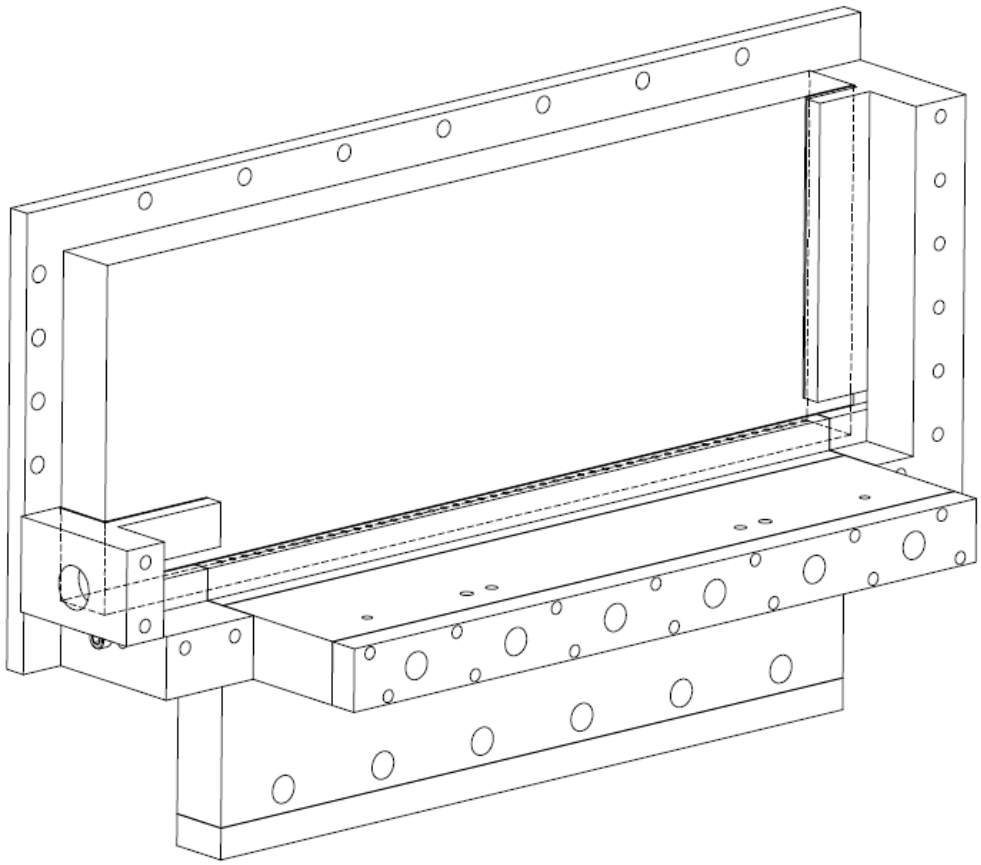

Figure 4.1.1 Schematic drawing of eLMDE test section in isometry view

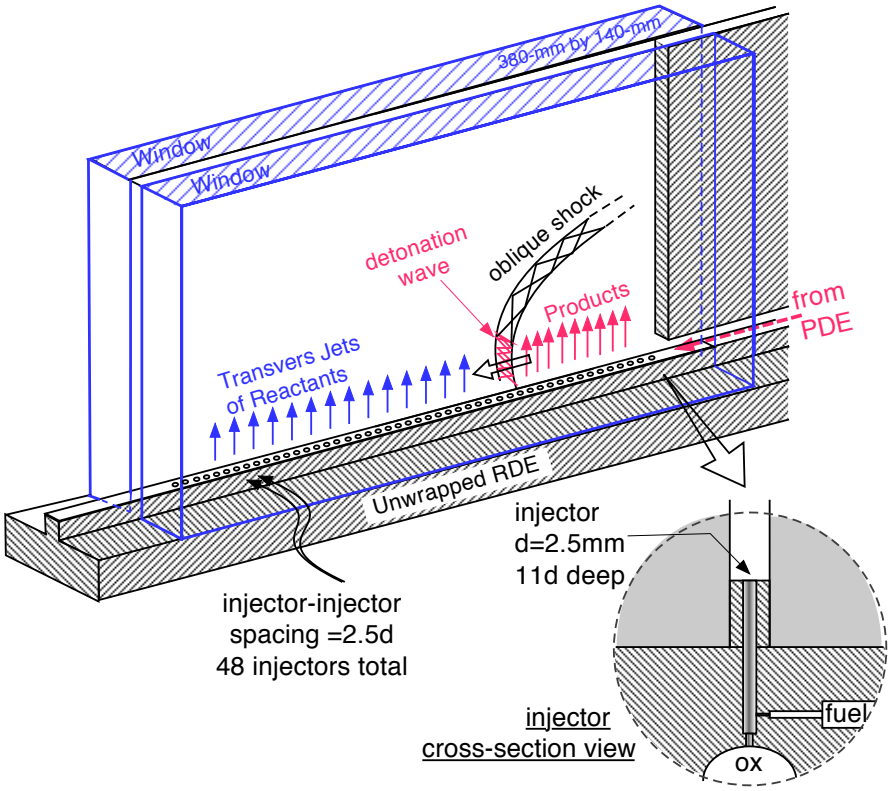

(a)

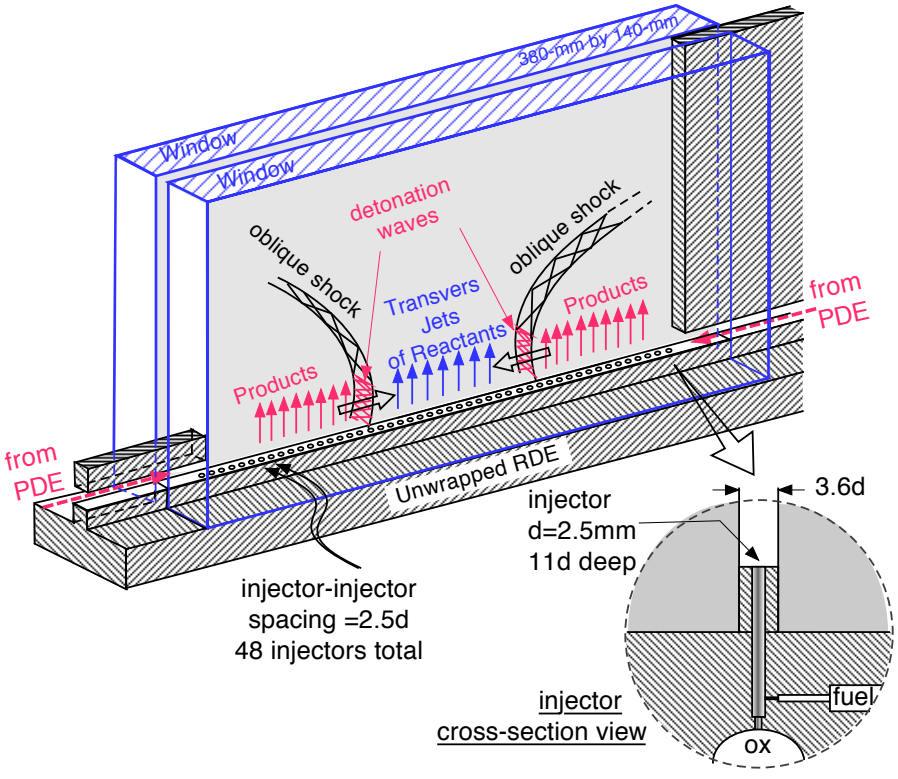

(b)

Figure 4.1.2 Experimental setup (a) a configuration for single wave and (b) a configuration for counter-propagating waves

Table 4.1.1 Experimental test conditions

Reference Test #		Injector Conditions		Combustor Conditions	
		Plenum-Jet Pressure Ratio, P_0/P_{jet}	Average Jet Velocity, V_{inj} [m/s]	Pressure Gain Ratio, P_2/P_1	Local Wave Velocity, D_{wave} [m/s]
Single Wave	Case 1	2.2	89	4.1	674±30
	Case 2	4.1	180	4.5	708±30
	Case 3	6.2	290	4.6	717±30
	Case 4	8.0	360	6.6	851±30
Counter Waves	Case 5	2.4	98	6.4~18	840±30 (LR) 1400±30 (RR)

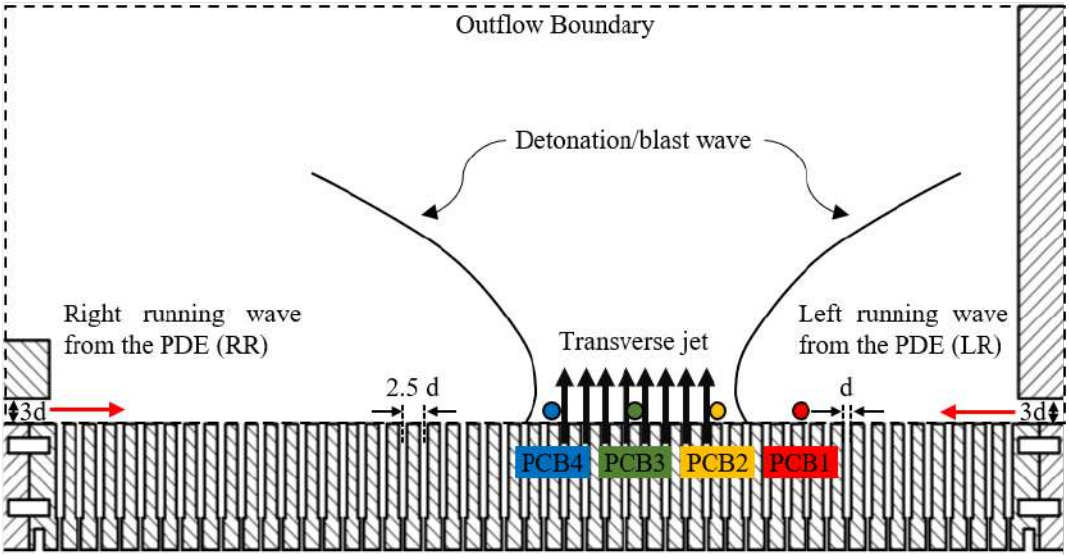

Figure 4.1.3 Schematic of location of the dynamic pressure transducers

Four dynamic pressure transducers (PCB 113B24) are flush-mounted along a side wall, near the exit plane of the injectors as shown in the Figure 4.1.3. First pressure transducer is located at an axial distance of 31d from the right end of the combustor, and subsequent transducers are mounted 10d apart from each other. Optical measurements were made using a high-speed camera (Phantom v2512) and CAVILUX Smart pulsing diode laser (640 nm). The schlieren visualization method was used to

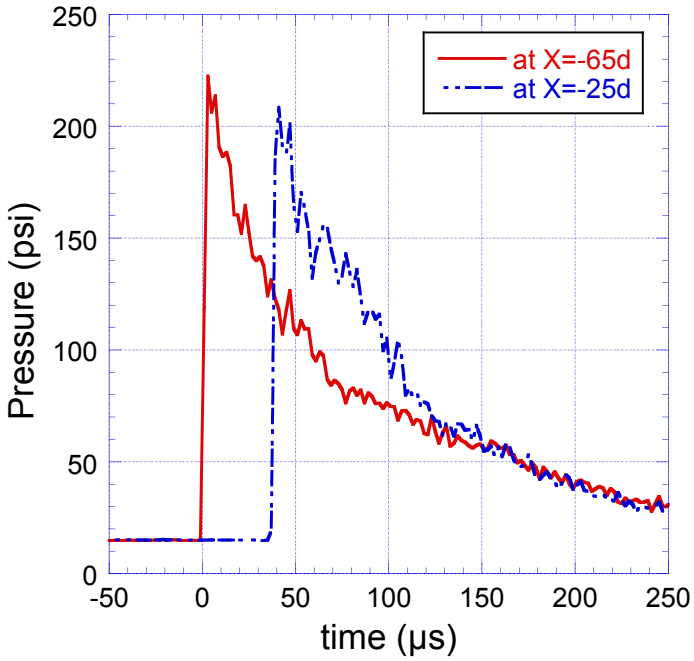

Figure 4.1.4 Pressure-time traces associated with a typical detonation wave before it enters the test section

capture the injector refresh. Also, wave propagation velocity is measured using both the high-speed visualization data and the pressure transducer results.

Pressure measurements using two additional pressure transducers mounted inside a pre-detonator tube were used to obtain more information about the initial wave strength entering the test section. Fig 4.1.4 shows a pressure-time trace associated with these measurements during a typical testing operation.

4.2 Refresh Jet from Single Wave

First, experiments were performed with a single-wave case with and without the refresh jets. The pressure data obtained from the four pressure transducers mounted along the combustor wall are presented in Figure 4.2.1. As the detonation wave enters

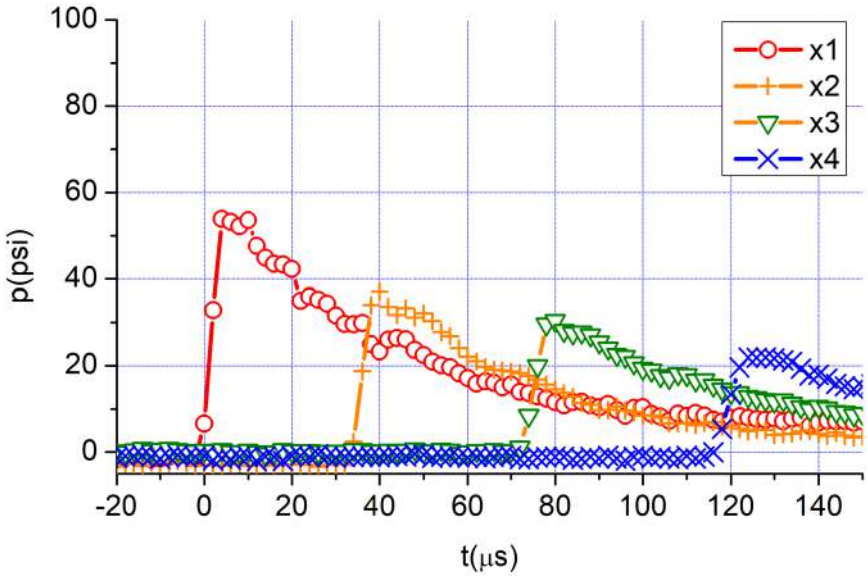

(a)

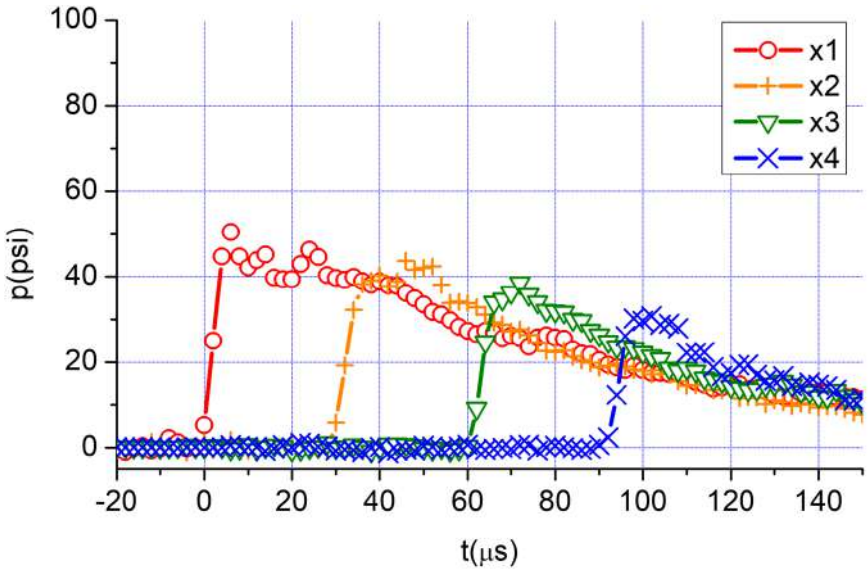

(b)

Figure 4.2.1 Pressure measurements for single-wave cases (a) with and (b) without the refresh jets

the test section and propagates along the channel which is deprived of the reactants, the wave decays into a blast wave and the strength weakens. The measurements with non-reacting jets indicate that peak pressures at x2, x3, and x4 are somewhat lower than the case without the refresh jets. A possible reason for this behavior is the entrainment

effect caused by the crossflowing jets. Other than this, there was no significant difference between the different mass flow rate cases. These pressure measurements represent the injector exit conditions after the wave passage over the injector flowfield.

Also, high-speed schlieren visualization was applied for these investigations. Figure 4.2.2 shows the high-speed schlieren images for low flow rate, case 1. Images were taken at 100kHz. Here the wave propagates from right to left. Surrogated fuel was injected from the eight highlighted injectors in the middle. Time t=0μs was chosen when the wave arrives at the highlighted injectors. Wave transition over the injectors and the refresh jets start to develop. Image at 160μs shows the appearance of the first refresh jets. Following the establishment of the first refresh jet, a subsequent refresh jet is developing. After a time delay, ~200μs, the jet seems to oscillate.

Figure 4.2.3 shows the high-speed schlieren sequence images for high flow rate, case 4. It was taken at 100kHz and wave is moving from right to left. Similarly, surrogated fuel was injected from the eight highlighted injectors in the middle and time t=0μs was chosen when the wave arrives at the highlighted injectors. Refresh jet starts to develop after the wave passage but earlier than the low flow rate case. Higher flow rate case shows more quicker refresh jet rebound with a shorter delay time and grew faster.

The images were used to obtain quantitative information regarding the refresh jet characteristics. Sequence of images were trimmed by each injectors. Only the injectors that are highlighted were chosen. Injectors were numbered from the most right or the first injector to encounter the wave one and continues until eight. Trimmed

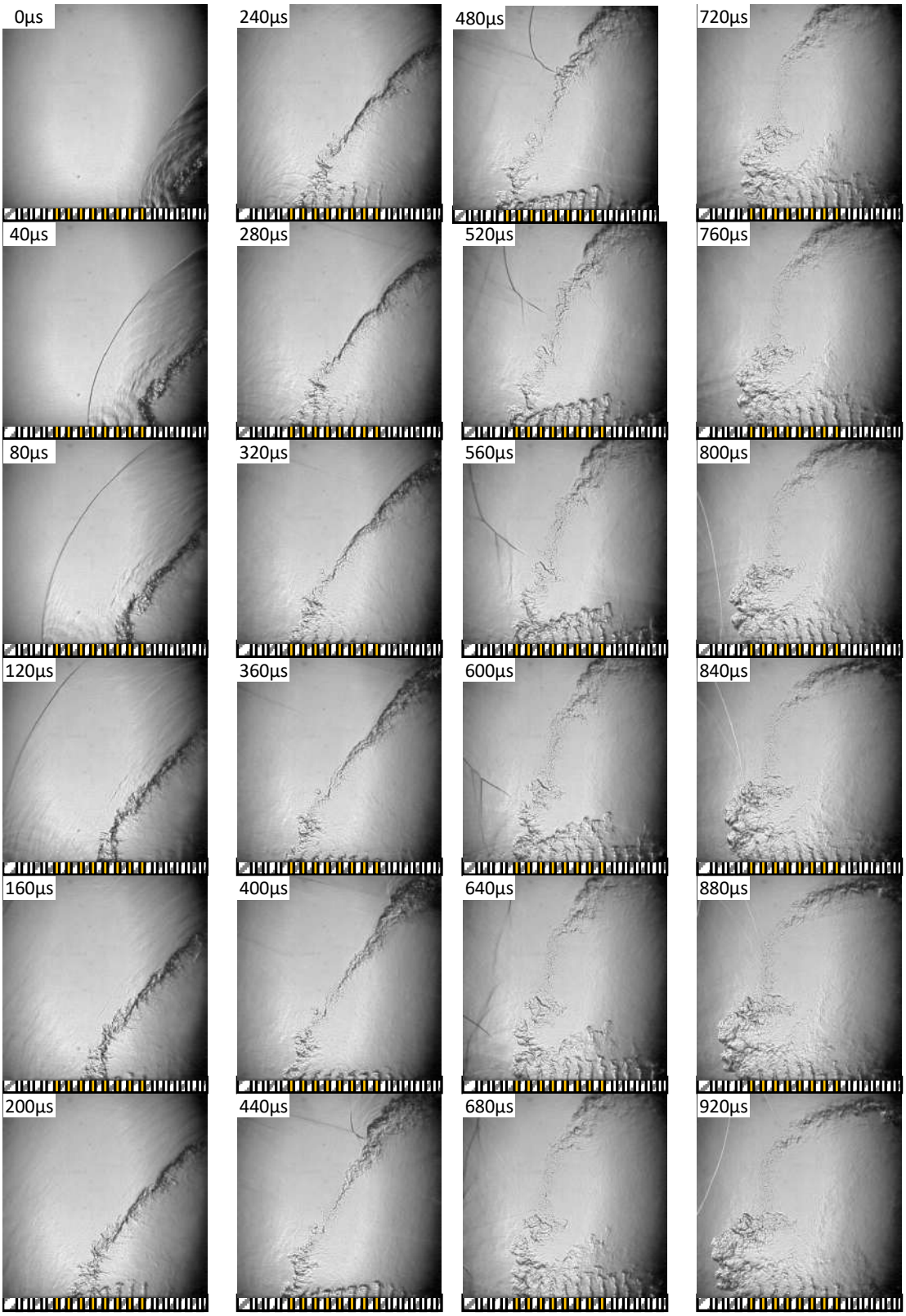

Figure 4.2.2 Sequence of injector refresh after single wave passage for Case 1

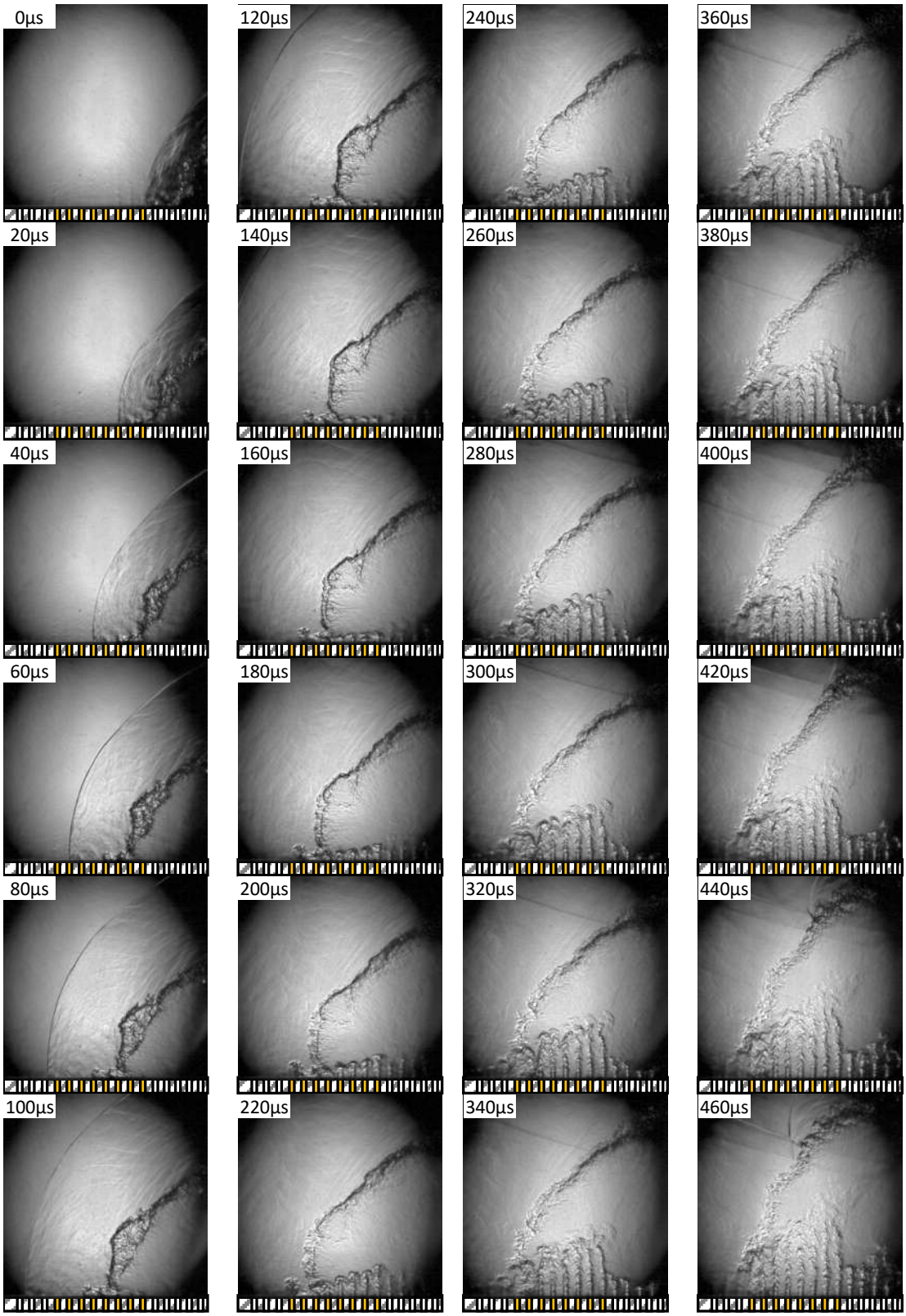

Figure 4.2.3 Sequence of injector refresh after single wave passage for Case 4

images were composed to a single image showing refresh jet development by time as shown in Figure 4.2.4 – 4.2.7.

Figure 4.2.4 represents a composite image showing the development of the refresh jet over the injector #1. Recovery behaviors of various refresh jets following each imposed wave passage are shown for four different mass flow rates in Figure 4.2.4 – 4.2.7. Figure 4.2.4 shows the injection refresh of the lowest mass flow rate case. It takes a relatively long delay time to establish the similar jet height in comparison to other cases. After the first refresh jet front established, there is a subsequent refresh jet front developing after a time delay suggesting jet oscillations. It can be seen that the characteristic time difference between the first and second delays is a little more than 200 μs in this case.

For Case 2 results with a higher mass flow rate shown in the Figure 4.2.5, refresh jet oscillation behavior was not as obvious as in Case 1. This implies that there was a bit more damping in this case with a greater mass flow to overcome the exit pressure. Nonetheless, the first injection refresh time delay remains roughly identical to that from the Case 1. For Case 3 (Figure 4.2.6), the ensuing flowfield appeared significantly different from those in Cases 1 and 2. For both Cases 3 and 4 (Figure 4.2.7) with higher mass flow rates, the refresh jets not only rebound more quickly with a shorter delay time, but the jets grow faster inside the combustor.

Images from the Figure 4.2.4 – 4.2.7, the jet front's height is measured for the first three injectors. The each height was measured from the image subjectively. Assuming the refresh jet develops linearly, linear regression fit was applied to the

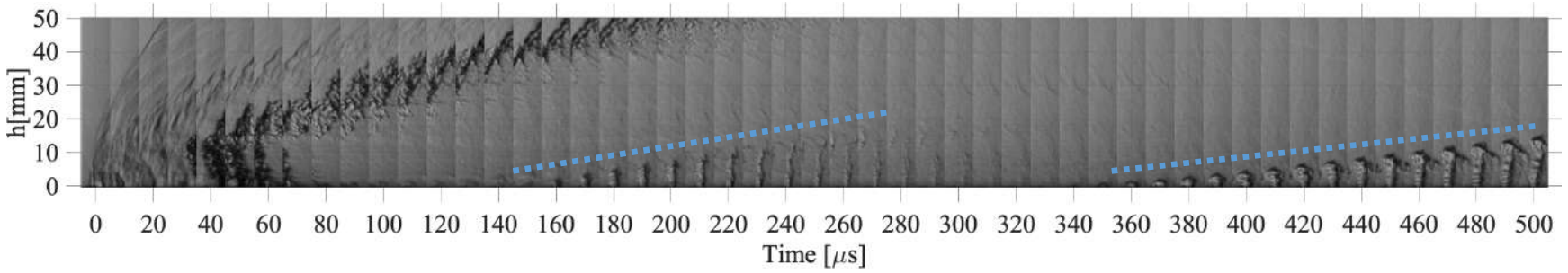

(a)

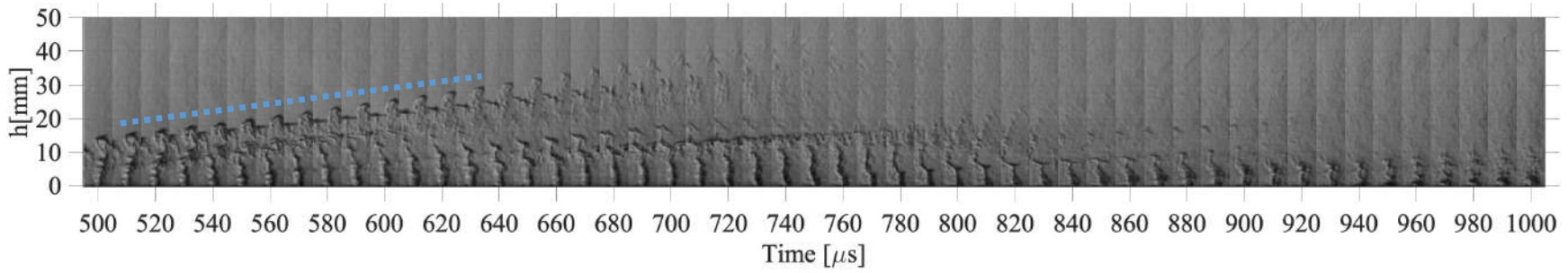

(b)

Figure 4.2.4 Composite images showing the onset and growth of the refresh jet from injector #1 following the wave passage for Case 1 (a) from 0 to 500 μs and (b) from 500 to 1000 μs

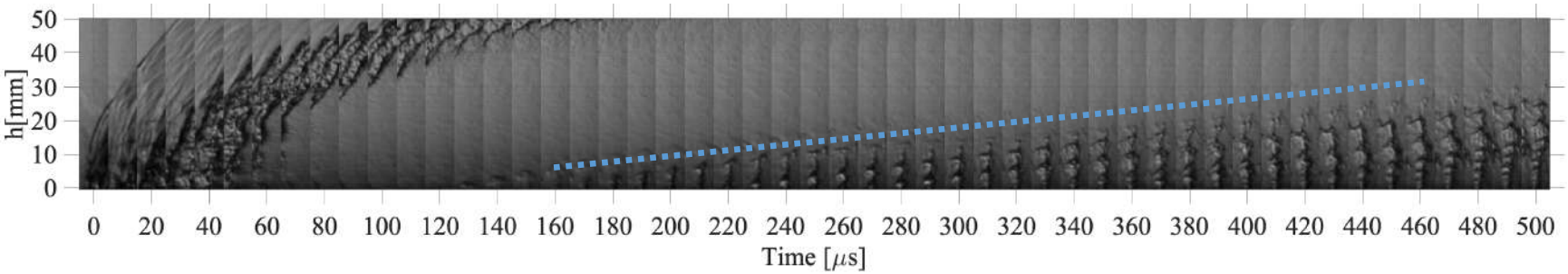

Figure 4.2.5 Composite images showing the onset and growth of the refresh jet from injector #1 following the wave passage for Case 2 from 0 to 500 μs

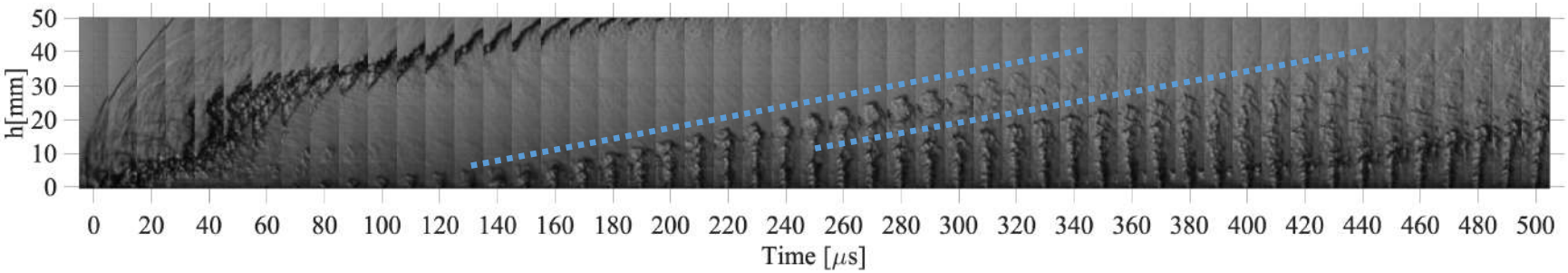

Figure 4.2.6 Composite images showing the onset and growth of the refresh jet from injector #1 following the wave passage for Case 3 from 0 to 500μs

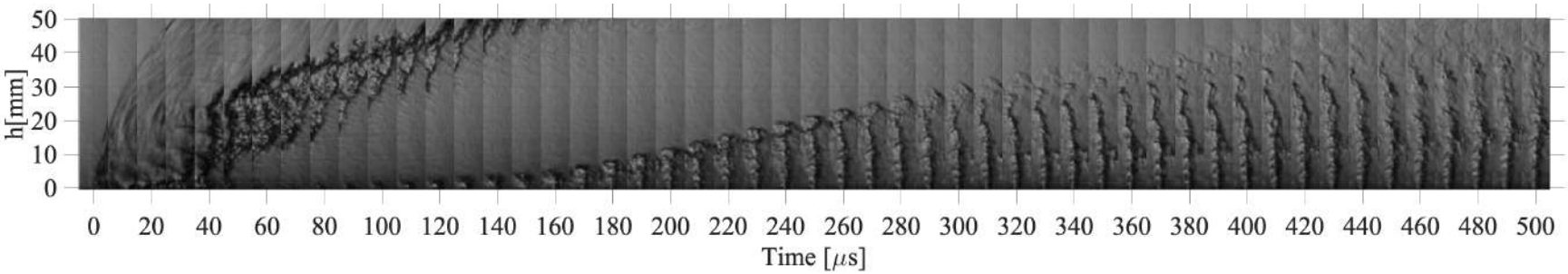

Figure 4.2.7 Composite images showing the onset and growth of the refresh jet from injector #1 following the wave passage for Case 4 from 0 to 500 μs

height data. From this, the x-intercept could be used to estimate the delay time of the refresh jet and the slope is used to obtain the refresh jet velocity.

The data for the growing refresh jets for Case 1 is deduced from the schlieren images and plotted in Figure 4.2.8. The refresh jet first appears after a delay time of about 130-150 μs, followed by the second refresh front at about 200 μs later from the first refresh. Delay times and initial velocity information for the first three injector jets are summarized in Table 4.2.1.

Table 4.2.1 Characteristic time delays and initial velocities of 1st and 2nd refresh jets for Case 1 condition

	1st Refresh Jet		2nd Refresh Jet	
	t_{delay} [μs]	V_1 [m/s]	t_{delay} [μs]	V_2 [m/s]
Injector #1	151.3	135.7	353.4	90.8
Injector #2	129.4	139.2	349.0	73.5
Injector #3	134.4	141.4	-	-
Average	138±9	139±3	351	82

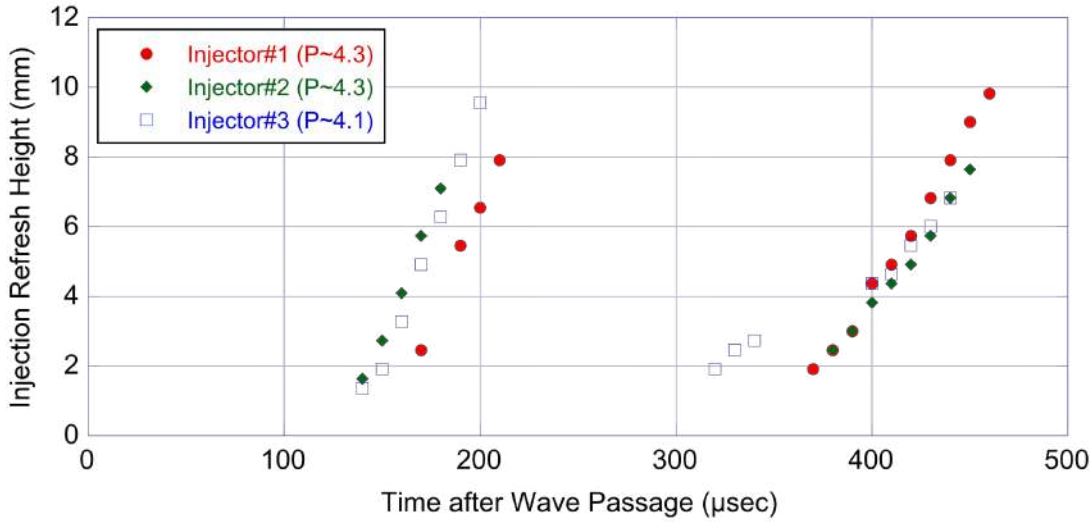

Figure 4.2.8 Growth of refresh jets for Case 1 condition

Figure 4.2.9 shows the growth of the refresh jets for Case 4. The refresh jet first appears after a time delay of about 80-150 μs. Interestingly, there seem to be two different velocities associated with refresh jet fronts. The first one appears to be a slower jet just overcoming the high pressure at the jet exit, while the second refresh with a faster velocity seems to be similar in characteristic with the other cases. The measured time delay data and the initial velocity data for the Case4 are reported in Table 4.2.2.

Table 4.2.2 Characteristic time delays and initial velocities of 1st and 2nd refresh jets for Case4 condition

	1st Refresh Jet		2nd Refresh Jet	
	t_{delay} [μs]	V_1 [m/s]	t_{delay} [μs]	V_2 [m/s]
Injector #1	80.9	63.2	143.7	188.3
Injector #2	74.8	57.0	146.5	186.1
Injector #3	96.2	88.0	148.5	207.9
Average	84±9	69±3	146±2	194±10

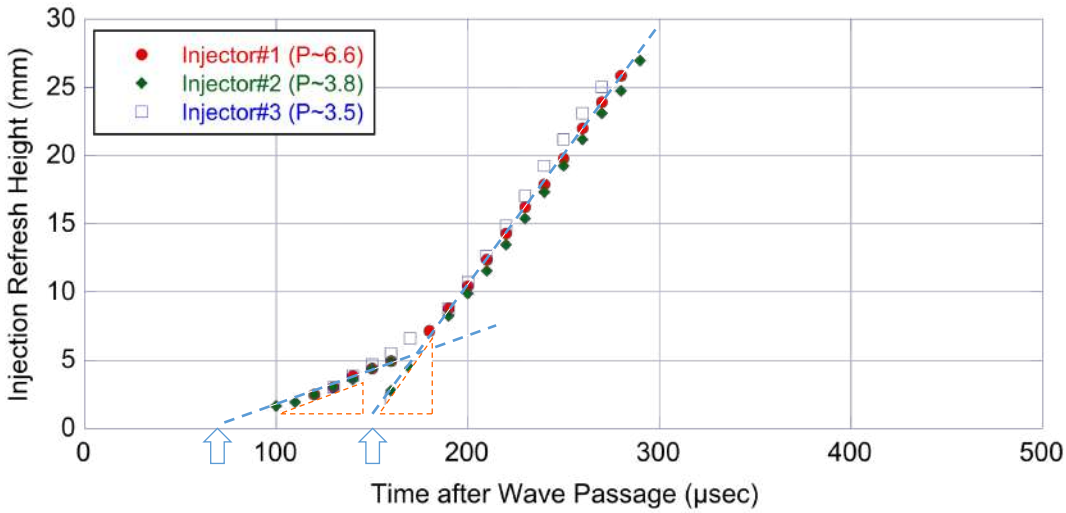

Figure 4.2.9 Growth of refresh jets for Case 4 conditions

For all the cases considered, there seems to be one common characteristic time delay around 140±10 μs. As the mass flow rate increases, however, the refresh jets may recover sooner if its stagnation pressure can overcome the combustor pressure. Such delay time depends on the average jet flow rate, which is related to its stagnation pressure. In other words, for a higher mass flow rate case, jet stagnation pressure can shorten the refresh time delay by overcoming the injector exit pressure.

4.3 Counter Propagating Waves

When rotating detonation engine operates, multiple waves appear inside the combustor. Frequently, counter-propagating waves are observed, and fundamental characteristics are not understood clearly. Here, using the advantage of accessible of clear observation of the detonation waves under confined condition like RDEs, collision of different types of detonation waves, detonation wave and decoupled shock-flame wave, were generated from modifying the experimental setup. This was done from 1) adding another pre-detonator and transition component at the other end of the eLMDE combustor, 2) varying the amount of spilled gaseous fuel and oxidizer from the connected pre-detonator, and 3) changing the gas that is injected inside the eLMDE combustor from ethylene gas and oxygen gas to surrogated reactant. From these modification, three different types of collision cases were able to simulate.

When ethylene gas and oxygen gas was injected inside the eLMDE combustor both detonation wave propagating from each side was able to survive from initial quenching. Second, changing the injected gas inside the eLMDE combustor to surrogate reactant, nitrogen gas, both side detonation waves were unable to be recover

Table 4.3.1 Wave speed properties before and after the collision

	Detonation wave vs Detonation wave	Decoupled shock-flame wave vs Decoupled shock-flame wave	Detonation wave vs Decoupled shock-flame wave
Approaching Wave Velocity (Left/Right) [m/s]	2100/2000	620/620	940/600
Approaching Wave Mach # (Left/Right)	6.4/6.2	1.9/1.9	2.9/1.8
Wave speed after collision (Left/Right) [m/s]	1200/1200	430/430	-/680
Wave Mach # after collision (Left/Right)	0.93/0.97	0.3/0.3	-/0.5

from the initial quench and generated collision of decoupled shock-flame waves. Last, varying the timing of both ethylene and oxygen gas valves from the first case, collision between detonation wave and decoupled shock-flame wave was established. Table 4.3.1 shows the wave speed properties before and after the collision.

4.3.1 Detonation wave vs. Detonation wave

Figure 4.3.1.1 shows the collision of two counter propagating detonation waves using schlieren method. Images were taken at 250 kHz and shows 21 injectors in the view field. Defining time 0μs when wave front of two waves are closest, it is clear that fully developed detonation wave is approaching toward each other at t=-4μs. Also, in the background space between two waves, reactant gas jet from the injectors are observed. Both waves still survive after collision and continues to propagate drifting apart. Assuming reactant gas that was injected was completely burnt after the

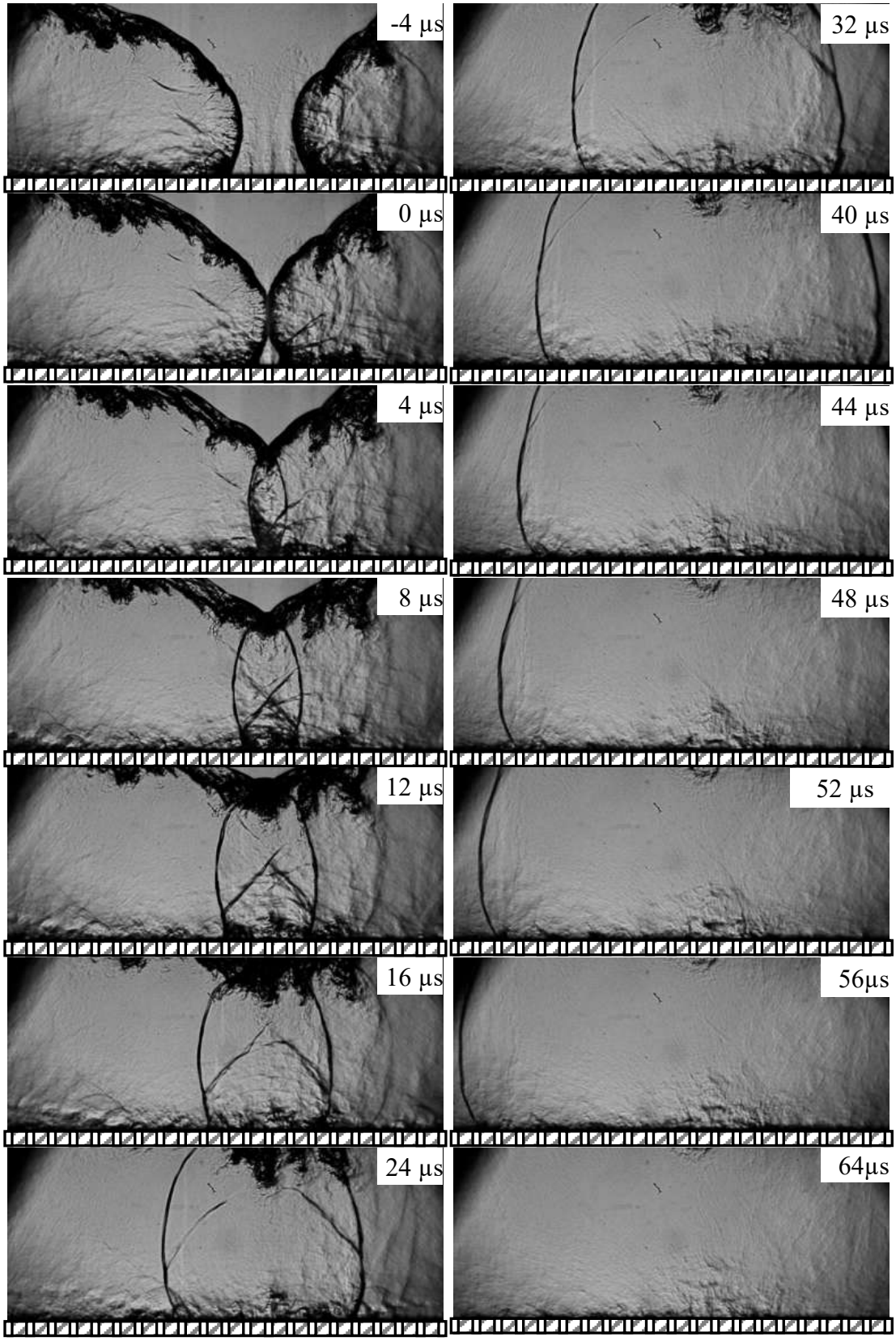

Figure 4.3.1 Sequence of before and after collision between detonation waves

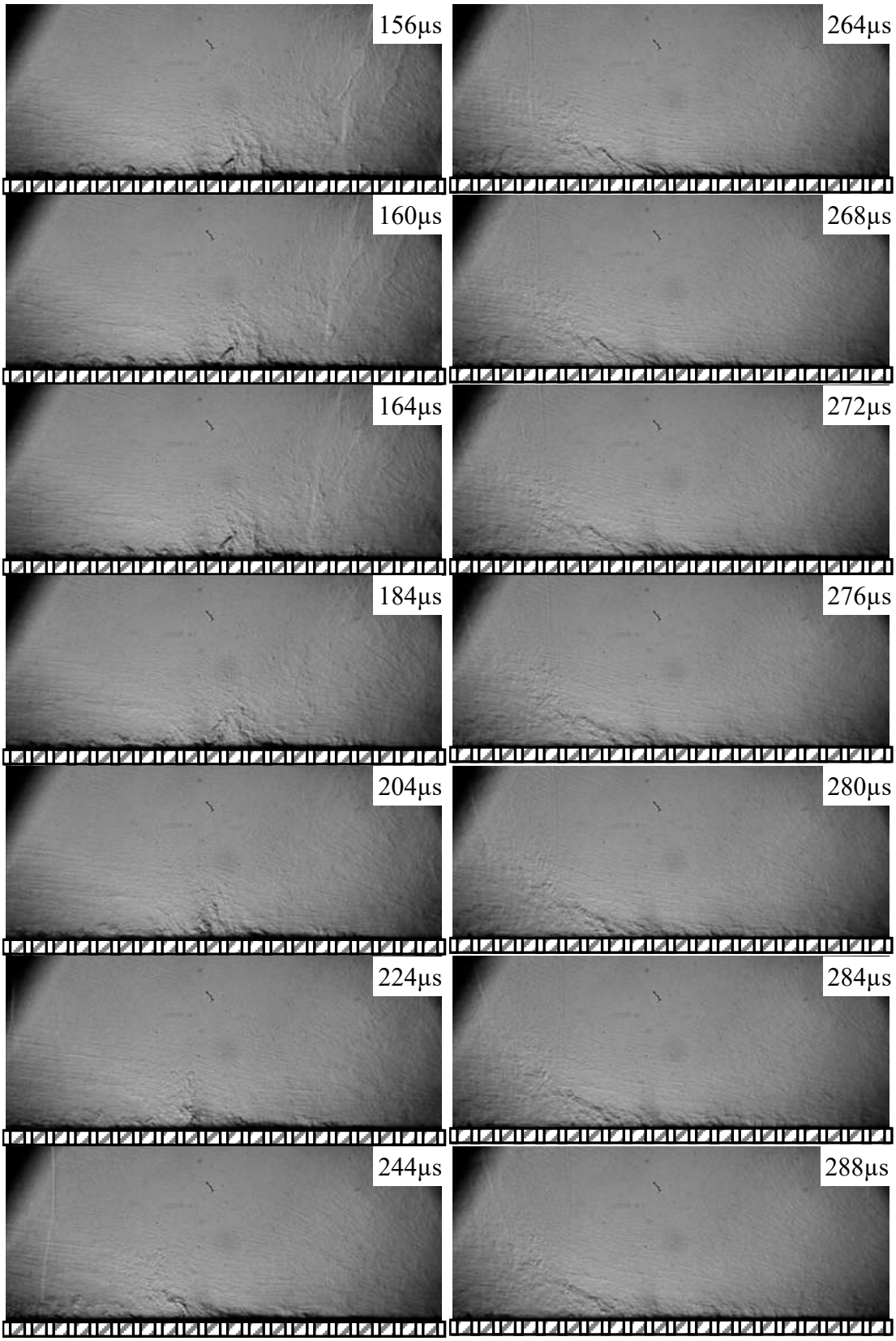

Figure 4.3.2 Sequence of flowfield change and refresh jet after collision

detonation wave, waves after the collision would meet hot product of detonation waves with no reactant to combust. After 8μs from collision, it shows that some structure of shock wave is attached to the propagating wave front. In addition to this, reflected shocks generated from the injector opening are observed. When tracking the reflected shock created from left to right running detonation wave at the left bottom corner, reflected shocks meet with the wave after collision approaching from right around 20μs. At 24μs, wave front of the right to left running wave meet the reflected shock from the injector. The reflected shock is still observed and appears from the injector one after the another. No refresh jet from the injector are observed, which may imply pressure field after the collision is sufficiently high that injection cannot `occur. However, it is not certain in this case suspecting insufficient mass flow from the injector. It is uncertain due to nature of eLMDE's injecting method. 8 injectors are connected to small reservoir that doesn't guarantee sufficient back pressure once it is opened initially. Tracking the propagating wave front of sequence of images obtained from the high-speed camera as shown in Figure4.3.1.1, speed of wave propagating before and after the collision is estimated and is shown in the Figure 4.3.2.1. Figure shows the wave speed at the distance from the collision occurred. Here RR represents right running, meaning wave is propagating from left to right. Wave speed was estimated from tracking the wave front at three different heights. It shows that both right running and left running wave does not show much difference in terms of height, which indicates that even though wave is not straight it is propagating evenly. Both right running and left running waves are approaching at similar speed and speed reduces rapidly after the

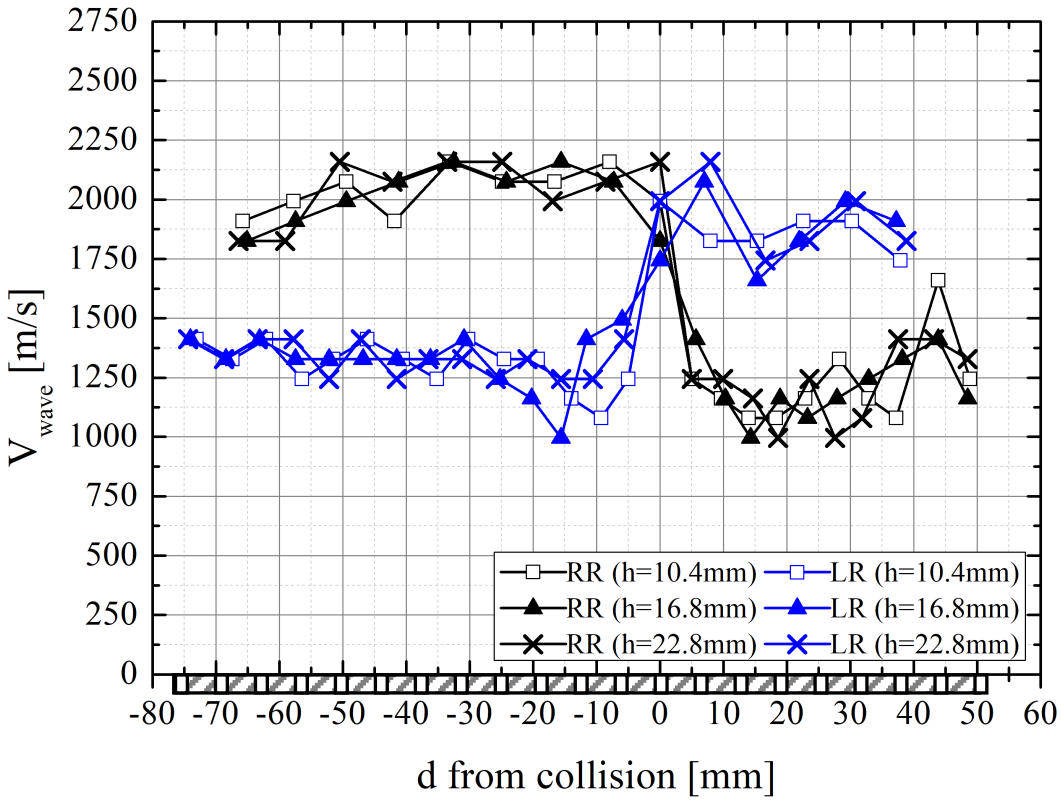

Figure 4.3.3 Velocity of right running (RR) and left running (LR) wave along the channel of eLMDE, showing distance with respect to the collision location

collision. Although the speed drops quickly, both waves propagate apart remaining at similar wave speed.

4.3.2 Decoupled shock-flame wave vs. Decoupled shock-flame wave

Decoupled shock-flame wave is decoupled detonation wave which shock and flame front detaches. This happens when there is not enough detonable mixture in the reactant so the reaction behind the shock wave could not support the wave to propagate. Thus, in order to create this condition, surrogate reactant, nitrogen gas, was injected thru the eLMDE injectors instead of reactant mixture.

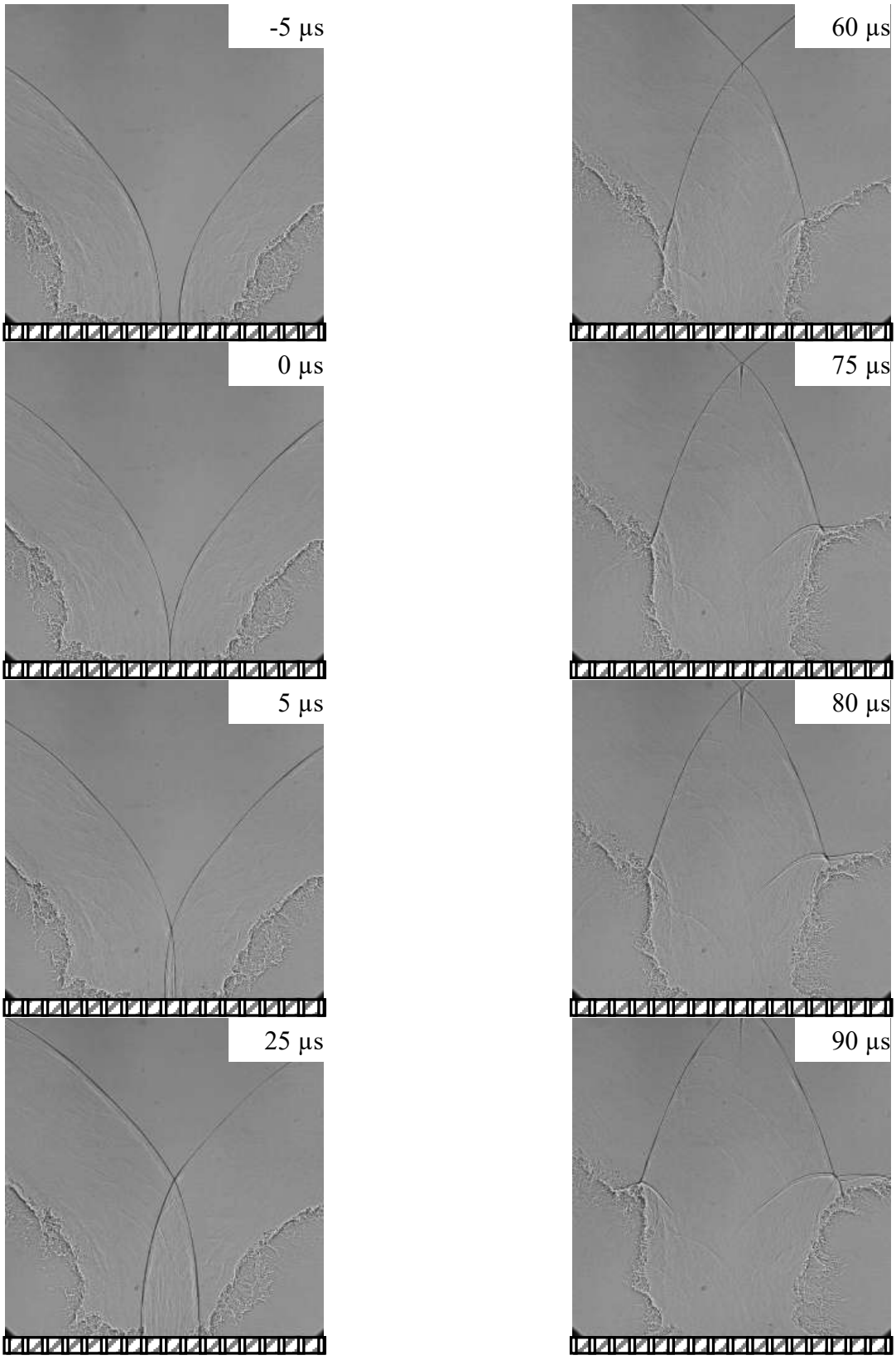

Figure 4.3.4 Sequence of collision between decoupled shock-flame waves-1

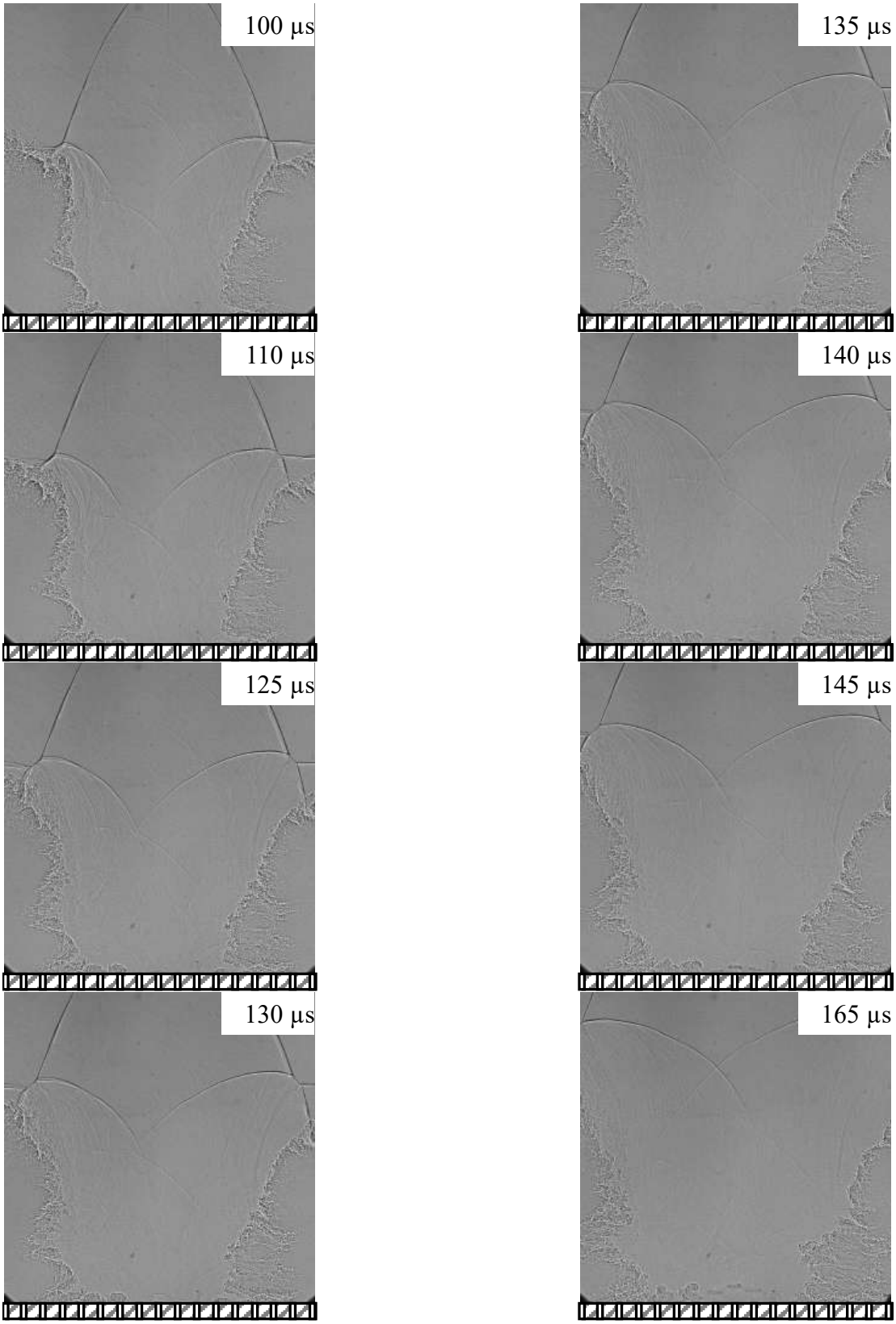

Figure 4.3.5 Sequence of collision between decoupled shock-flame waves-2

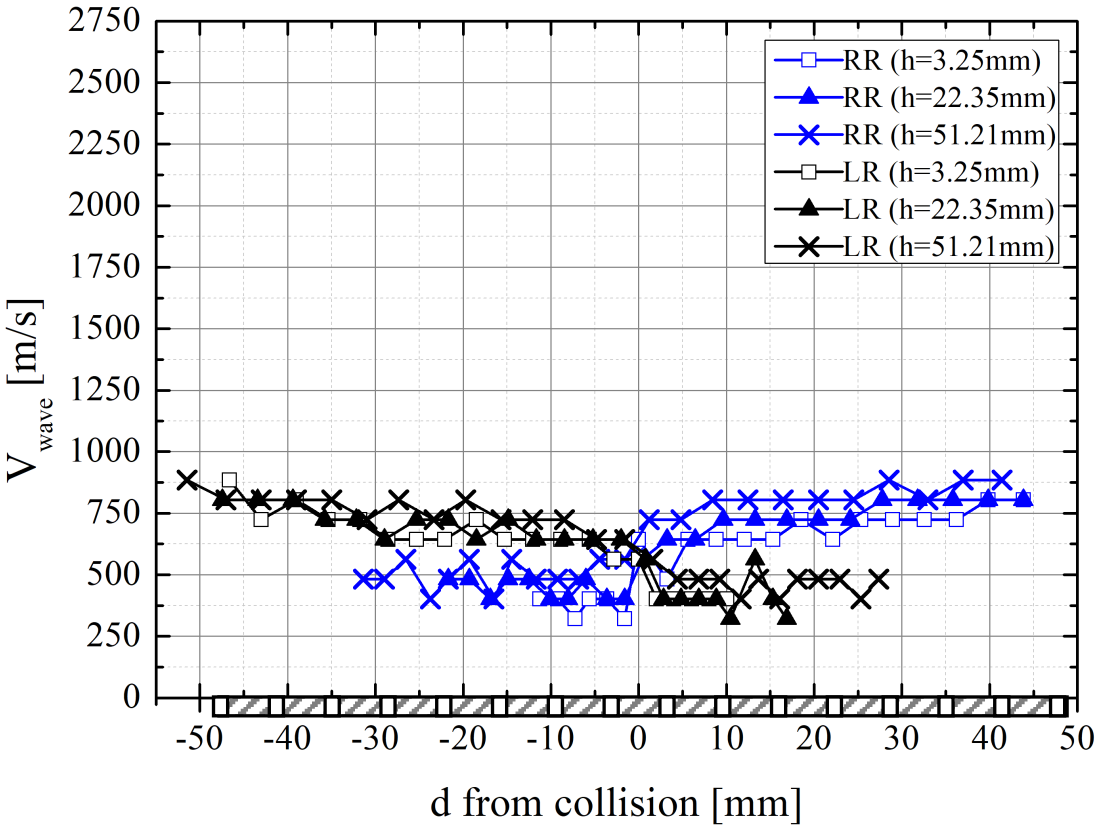

Figure 4.3.6 Velocity of right running (RR) and left running (LR) wave along the channel of eLMDE, showing distance with respect to the collision location

In Figure 4.3.2.1 and 4.3.2.2, t=0 μs is defined when two waves collide each other. Here, surrogate gas is shocked after the shock front and before the flame front. After collision, overlapped region is shocked again from the wave propagating toward it. By tracking the location of the wave front for each sequence of images, wave speed from the stationary reference frame is obtained along the eLMDE channel as shown in the Figure 4.3.2.3. Wave speed is plotted at relative distance from where the collision occurred. Wave was approaching relatively similar speed and after the collision both waves have survived from it and continue to propagate in the same direction it traveled before the collision.

After the collision, each wave encounters the flame front coming toward it. The flame front seems to elevate the temperature and change the flow to be subsonic. There are three interesting points to point out. 1) upper middle along the interaction points 2) interaction between flame front and right running or left running wave 3) location of where the first refresh jet appeared.

First point shows the development of Mach stem from the two shock wave meet at an angle from t=60μs. At t = 80μs, it clearly shows the Mach stem has grown and is propagating outside the view field.

Left and right running waves meet the flame front heading its way and the reflected shock from the flame front seems to interact with the incident shock. Irregular reflection from the flame front causes Mach stem which could be confirmed when t=60-90μs for right running wave and t=80-100μs for left running wave, respectively. After the Mach stem is developed it follows along the flame front.

Last, looking at adjacent injector where the wave collision happens at t=130μs, bow shock appears from the injector. From t=135μs image, material interface appears following the bow shock. This is likely the refresh jet that was suppressed from the wave. Observing the images at t=145 and 165μs, refresh jet seems to develop faster at the injector closer to the wave collision. This may imply that even though the wave collision created higher pressure, the waves that pass through may have suppressed the injector again which led the adjacent injector from the collision to face quicker pressure decay and faster refresh jet.

4.3.3 Detonation wave vs. Decoupled shock-flame wave

In this case, right running detonation wave collide with the left running decoupled shock-flame wave. t=0μs was defined similarly as previous cases. Before the impact, t=-4μs, right running wave is clearly decoupled and shock front and flame is detached sufficiently. On the other hand, the left running detonation wave starts to detach leaving only product after the wave passage. From t=0μs to t=20μs, detonation wave seems to relatively holding its position but right running shock front is passing through the detonation wave and shock wave is propagating right running.

Since the flame front of the right running wave is detached enough from the shock front, it is clear that compressed reactant exists between the shock and flame front. At t=24μs, reactant is sufficiently compressed from both left and right running waves and temperature is elevated enough to cause a re-ignition. Bright location is where the re-ignition occurred. This is clearly a deflagration to detonation transition (DDT). This is a good example of how counter propagating waves could be created inside the RDE combustor. It shows that the stronger left running detonation is now turned into right running wave. Additionally, in this case because the right running detonation wave left no reactant after the passage, re-ignited wave could not sustain to be detonation wave, but if there was detonable reactant in its passage, counter propagating detonation wave could have occurred. Assuming this was inside the actual RDE combustor, this could imply that right running shock wave could cause another DDT if it encounters the similar situation, which would again change the direction of the wave and the RDE combustor would be operating in a so-called slapping mode.

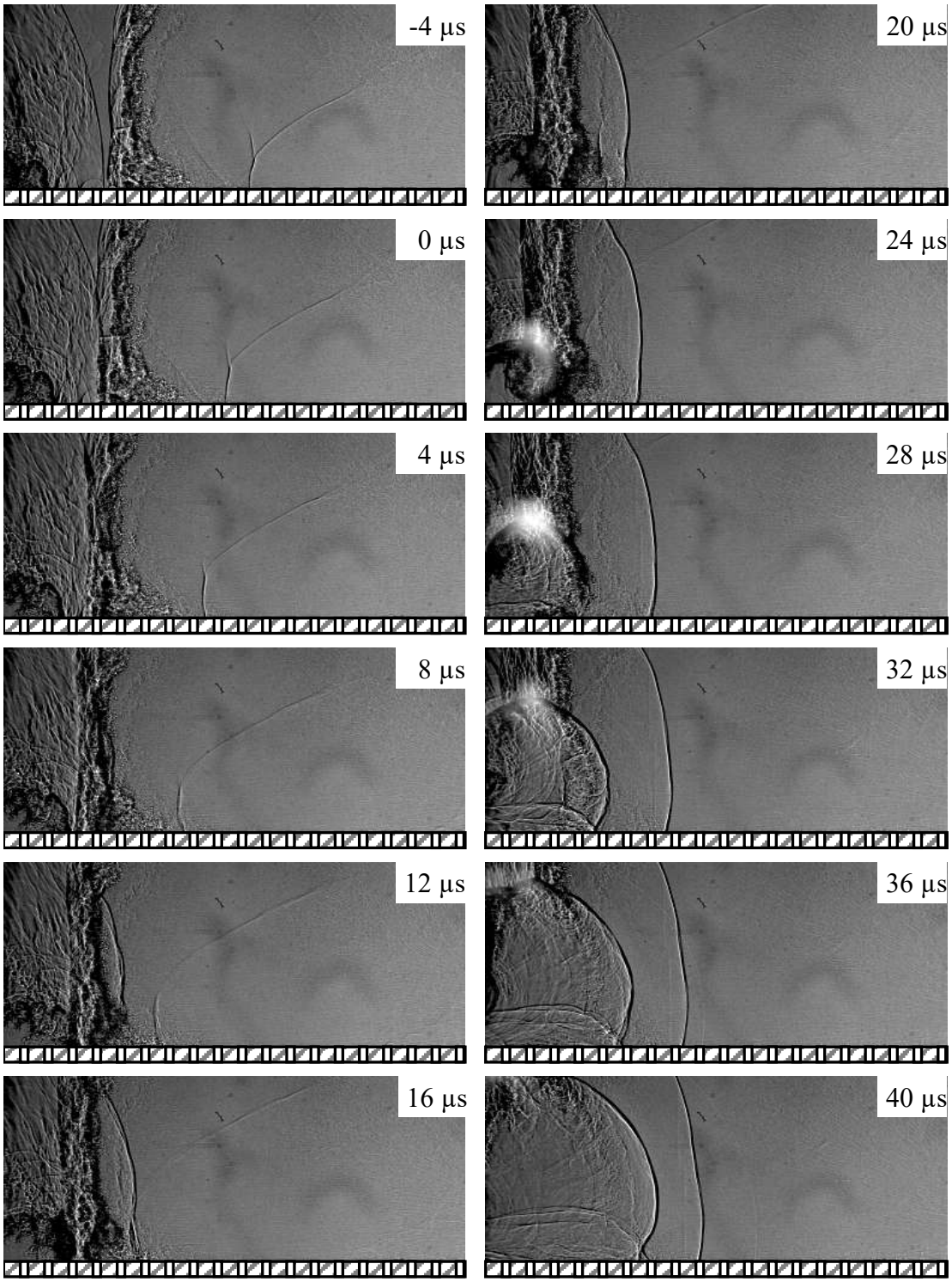

Figure 4.3.7 Sequence of collision between detonation wave and decoupled shock-flame wave

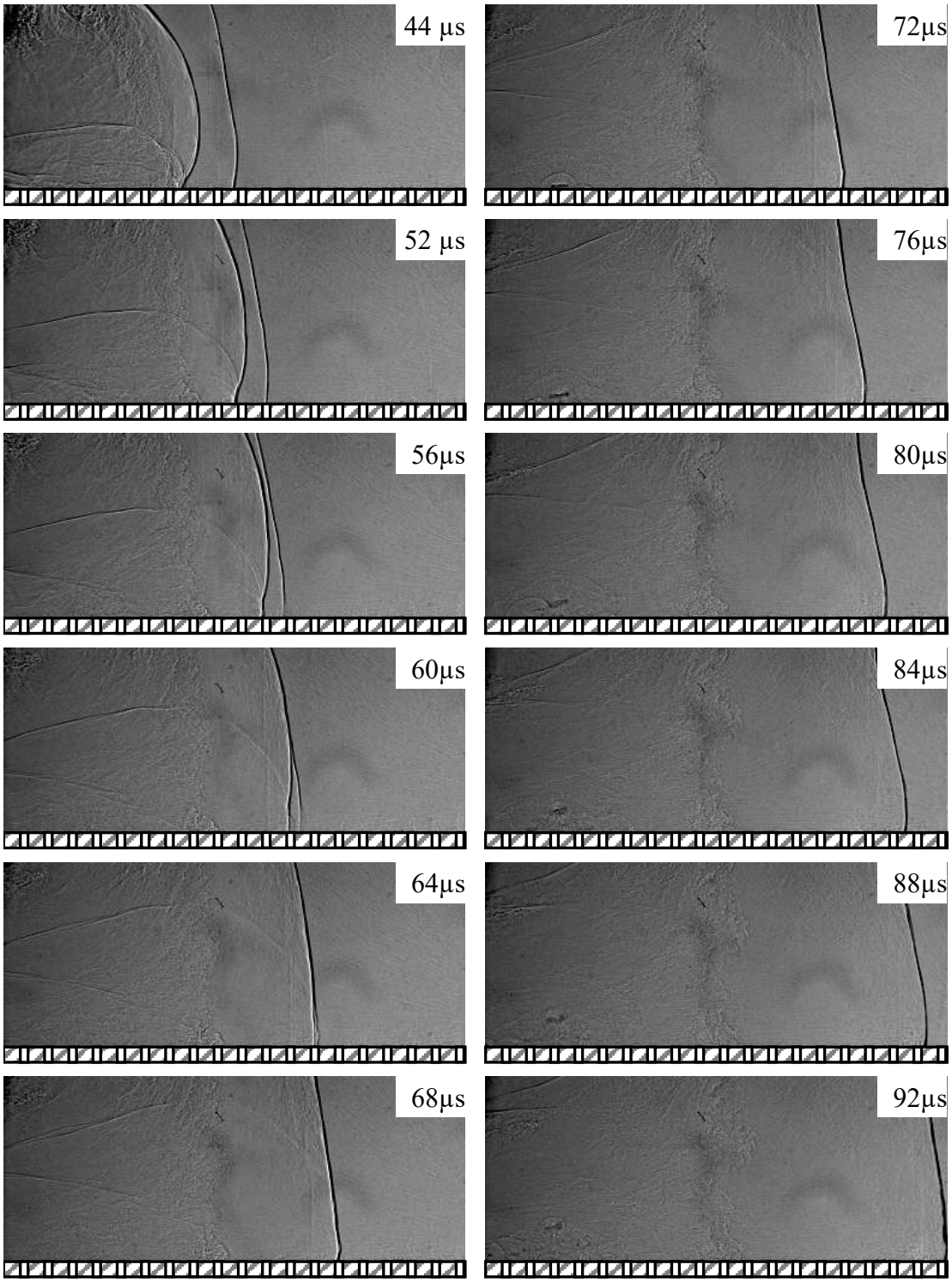

Figure 4.3.8 Sequence of re-ignited wave catching up right running wave after collision

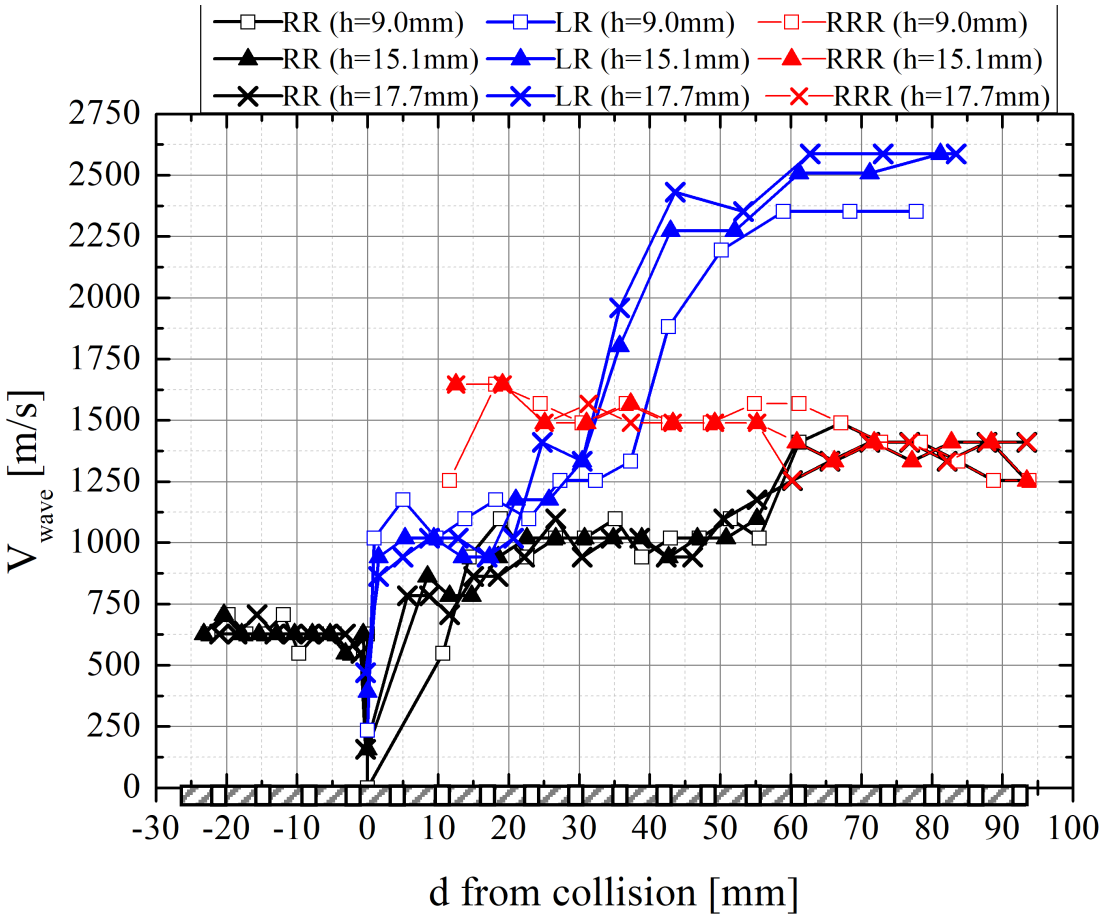

Figure 4.3.9 Velocity of right running (RR) and left running (LR) wave along the channel of eLMDE, showing distance with respect to the collision location

It is not clear what kind of wave would propagate left running, but the images from t=32μs show that the re-ignited wave starts to catch up the initial right running shock wave after the collision. Figure 4.3.3.3 shows the wave velocity from the stationary observer reference frame. After the collision, right running wave have increased its wave speed and eventually overlaps with the re-ignited right running (RRR) wave.

Another interesting point could be observed from the injector when t=72μs. A bow shock created from the injector exit appears and the refresh jet continues to grow. Adjacent injector from the left running and right running wave is 4th injector from the

left. However, the injector that shows the refresh jet is 3rd injector. Going back to the Figure 4.3.3.1 when t=24μs, adjacent injector to the re-ignition is 3rd injector. It is not clear since the injector reservoir are connected, but it is a reasonable explanation since the re-ignition created detonation wave for a while.

4.4 Refresh Jet from Counter Propagating Waves

Figure 4.4.1 shows the pressure-time traces associated with the counter-propagating two-wave cases. Similar to the single-wave cases, the pressure amplitude is higher without the refresh jets than with the jets. Figure 4.4.1(a) shows that the right-running wave enters the injector area of interest earlier than the left-running wave. Also, it can be deduced that the right-running wave is faster than the left-running wave. Finally, at x2, both waves have collided, and the amplitude reaches the highest value around t=40μs.

Visualization images in Figure 4.4.2 could be used to help better understand the interaction process shown in Figure 4.4.1. In the first phase, two detonation waves approach from each respective side and collide around injector #5. Since there is no reactant being injected, the waves quench over the jet flowfield and become blast waves. Then the strength of each wave decreases as it propagates further away. Nevertheless, the collision of the two waves in this case sets up a higher pressure jump initially over the affected injector exit. Other injectors face two smaller pressure peaks with the waves arriving successively but propagating in the opposite direction. They cause even slower recovery than the injector over which the waves have collided.

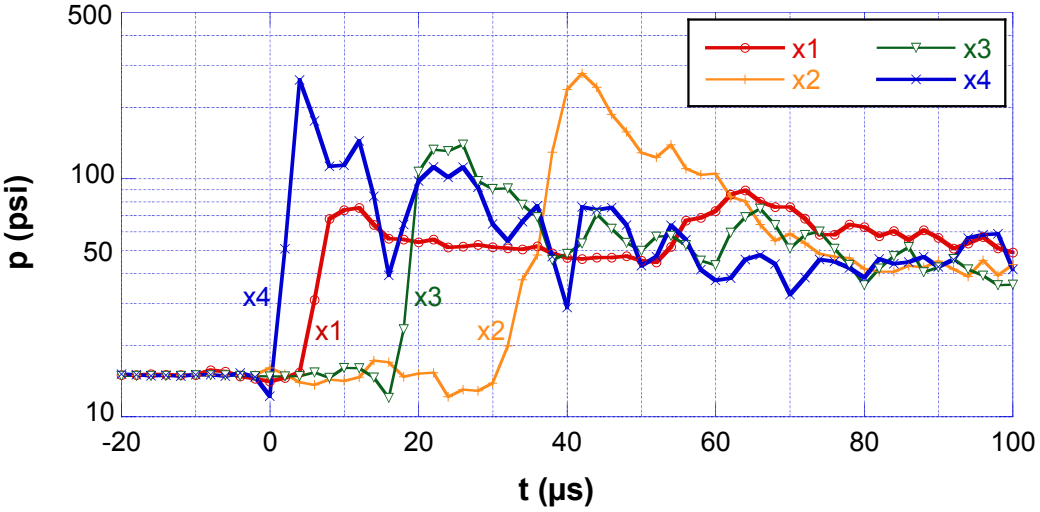

(a)

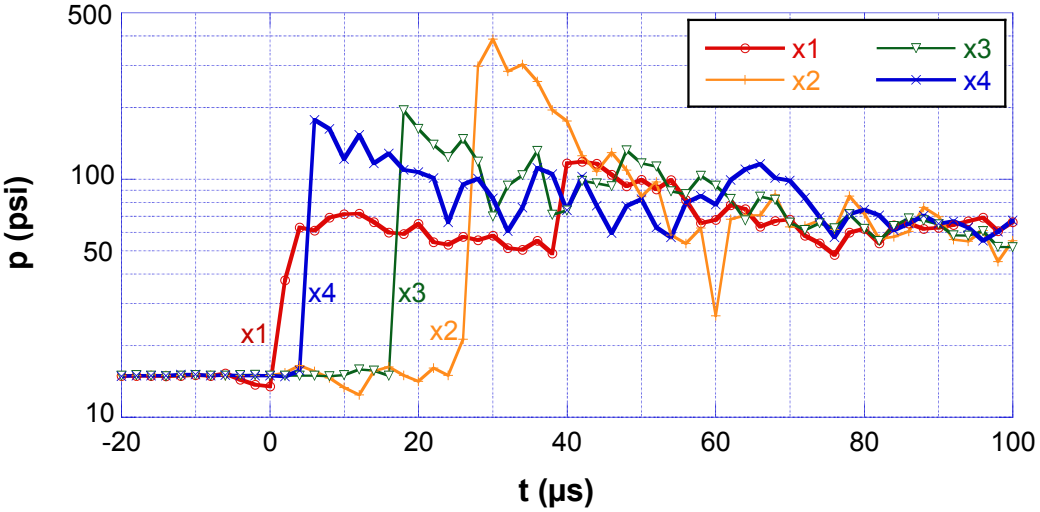

(b)

Figure 4.4.1 Pressure measurements for two-wave cases (a) with and (b) without the refresh jets

In the second phase, each wave interacts with the products, and weak waves pass by each other. This behavior was also observed in Figure 4.4.1. Following the intersection of the two waves after the collision, it could be seen in Figure 4.4.2 that a Mach stem was generated from the crossing point.

Figure 4.4.3 shows the injector refresh behavior following the wave collision. Figure 4.4.3(a) shows the first refresh that occurs after about 350 μs from the time of wave collision. This time delay is much longer than the single wave cases, in which a similar mass flow rate was injected into the combustor (Case 1). Also, each injector response is different since they were exposed to a different pressure field following various patterns of the two wave passages, depending on the location of the injector. For the single-wave cases, the refresh patterns from a bank of adjacent injectors are quite similar. The refresh jets line up monotonically following the wave passage direction. For the cases involving counter-propagating waves, However, the refresh jet closest to the collision location recovered more quickly than the refresh jets from other injectors away from the collision point.

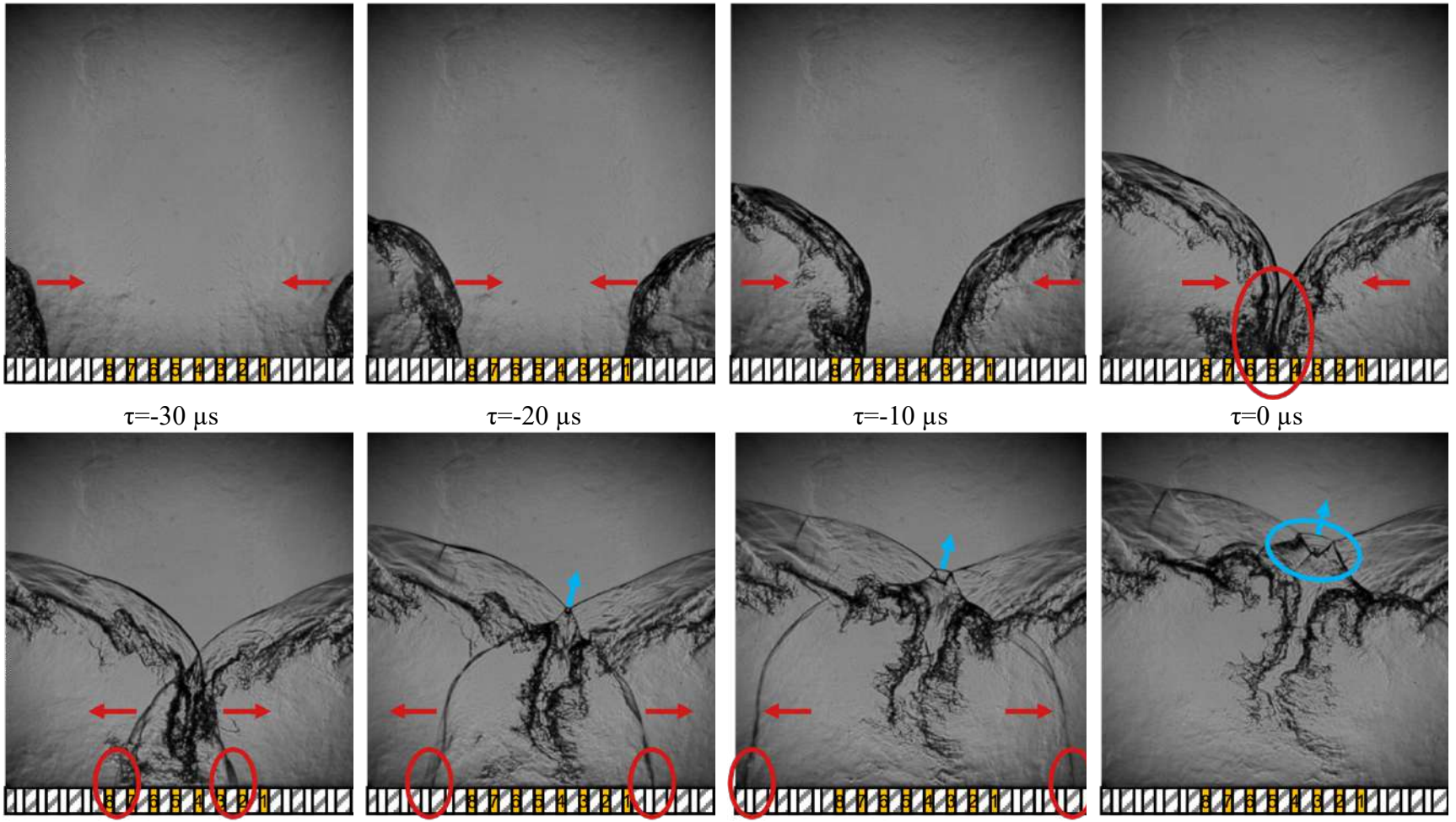

Figure 4.4.2 Sequence of images showing two counter-propagating waves colliding over the injectors. (a) before the wave collision, and (b) after the wave collision

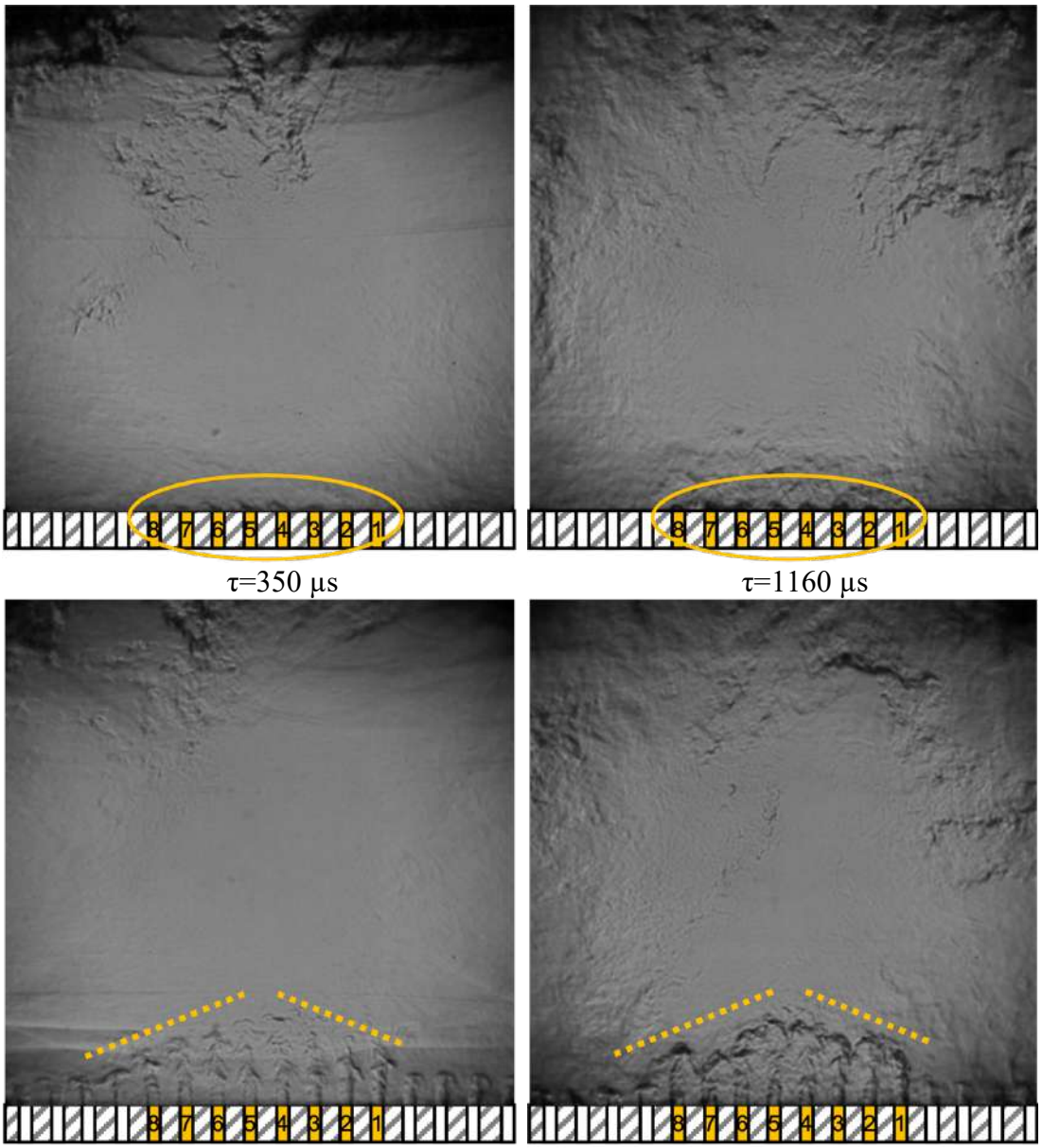

Figure 4.4.3 Injector refresh after wave collision. (a) first refresh after 350 μs, and (b) second refresh after 1160 μs

Chapter 5: Detonation Wave-Fuel Droplet Breakup in Unwrapped RDE Combustor

5.1 Test Conditions

In the previous study, the linear model detonation engine (eLMDE) [14,72,83,84] was designed to simulate the RDE combustor that is unwrapped in a linear direction. Figure 5.1.1 illustrates three typical types of detonation waves observed in the eLMDE when reactant is injected from the injector below and wave is propagating left to right. Figure 5.1.1(a) shows the detonation wave propagating in the region of Mach number 6.7-7.8 and consists of a gradually inclined detonation wave in the front and an oblique shock following. Figure 5.1.1(b) illustrates the weakly-coupled wave propagating in the region of Mach number 3.4-3.8 and consists of a deflagration zone behind the wave. Finally, in Figure 5.1.1(c) the decoupled shock-flame wave, leading shock wave propagates at a Mach number of 2.5-2.7, followed by the flame front. In present work, these three different types of detonation waves were chosen to understand the interaction between the detonation wave and liquid fuel droplet.

A schematic drawing of the detonation channel Is shown In Figure5.1.2. As Fig 5.1.2 indicates, bottom injector was removed and replaced with smooth surface. Thus, ethylene-oxygen gas filled from a pre-detonator is the main source of the reactant that sustains the detonation wave. The equivalence ratio of ethylene and oxygen gas that was injected from the pre-detonator was stoichiometry and expected to get partially mixed as it gets pushed in to the eLMDE channel. In order to repeatably generate three different types of detonation waves, injection timing of ethylene and oxygen gas was

precisely controlled at the pre-detonator, which led to controlled amount of reactant gas spilled inside the eLMDE. Specific information of Mach number and velocity of three types of waves are listed in Table 5.1.1. The uncertainty is based on the statistical dispersion.

The liquid droplet is suspended inside the eLMDE channel, as shown in Figure 5.1.2. A thin stainless steel dispensing needle is located 4.25" (d) downstream of the entrance and 0.75" (h_2) above the bottom surface. Various size of needle was used to generate different size of droplet. The droplet diameter is measured for each test using the calibrated visualization images and is listed in the Table 5.1.2. In this paper, dispensing needle has ID of 0.006" and OD of 0.012" and consist of blunt end. 1*ml* syringe is connect to the dispensing needle and located outside of the detonation channel. Location of the liquid droplet was chosen far downstream from the channel entrance for a detonation wave to develop from the inlet of the eLMDE. As indicated in the Table 5.1.2, Ethanol, JP-8, and water was used for the liquid fuel.

Two planar quartz windows allow to image the flowfield inside the channel. High-speed shadowgraph and schlieren visualization are taken by Phantom v2512. In addition, chemiluminescence and luminescence images were taken to verify the reaction after the wave collides the liquid droplet. Two different frame rates are used to capture a different aspect of the breakup process. A faster frame rate, 500 *kHz*, is used to capture the initial breakup of the liquid droplet; meanwhile, a slower frame rate, 200 *kHz*, is used to observe the end process of vaporization.

For pressure measurement, one of the planar quartz windows is replaced with a metal window that has four slots for high frequency pressure sensors (PCB 113B24)

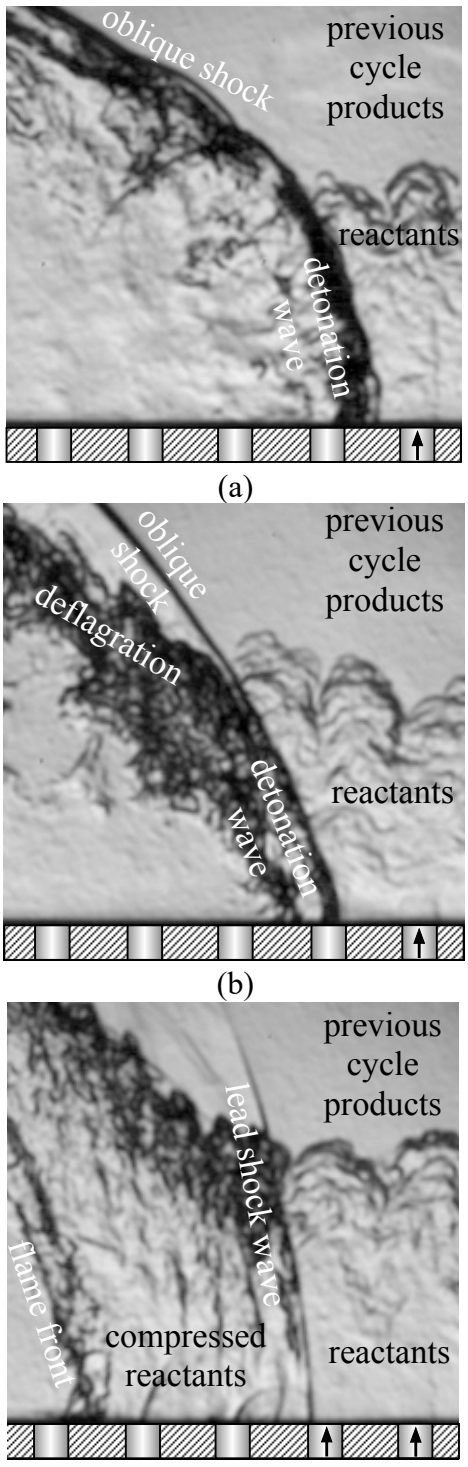

Figure 5.1.1 Types of detonation waves observed in a model RDE combustor using C2H4-O2 reactants. (a) detonation wave propagating at 2.2 *km/s*, (b) weakly-couple detonation wave at *1.0 km/s*, and (c) decoupled lead shock wave at 690 *m/s* [14,72]

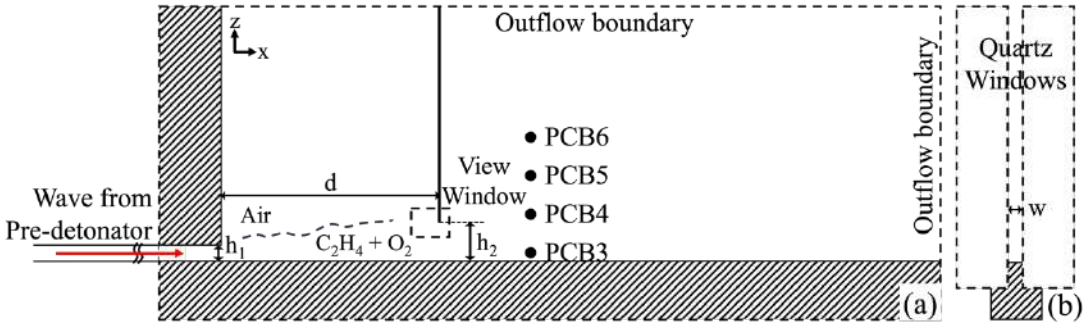

Figure 5.1.2 Schematic drawing of experimental setup

Table 5.1.1 Flow conditions for fuel droplet in wave experiments

Fuel Droplet-in-Detonation Wave Test Cases	Reactant gas	Velocity of Approaching Wave [m/s]	Mach No. of Approaching Wave
Detonation Wave	$C_2H_4 + O_2$	2168 ± 160	7.3 ± 0.5
Weakly-Coupled Wave	$C_2H_4 + O_2$	1165 ± 70	3.6 ± 0.2
Decoupled Shock-Flame wave	$C_2H_4 + O_2$	877 ± 30	2.6 ± 0.1

Table 5.1.2 Droplet information

Droplet diameter [*mm*]	Type of liquid fuel
1.7 – 2.1 ± 0.1	Ethanol, JP-8, Water

which were used to record at 500 *kHz*. Figure 5.1.2 shows four dynamic pressure measurements positioned in vertical array relative to where liquid droplet located z = -0.625”, 0.125”, 0.875”, and 1.626”, respectively. Individual tests are conducted to characterize the wave profile near the liquid droplet by positioning the liquid droplet relative to the PCB at x = -1.75”, -1”, and 0”. Figure 5.1.3 shows pressure measurement of vertical array of detonation wave and decoupled shock-flame wave. The pressure measurement shows that the pressure rise is roughly about two times of the decoupled

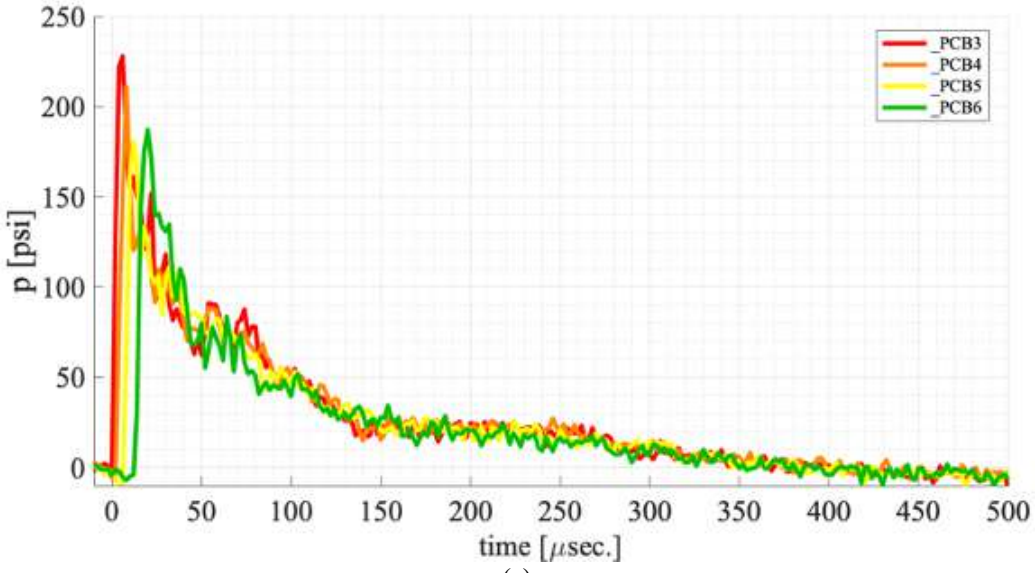

(a)

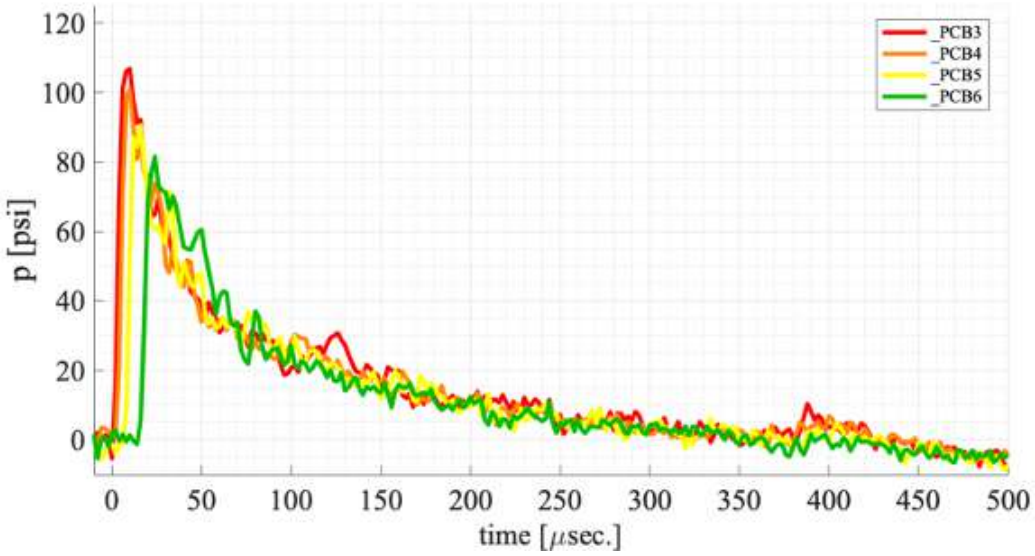

(b)

Figure 5.1.3 Pressure measurement of (a) detonation wave and (b) decoupled shock-flame wave

shock-flame wave for detonation wave and as the wave passes by pressure decays.

Furthermore, dynamic pressure was measured with and without the liquid droplet suspended inside the eLMDE combustor to verify the effect from the existence of the droplet. Figure 5.1.4 shows the average pressure measurement from multiple

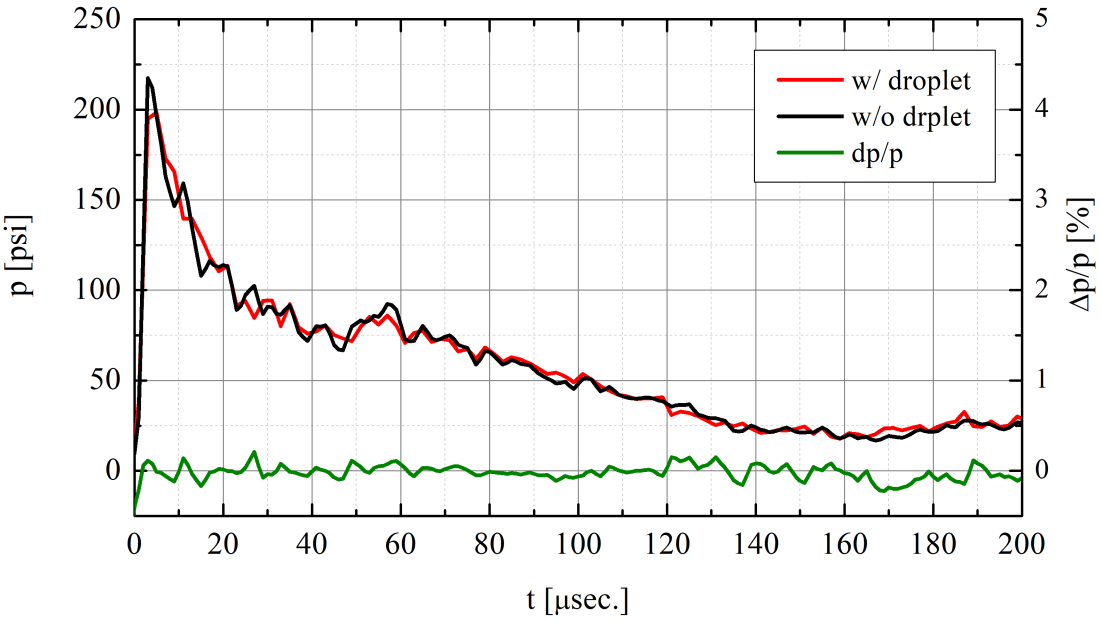

Figure 5.1.4 Average dynamic pressure of detonation wave with an without liquid fuel droplet

tests. The plot shows the dynamic pressure measured at the closest location from the liquid droplet (z=0.125”). It shows that existence of the droplet has no significant effect on the pressure rise from the detonation wave passage from the appearance of the liquid droplet.

5.2 Ethanol Droplet Breakup from Detonation Wave

In the time-sequenced images of Figure 5.2.1, a detonation wave propagates from left to right through a layer of well-mixed ethylene-oxygen mixture and an ethanol droplet is suspended in the wave propagation path. High-speed shadowgraph images are captured at every 2μs interval, with the reference time of t=0 μs denoting the instant when the detonation wave reaches the fuel droplet. The wave speed in the horizontal direction (x-axis) was measured to be 2.2km/s at this point. Initial deformation of the

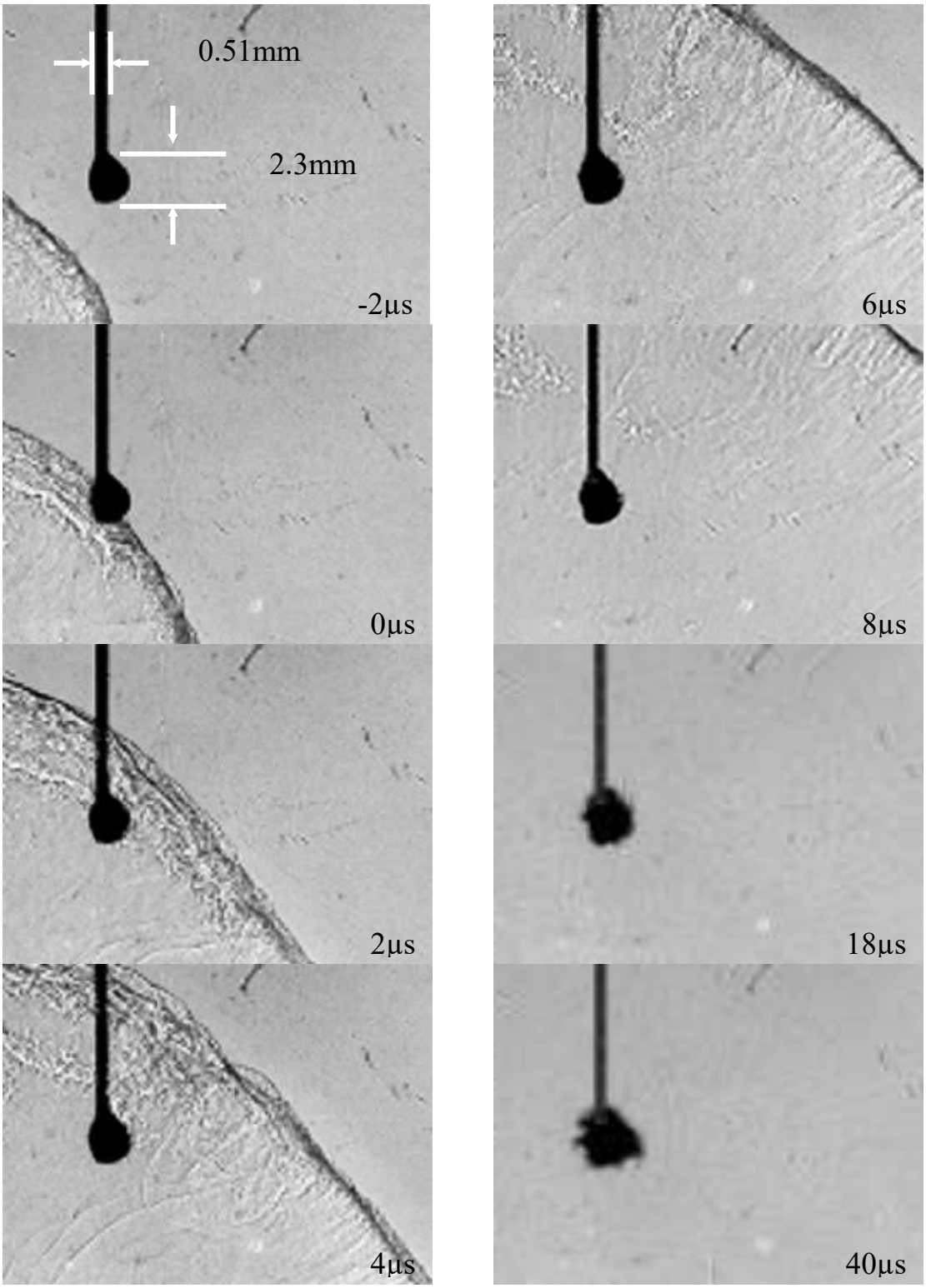

Figure 5.2.1 C_2H_4-O_2 detonation wave propagating over a suspended ethanol droplet

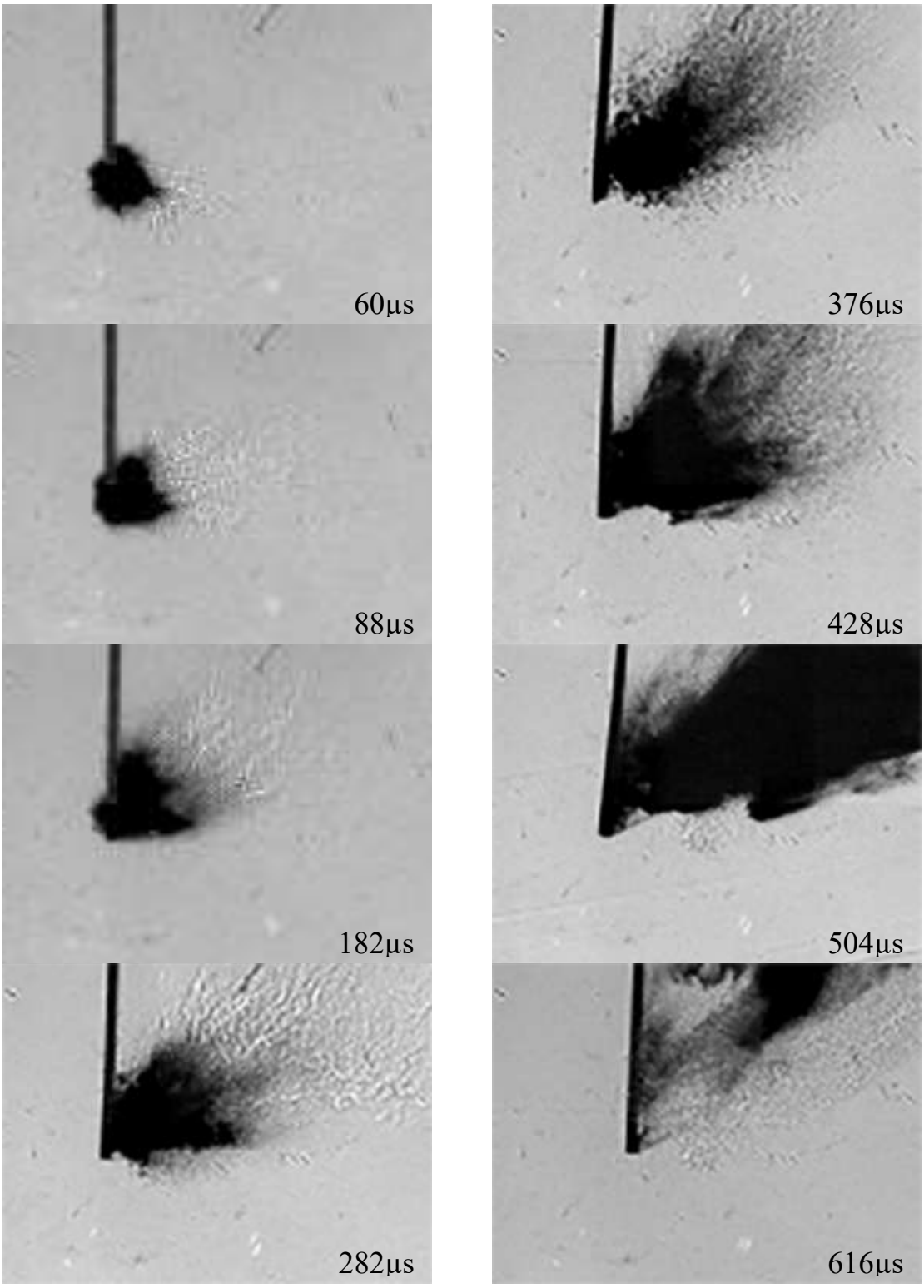

Figure 5.2.2 C_2H_4-O_2 detonation wave propagating over a suspended ethanol droplet

fuel droplet is observed after t=6μs. At t=8 μs, wavy structure starts to develop on the surface of the droplet. Wavy structure grows as time evolve as shown in t=18μs. After t=40μs droplet deforms significantly and starts to show some atomization on the surface of the droplet. At t=60μs, wavy structure starts to disappear, and liquid droplet starts to spread out. Sign of atomization starts from the surface and starts to spread downstream. Significant breakups and ligaments are observed at around t=88μs as the vaporizing streaks convect downstream in the wake of the droplet by the wave-induced flowfield. Beyond t=182μs, many fragments of scattered droplet clusters continue to spread out. At around t=428μs, the fuel becomes atomized almost completely, and at around t=500μs, it turns into a cloud-like structure suggesting high-level of vaporization. Darkened area increases as the cloud scattering develops and then quickly fades away. It should be noted here that the detonation wave-induced flow speed around the droplet should rapidly decrease over time as the wave propagates away from the droplet.

5.3 Ethanol Droplet Breakup from Weakly-coupled Detonation Wave

Weakly-coupled detonation wave, which was defined as wave speed slower than detonation wave and consists of deflagration zone behind from previous chapter, was examined to observe the interaction between the wave and the ethanol droplet. Figure 5.3.1 shows the time sequence of ethanol droplet breakup from the weakly-coupled detonation wave. Since weakly-coupled detonation wave is detached from the following flame front, shock wave encounters the liquid droplet first. t=0μs is defined when the shock wave collides the liquid droplet surface. As soon as shock wave pass

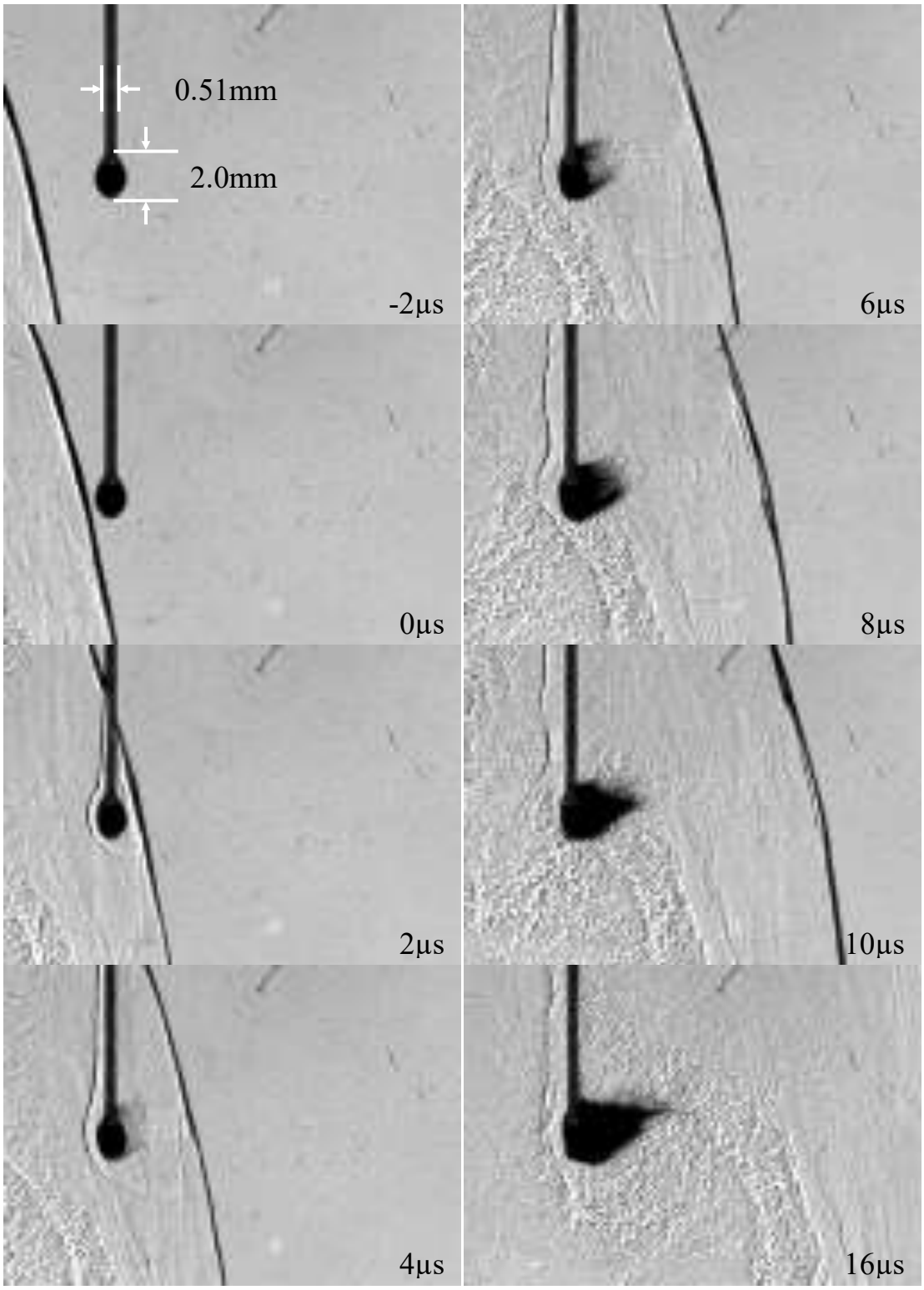

Figure 5.3.1 C_2H_4-O_2 Weakly-detonation wave propagating over a suspended ethanol droplet

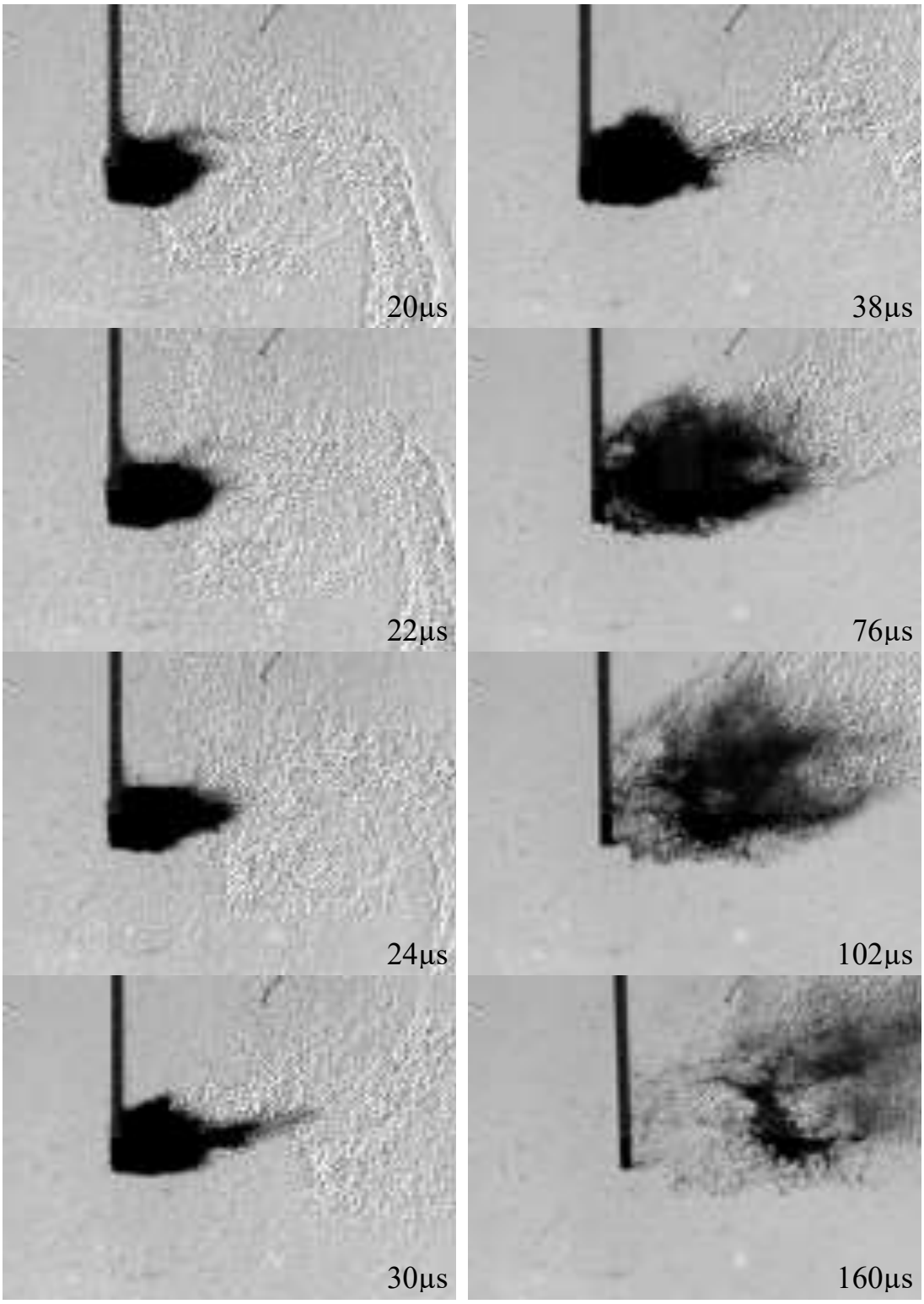

Figure 5.3.2 C_2H_4-O_2 Weakly-detonation wave propagating over a suspended ethanol droplet

through the liquid droplet at t=2μs, a bow shock is created in front of the liquid droplet. At the next time step, t=4μs, streaks from the liquid droplet surface are observed, which implies initial breakup of a liquid droplet. This is significantly earlier than the initial breakup from the detonation wave. Also, the breakup process seems to show different trend from the detonation wave case. Strips of liquid droplet spread out along downstream until t=10μs. At t=6μs, flame front arrives, and the bow shock starts to disappear as the flame front propagate downstream. As the flame front pass though the liquid droplet, the breakup shape starts to change. Strips disappeared and started to spread out wider. After the flame front propagation, liquid droplet shows large area of atomization and vaporization at the trailing side of the liquid droplet. Region of breakup, dark area, gets wider and atomization and vaporization area also gets wider as time passes. Around t=102μs liquid droplet starts to detach from the dispensing needle and completely detach around t=160μs.

5.4 Ethanol Droplet Breakup from Decoupled Shock-flame Wave

The droplet breakup and atomization behavior associated with a decoupled shock-flame wave is different from the breakup of detonation wave case but similar to the breakup from weakly-coupled detonation wave case as described in the previously chapter. In Figure 5.4.1, a decoupled wave propagates from left to right through a poorly-mixed ethylene-oxygen mixture and again over a suspended ethanol droplet. Using a similar approach as previous case, the reference time frame of t=0μs is associated with the timing of the wave arrival on the droplet surface. For this case, the

lead shock wave speed was around 0.88 *km/s* in the horizontal direction. The wave propagation speed is substantially lower than the previous case, but the wave-induced flow still establishes a bow shock around the fuel droplet suggesting that the relative Mach number is supersonic. This bow shock starts to appear as soon as the lead shock wave arrives on the droplet (t=0μs). It can be observed that the droplet deformation and subsequent ligament formation starts at around t=4μs, much sooner than the detonation wave case. Initial breakup observed is shearing of the fuel droplet from the outer surface layer of the droplet. Comparing to the previous cases, existence of the bow shock clearly enhances the initial breakup process, which implies that the supersonic flow induced from the wave has substantial effect on the breakup process.

From t=16μs, flame front followed by the lead shock starts to get closer to the bow shock. As the flame front approaches, the bow shock that was sitting in front the droplet starts to disappear, which indicates that the increased local temperature may increase local speed of sound. Shearing on the surface develops and a long tail of fuel fragments is observed in the droplet wake during t=20~40μs. This trailing tail of fuel fragment is much longer than what was observed from the weakly-coupled detonation wave case. This could be explained from the distance between the shock and flame front. Since the decoupled shock-flame wave has longer distance between the shock and flame front compared to the weakly-coupled detonation wave, liquid droplet is exposed to the supersonic slip flow much longer. Thus, liquid droplet collided with weakly-coupled detonation has relatively short time to be stripped and the decoupled shock-flame wave have longer time to be stripped. This could be confirmed from the

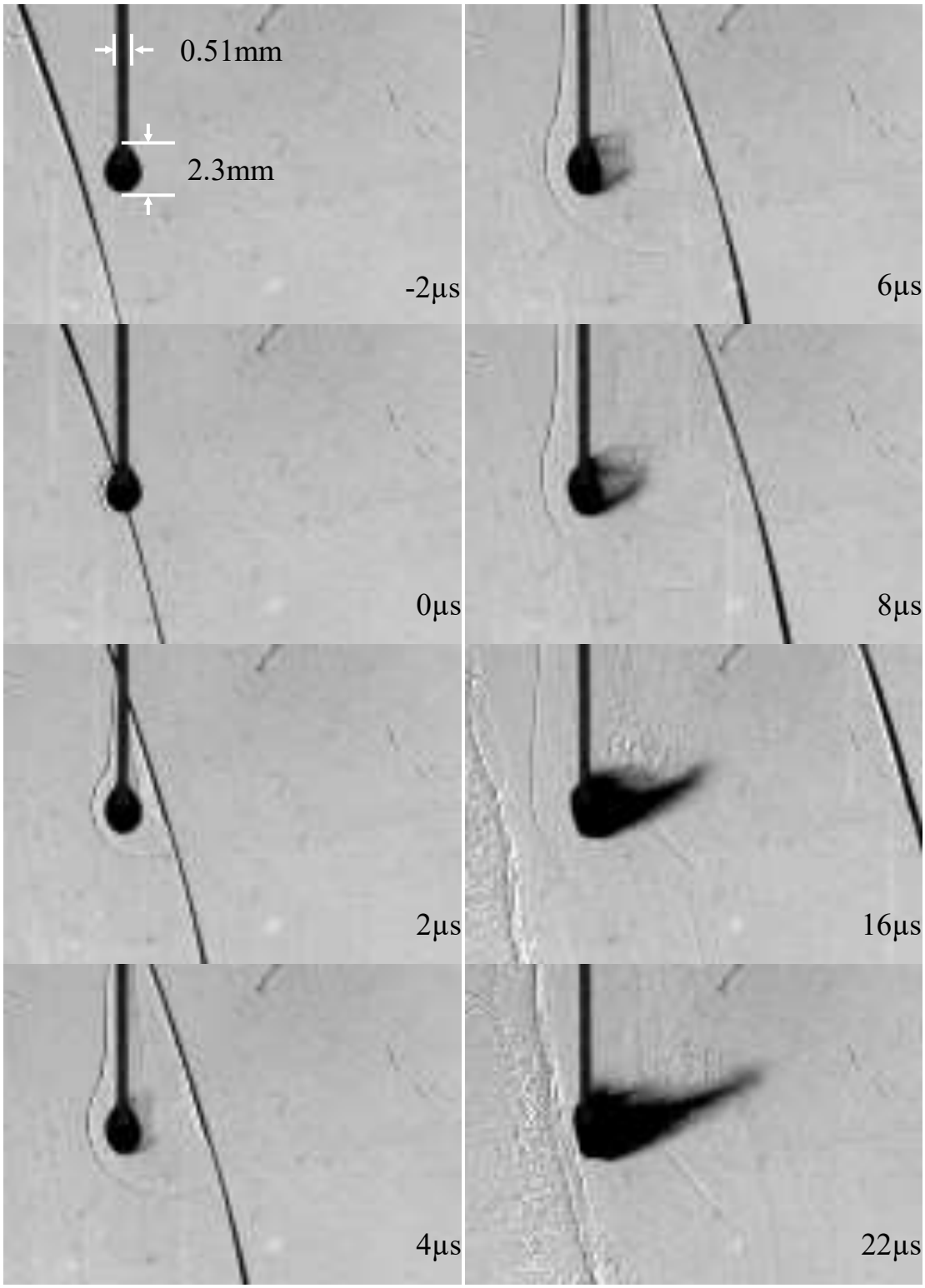

Figure 5.4.1 Lead shock wave, decoupled from the flame fronts, propagating over a suspended ethanol droplet

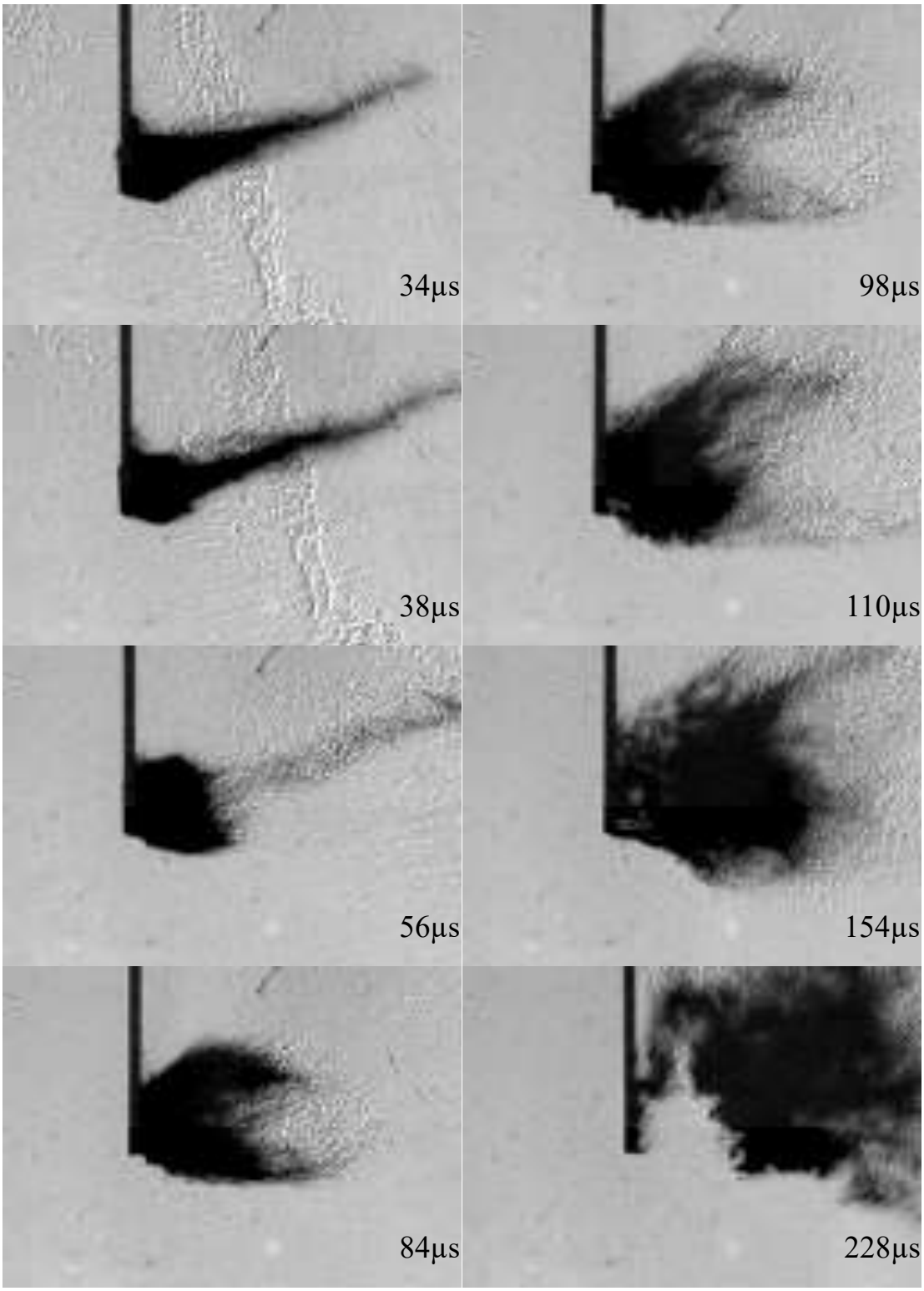

Figure 5.4.2 Lead shock wave, decoupled from the flame fronts, propagating over a suspended ethanol droplet

arrival time of the flame front, it takes more than 10μs for the flame front of decoupled shock-flame wave to arrive than the flame front of weakly-coupled detonation wave.

During the period when the flame front is passing through the trailing tail of liquid droplet fragment, the thickness of the tail gets thinner as if the flame fronts stretching the trailing tail as shown in the Figure 5.4.2 t=34μs and t=38μs. This behavior is noteworthy because this is the longest area that the liquid droplet had spread downstream among all three cases presented here. In similar time frame, liquid droplet collided with the detonation wave barely started to spread out.

After the propagation of flame front flow seems to continue downstream and the liquid droplet convects with the flow. From this time period, a different phase of the liquid droplet shattering starts at t=~60μs. As the trailing of the liquid droplet fades away (t=56μs*)*, the area of shattering increases and gets wider in the vertical direction. Also, some structure of atomization/vaporization starts to get observed at the trailing of the shattering. Another thing to point out is the different shapes of spread out of the liquid droplet in three cases.

In the detonation wave collision case, liquid droplet spread out in much later time (t=182μ) and spread out in skewed angle. Next, dispersion of liquid droplet for weakly-coupled detonation wave collision case occurred at t=76μs forming cloud like expansion. Lastly, liquid droplet from the decoupled shock-flame wave spread out and shows similar atomization and vaporization at t=84μs. However, it shows different dispersion shape. It shows more spreading from top and bottom and shows most wide area of spreading among the cases.

The shattered area increases and more atomization and vaporization area are found after t=84μs. The shattered liquid droplet started to detach from the needle at around t=154μs and completely detaches around t=228μs. This is slower than the weakly-coupled detonation wave, which may suggest the flowfield has lower convection speed than the weakly-coupled detonation wave case.

5.5 Analysis of the Ethanol Droplet Breakup

The breakup process of the liquid fuel droplet between the detonation wave-droplet interaction and the decoupled shock-droplet interaction shows different behavior. First, the timing of the initial breakup process is different as shown in the Figure 5.5.1. When a lead shock from the decoupled shock-flame wave passes, clear evidence of liquid droplet breakup is noticed early as at t=4μs. On the other hand, until t=34μs, only slight deformation on the surface of the liquid droplet is observed and no stripping occurs.

Second, in the decoupled wave case, a bow shock is observed ahead of the fuel droplet in the wave-induced flowfield, and initiates shock-enhanced droplet breakup. However, at similar time sequence, detonation wave case doesn't show any feature in terms of flowfield change. It only shows the deformation of wrinkle/wavy shape on the surface of the liquid droplet. As shown in Figure 5.5.1, there is no sign of shearing of the liquid droplet for the detonation wave case even when the shearing tail from the decoupled wave breakup disappear after the flame front passes by.

Next, due to the earlier breakup initiation, breakup appears wider with decoupled wave interaction compared to the detonation case at the similar time sequence. The earlier initial deformation from shock wave led to earlier and wider

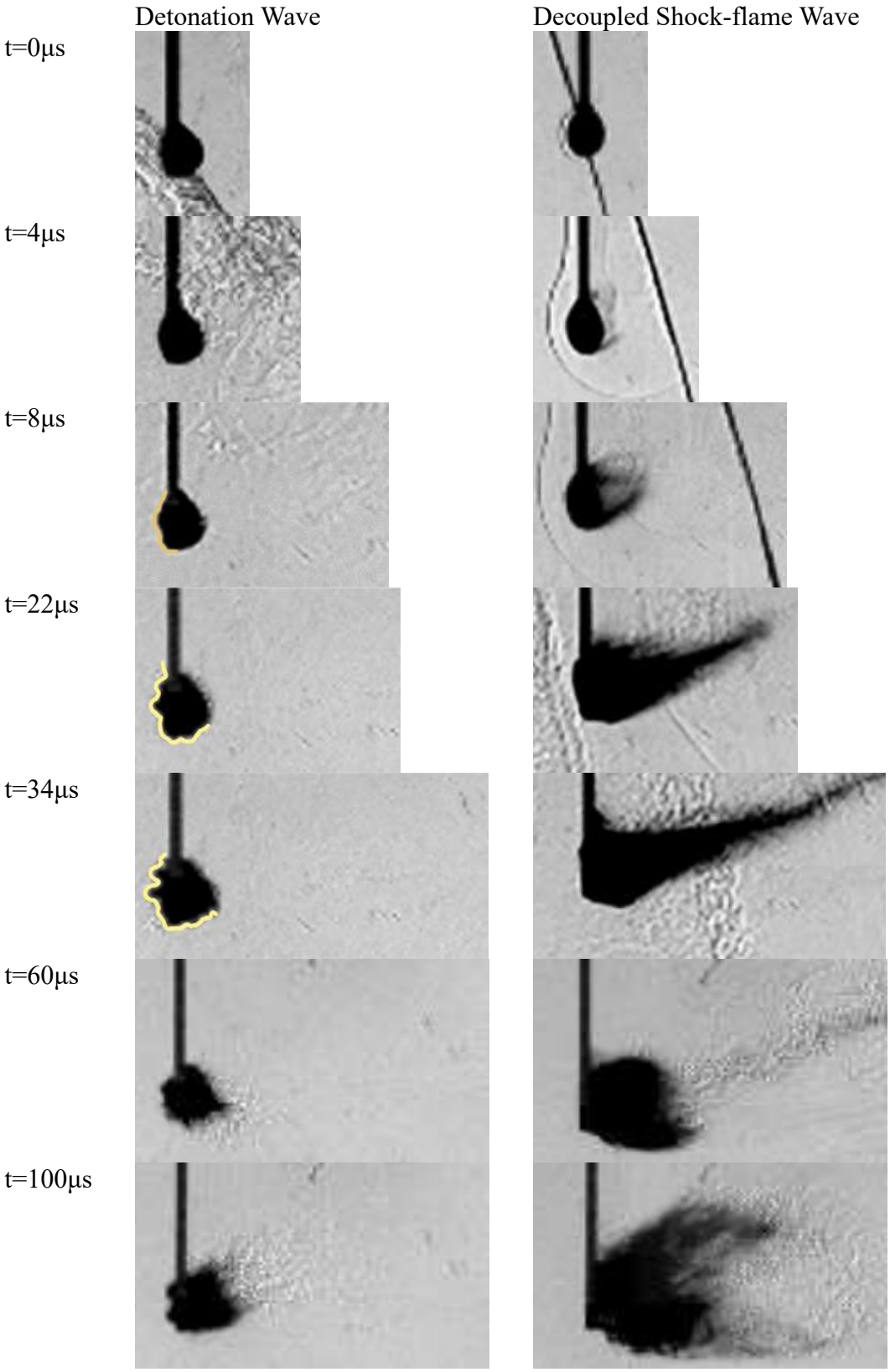

Figure 5.5.1 Comparison of breakup sequence for (a) detonation wave and (b) decoupled shock-flame wave

dispersion at t=60μs as shown in the Figure 5.5.1. For the detonation wave to vaporize the liquid droplet as the decoupled wave had at t=60μs, it took more than 100μs to disperse roughly about the same.

The main physical explanation for the difference in the initial breakup could be from the aerodynamic effect. As mentioned previously, the difference noticed in the initial stage of a breakup is the presence of the bow shock in front of the liquid droplet after the wave passes. A bow shock is established in front of the liquid droplet for the decoupled wave case. The existence of the bow shock means the induced velocity from the wave is supersonic.

The difference comes from the surrounding gas. The surrounding gas after the shock wave is shocked reactant, while the downstream of the detonation wave is the detonation product, as shown in Figure 5.5.2(a). Considering the conditions conducted in this study, the induced velocity is greater when the detonation wave is propagating at a higher speed than the shock wave, as shown in Figure 5.5.4(a). The induced velocity from the detonation wave is 1.0 *km/s*, while it is 670 *m/s* from the decoupled wave at the same time sequence from the impact.

Although the slip velocity is greater for the detonation case, the Mach number for induced velocity is subsonic. Since the detonation product has a higher speed of sound than the shocked reactant due to the increased temperature from the reaction and compression from detonation wave, the flowfield induced from the detonation wave cannot reach supersonic. This could be shown from the Figure 5.5.4(b). For all wave Mach number for detonation wave, induced flow Mach number remains subsonic.

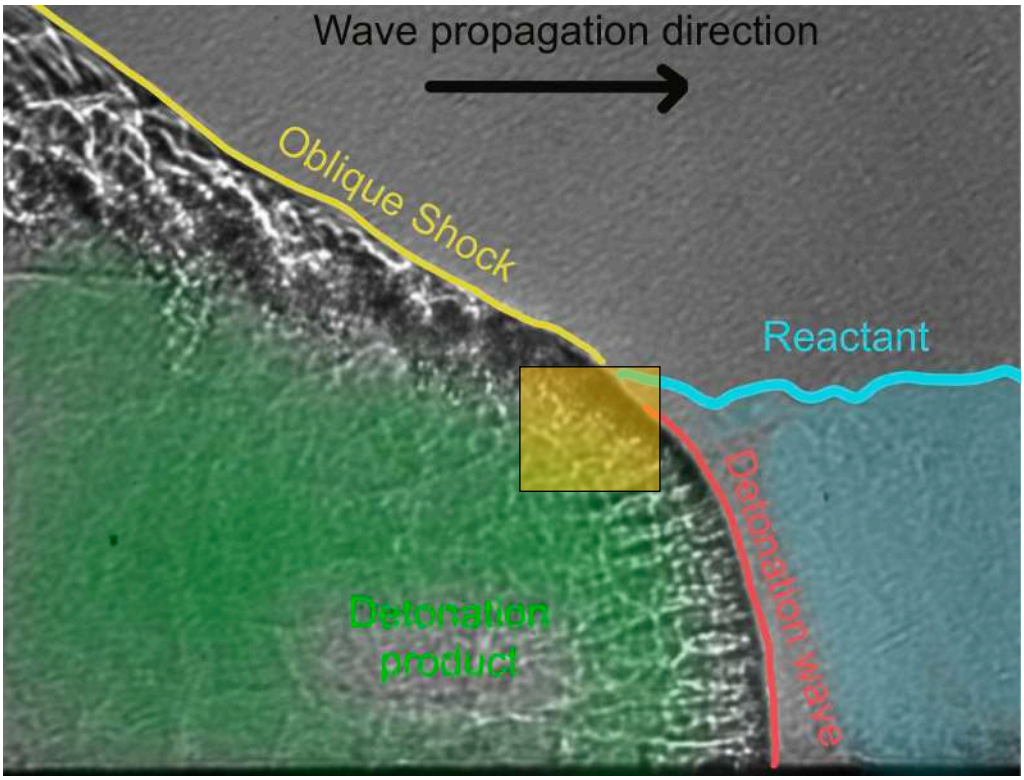

(a)

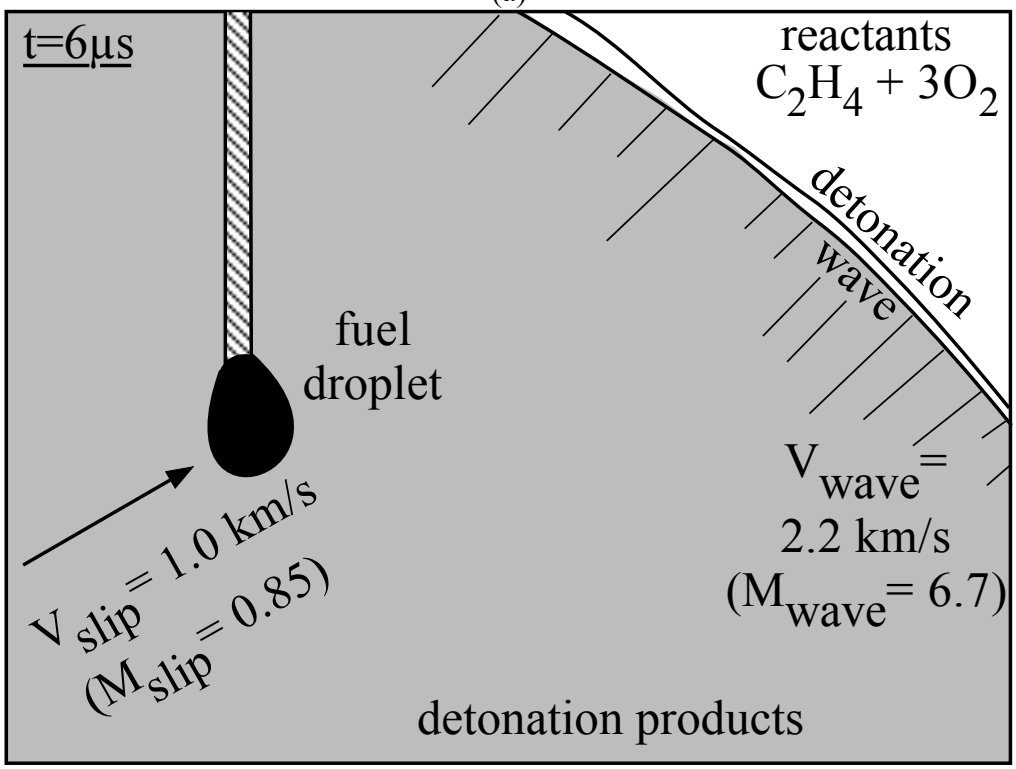

(b)

Figure 5.5.2 Illustration of fuel droplets subjected to the detonation wave-induced flows 6μs after the wave passage

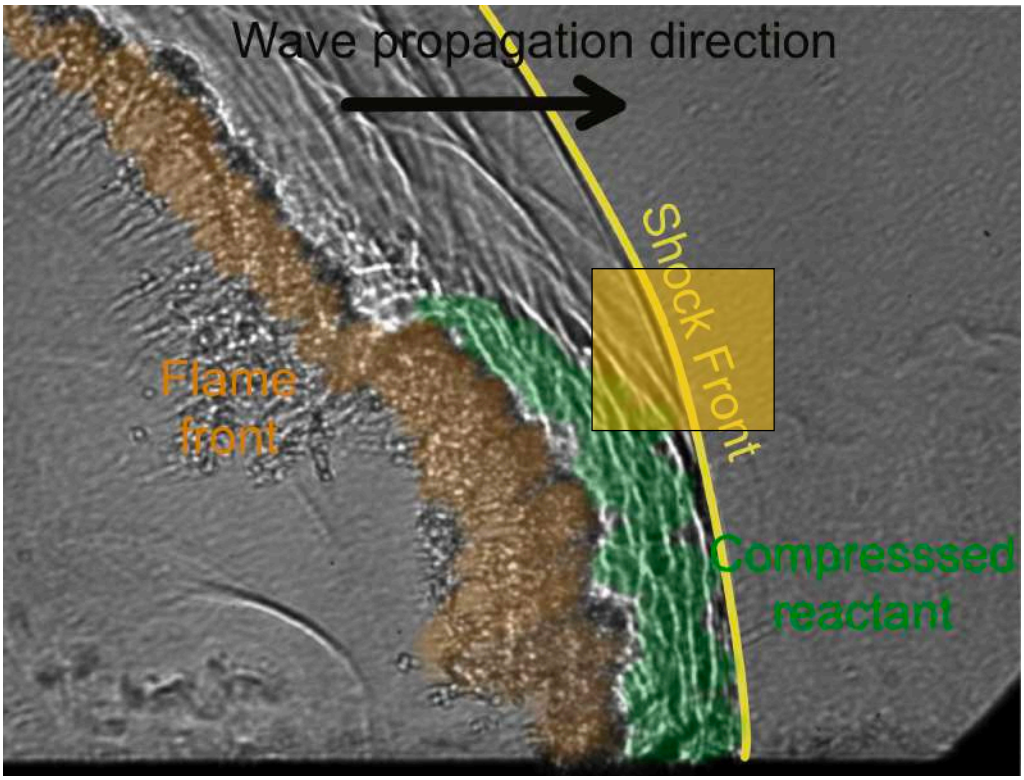

(a)

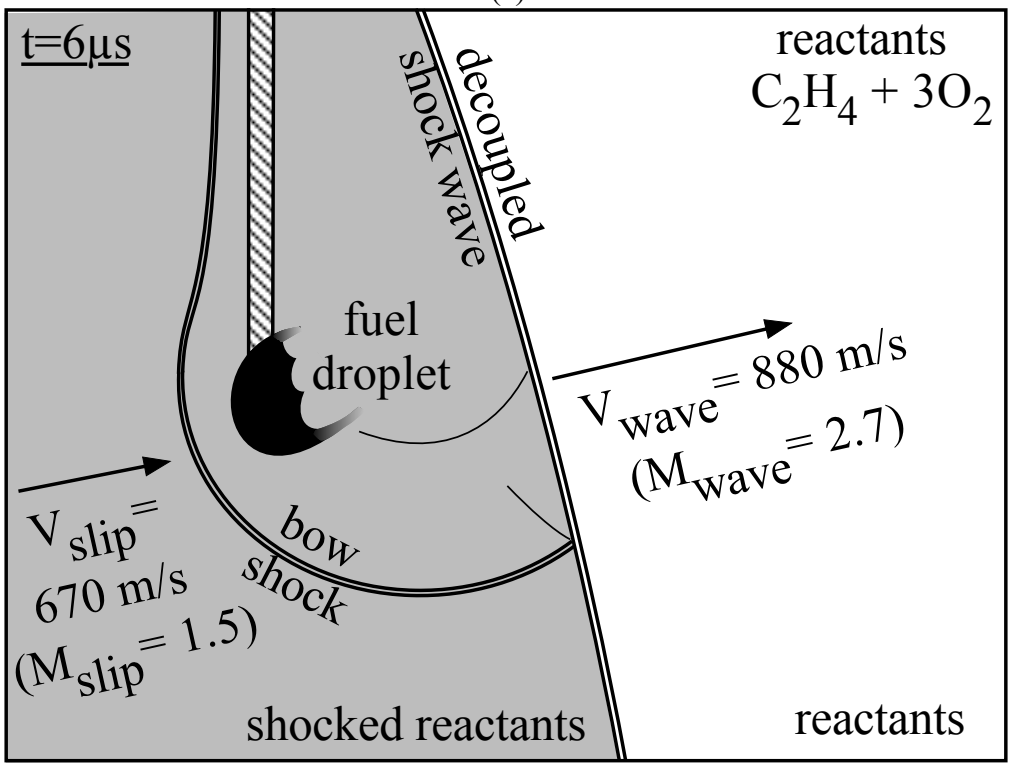

(b)

Figure 5.5.3 Illustration of fuel droplets subjected to the decoupled wave-induced flows 6μs after the wave passage

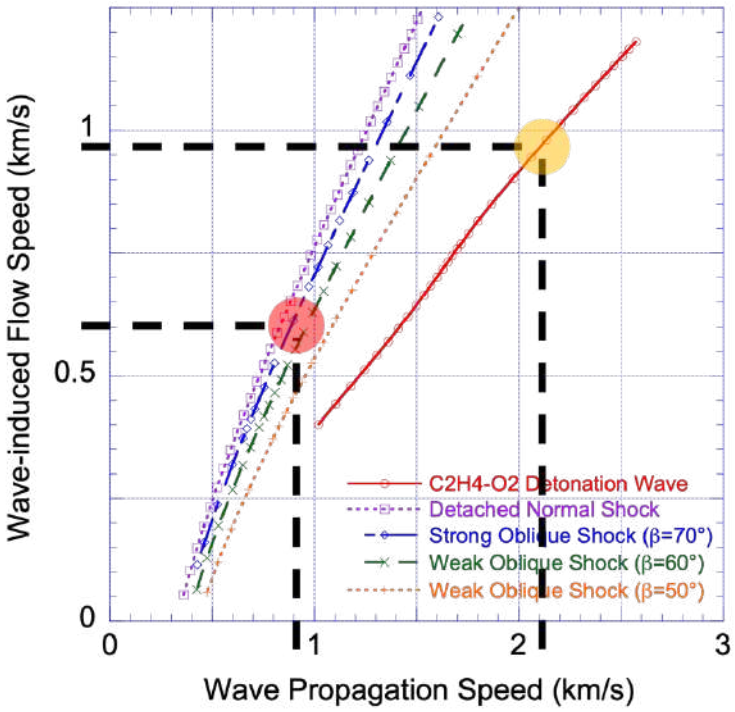

(a)

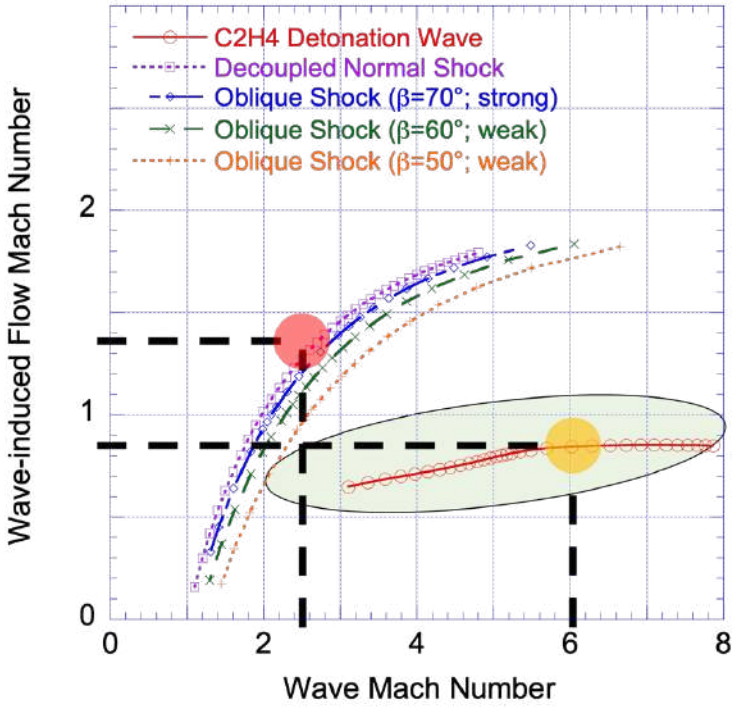

(b)

Figure 5.5.4 Comparison of the speed of wave propagation and the wave-induced (a)flow speed and (b)Mach number in its wake

In contrast, induced velocity from weakly-coupled or decoupled waves is supersonic if the shock wave propagates greater than Mach 2, as shown in Figure 5.5.4(b). Maintaining the slip velocity at supersonic in weakly-coupled or de coupled wave cases, a bow shock could be sitting in front of the liquid droplet as illustrated in Figure 5.5.3. This supersonic flow initiates the shearing of the outer layer of the liquid droplet due to the rapid pressure gradient on the liquid fuel droplet surface, which enhances the earlier breakup. Specific approaching and induced wave speed and Mach number for the corresponding case is listed on the Table 5.5.1.

Using the estimated speed of the wave, the induced Mach number (M_{slip}), Weber number (We) and Reynolds number (Re_D) were estimated as shown in the Table 5.5.2. Induced Mach number is defined as

$$M_{slip} = \frac{u_{slip}}{c} \tag{5.1}$$

where u_{slip} is the induced gas velocity immediately after the wave passage and c is speed of sound. Weber number is often considered in analyzing the multiphase flow, liquid droplet, and gas flow. It had been widely recognized as the breakup analysis is determined by the Weber number. Here Weber number is defined as,

$$We = \frac{\rho_g u^2 d}{\sigma} \tag{5.2}$$

Table 5.5.1 Wave speed and Mach number for approaching and induced detonation wave and decoupled shock-flame wave

	Detonation wave		Decoupled shock-flame wave	
	Wave Speed [m/s]	Ma	Wave Speed [m/s]	Ma
Approaching	2170	6.7	877	2.7
Induced	1000	0.85	670	1.5

Table 5.5.2 Non-dimensional parameter estimated from wave-induced flow immediately after wave passage (Ethanol droplet)

	M_{slip}	We	Re_D	Oh
Detonation wave	0.85	$2.3x10^5$	$4x10^4$	$6.4\ x10^{-3}$
Decoupled shock-flame wave	1.5	$2.2x10^5$	$2x10^5$	

where u is the gas velocity, ρ_g the gas density, d the initial droplet diameter, and σ the surface tension of the liquid droplet, respectively. The Weber number represents the ratio between the aerodynamic force and the cohesion force from the surface tension. It is well known that in high We regime (We~10^5) droplet breakup is categorized as catastrophic and stripping.

Also, the Reynolds number could be used to indicate the flow condition for the breakup behavior. Here the droplet-diameter based Reynolds number is defined as

$$Re_D = \frac{\rho_g u d}{\mu_g} \tag{5.3}$$

where ρ_g the gas density, u is the gas velocity, d the initial droplet diameter, and μ_g is the gas dynamic viscosity. Another parameter that could be used to explain the breakup could be Ohnesorge number. Ohnesorge number is defined as

$$Oh = \frac{\mu_d}{\sqrt{\rho_d d \sigma}} \tag{5.4}$$

where μ_d is the viscosity of the liquid droplet and ρ_d is the liquid droplet density. Ohnesorge number is ratio of droplet viscous forces to surface tension forces, so it does not reflect the flow condition. Thus, in order to find a distinct role for the initial breakup from the flow immediately after the wave passage, Ohnesorge number is not appropriate.

Table 5.5.3 Breakup mechanisms regime by range of Weber number [62]

Breakup Regime	We Range
Vibrational	We < 12
Bag	12< We < 50
Bag and Stamen	50 < We < 100
Sheet stripping	100 < We < 350
Catastrophic & Stripping	350 < We

Table 5.5.2 shows the estimated non-dimensional parameter from the wave-induced flow immediately after the wave passage. The Weber numbers for both detonation and decoupled shock-flame waves cases are in this same category, catastrophic and stripping, as shown in the Table 5.5.3. Also, both Reynolds numbers are well above to be turbulent flow and below the drag crisis, which occurs at Reynolds number in the range of 3.0×10^5 in case of sphere. This indicates that the drag coefficient is in a reasonable range to be considered the same. Hence, except for the induced Mach number, Weber and Reynolds numbers are estimated for detonation and decoupled shock-flame wave cases in the same regime. The slip Mach number falls in different regime, slip Mach number immediately after the detonation wave is subsonic and slip Mach number after the decoupled shock-flame wave is supersonic. This concludes that the slip Mach number has critical role in the initial liquid droplet breakup inside a rotating detonation engine.

Since the flow after the wave passage decays rapidly, long term breakup process

Table 5.5.4 Boiling point of liquid ethanol at peak pressure rise and half the peak pressure for detonation wave and decoupled shock-flame wave

	Detonation wave	Decoupled shock-flame wave
	Peak p	peak p
Pressure [psig]	242.8	121.5
Boiling point [K]	446	417

requires different explanation. One possible physical effect could be thermodynamic effect. Transient dynamic pressure measurement near the liquid droplet for detonation wave and decoupled wave are shown in the Figure 5.5.5. Dynamic pressure was measured at two closest locations (z=-0.625" and 0.125"). As shown in the Figure 5.5.5, detonation wave case clearly shows higher magnitude pressure rise compared to the decoupled shock-flame wave case. Clearly after 100μs, pressure trace decays relatively quietly. Due to the nature of dynamic pressure measurement, it is unclear how rapidly pressure field decays. However, it gives valuable information of peak pressure rise from the wave propagation.

From the peak pressure obtained from the dynamic pressure measurement boiling point of the liquid ethanol could be estimated. Table 5.5.4 shows the boiling point of liquid ethanol at the peak pressure for the detonation wave and decoupled shock-flame wave. There is about 30K difference in boiling temperature at each peak pressure. The pressure field after the wave rapidly drops due to the nature of the boundary condition the RDE holds; partially confined. It is uncertain how quick the pressure would drop inside the RDE combustor, but the pressure after the decoupled shock- flame wave would likely be lower than the detonation wave case. This suggests that decoupled shock-flame wave will always hold lower boiling point than the detonation wave passage. Since the boiling point changes more rapidly in the lower pressure range (under ~80psig) as shown in Figure 5.5.6, lower boiling temperature is expected in the long-term breakup process for the decoupled wave case. This could explain the faster atomization and vaporization for decoupled wave case that happens at later breakup process.

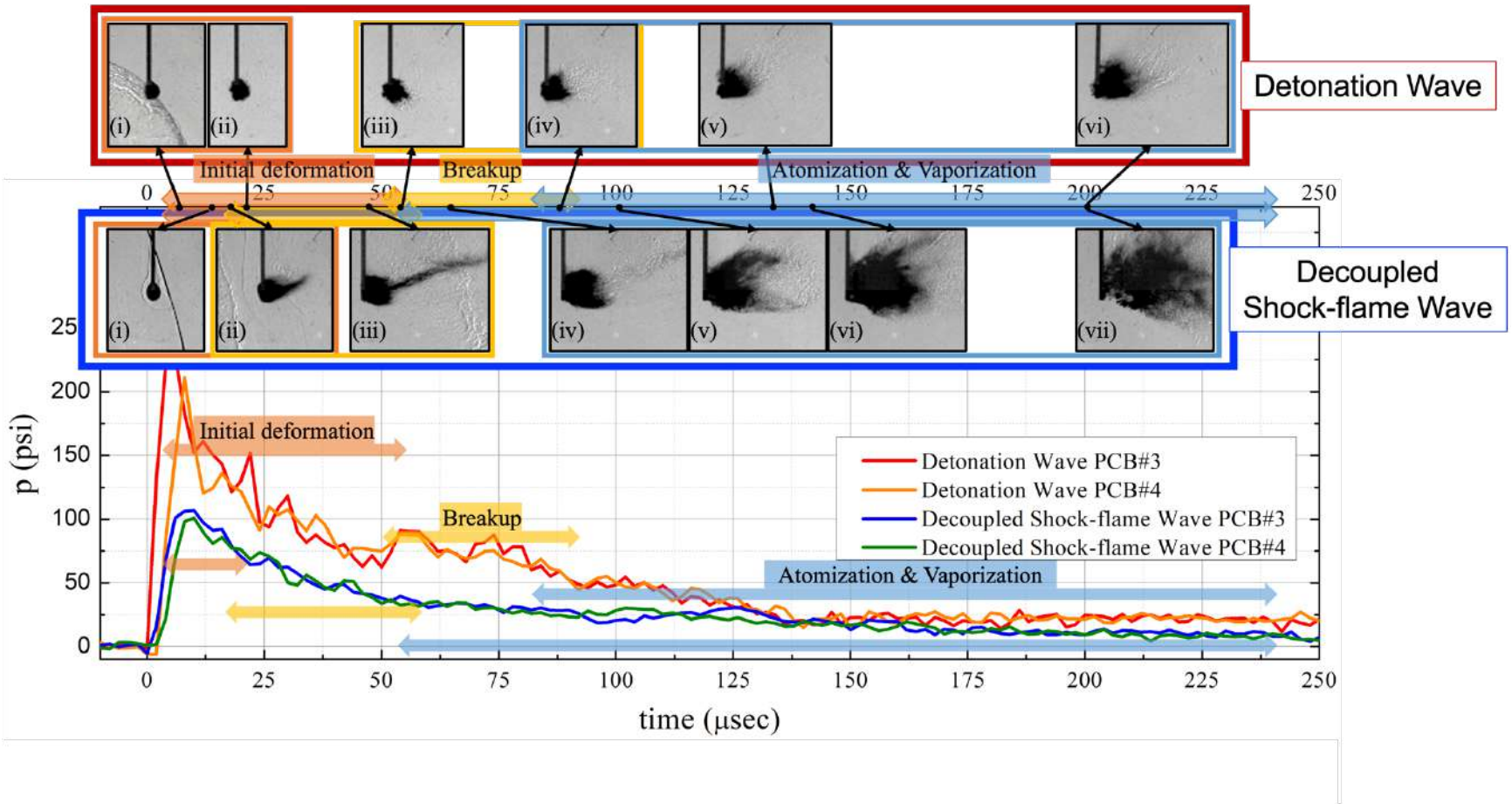

Figure 5.5.5 Pressure measurement for detonation wave and decoupled shock-flame wave cases until 200μs

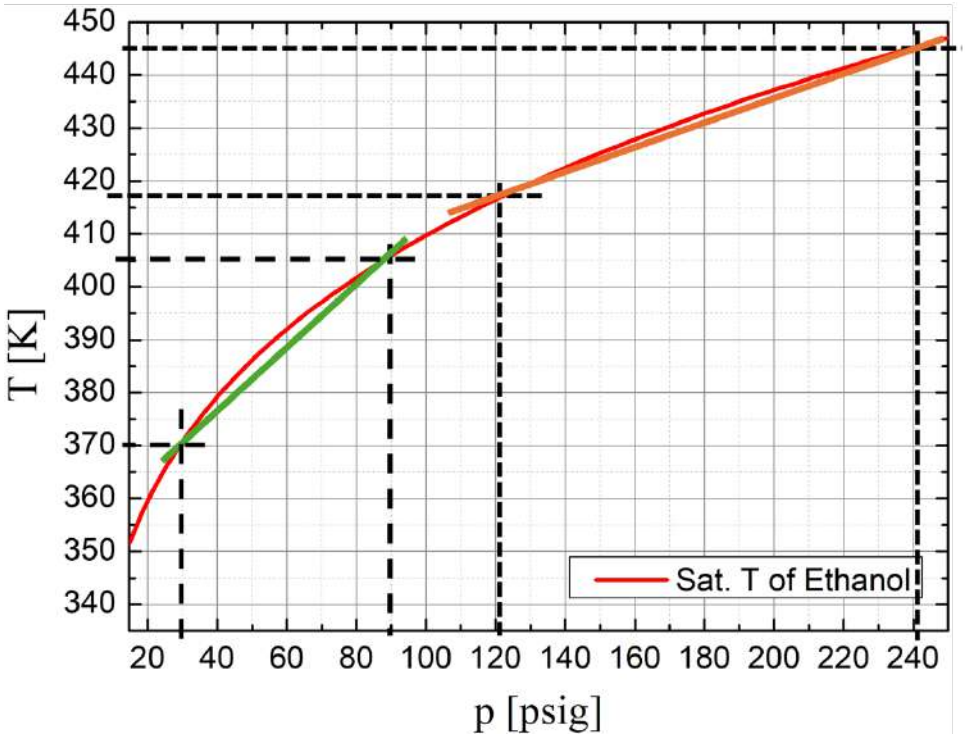

Figure 5.5.6 Estimated saturation temperature vs pressure of ethanol

5.6 JP-8 Droplet Breakup from Weakly-coupled Detonation Wave

Additionally, breakup process of JP-8 droplet from collision with weakly-coupled detonation wave was conducted. This was done to extend the work to practical usage of liquid fueled rotating detonation engine. The test condition for the JP-8 liquid droplet test is listed in the Table 5.6.1. Figure 5.6.1 shows the breakage of the JP-8 liquid droplet after the weakly-coupled wave passes over. Images were taken at 250

Table 5.6.1 Test conditions for JP-8 droplet test

Flow condition		Droplet condition	
Reactant	$C_2H_4 + O_2$	Liquid droplet	JP-8
Wave avg. Velocity [km/s]	1.1	Droplet height [mm]	2.3
		Droplet width [mm]	1.7

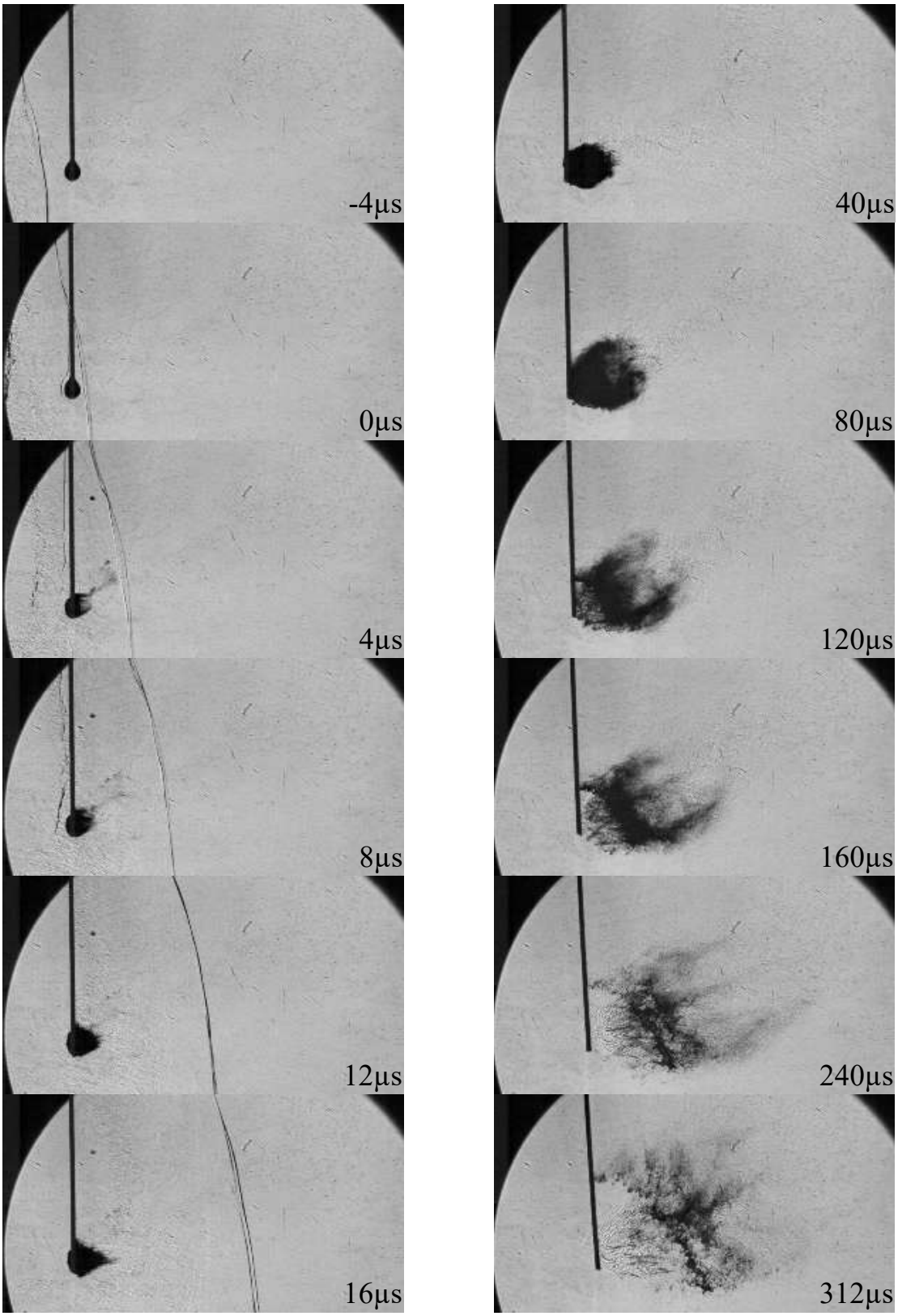

Figure 5.6.1 A lead shock wave, decoupled from the flame fronts, propagating over a suspended JP-8 droplet

kHz shadowgraph with a wider field of view than the previous images from the ethanol cases.

As shown in Figure 5.6.1, leading shock created bow shock in front of the liquid droplet at 0μs and the liquid droplet starts to strip at t=4μs. As noticed from the weakly-coupled detonation case, the trailing shear tail that was observed from the decoupled wave case is not observed. This is caused because the following flame front arrived earlier at t=8μs. Overall trend of breakup and dispersion of the liquid droplet is similar to the weakly-coupled detonation wave case. This indicates that the results that is obtained can be extended to different types of liquid propellent inside the rotating detonation engine combustor. Similar shape of wider dispersion is observed at t=16, 40μs. After t=120μs, the JP-8 liquid droplet starts to detach from the needle. Cloud- like area of darkening region reduces and leaves liquid ligament alike pattern as shown in 240μs. In addition, Figure5.6.1 does not show any sign of combustion from the atomized droplet of the JP-8. This may imply that the vaporized and atomized droplet does not meet the condition for a detonation wave to be sustained. 1) Atomized droplet is not in suitable size 2) pressure and temperature field after the wave is not adaptable to re-ignite 3) Atomized droplet didn't mixed with oxidizer enough and does not exist as detonable mixture.

5.7 Investigation of Liquid Water Droplet Breakup

Here additional tests were conducted to investigate the reaction of the liquid fuel. Instead of using propellent for the liquid droplet water was chosen. Figure 5.7.1 shows the sequence of water droplet breakup from a detonation wave collision. Similar

to the JP-8 case, images were taken at 250kHz and is looking at wider view. Due to the wider view, small features that was observed in the ethanol case may not show up. However, it will show all the features especially after the wider spread out since it occurs outside the smaller view.

Like the ethanol breakup from the detonation, no significant initial breakup appears. It is not clear vaporization and atomization is happening on the surface of the liquid droplet, but liquid droplet seems to breakup and deform quicker at t=32 and 48μs. At t=80μs, it starts to show significant spreading out. From this point water droplet seems to show quicker spread out.

In Figure 5.7.2, sequence of liquid water droplet breakup from decoupled shock-flame wave. Identical initial breakup process from ethanol-decoupled shock-flame wave was observed. Leading shock wave pass the liquid droplet and a bow shock sits in front of the liquid droplet. Striping from the liquid droplet behind bow shock is observed. Water has stronger surface tension than ethanol, but the results show that even with the stronger surface tension, rapid pressure gradient on the surface of water created after the bow shock still generated strips and cause the early initial breakup like ethanol.

It was unclear from the liquid fuel droplet whether it re-ignite or react during or after the breakup. Thus, using a non-reacting liquid, water, it was considered water liquid droplet breakup would show different trend compared to the liquid propellant cases. However, no distinguishing difference were found between the water and liquid propellant cases.

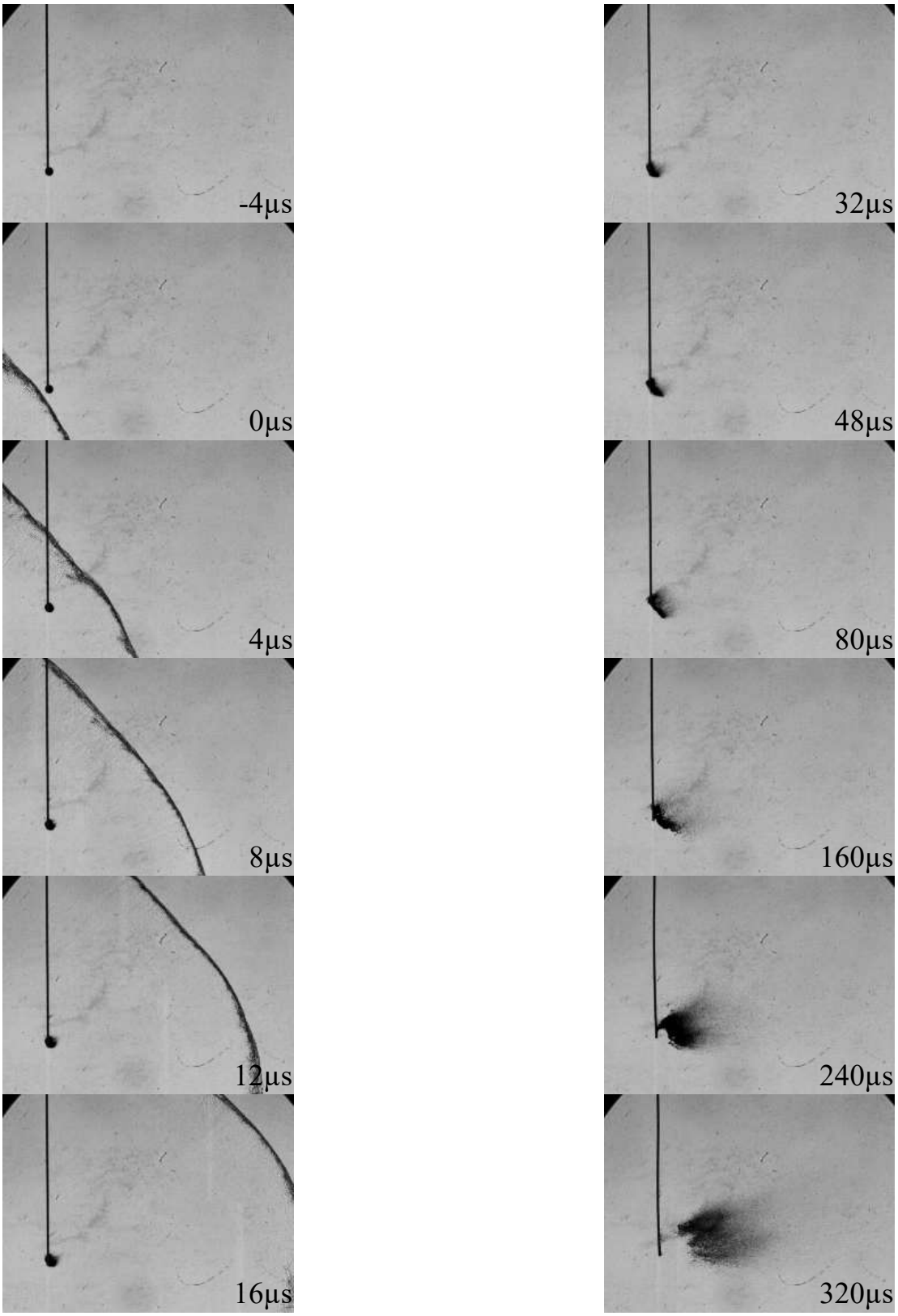

Figure 5.7.1 Water droplet exposed to the detonation wave

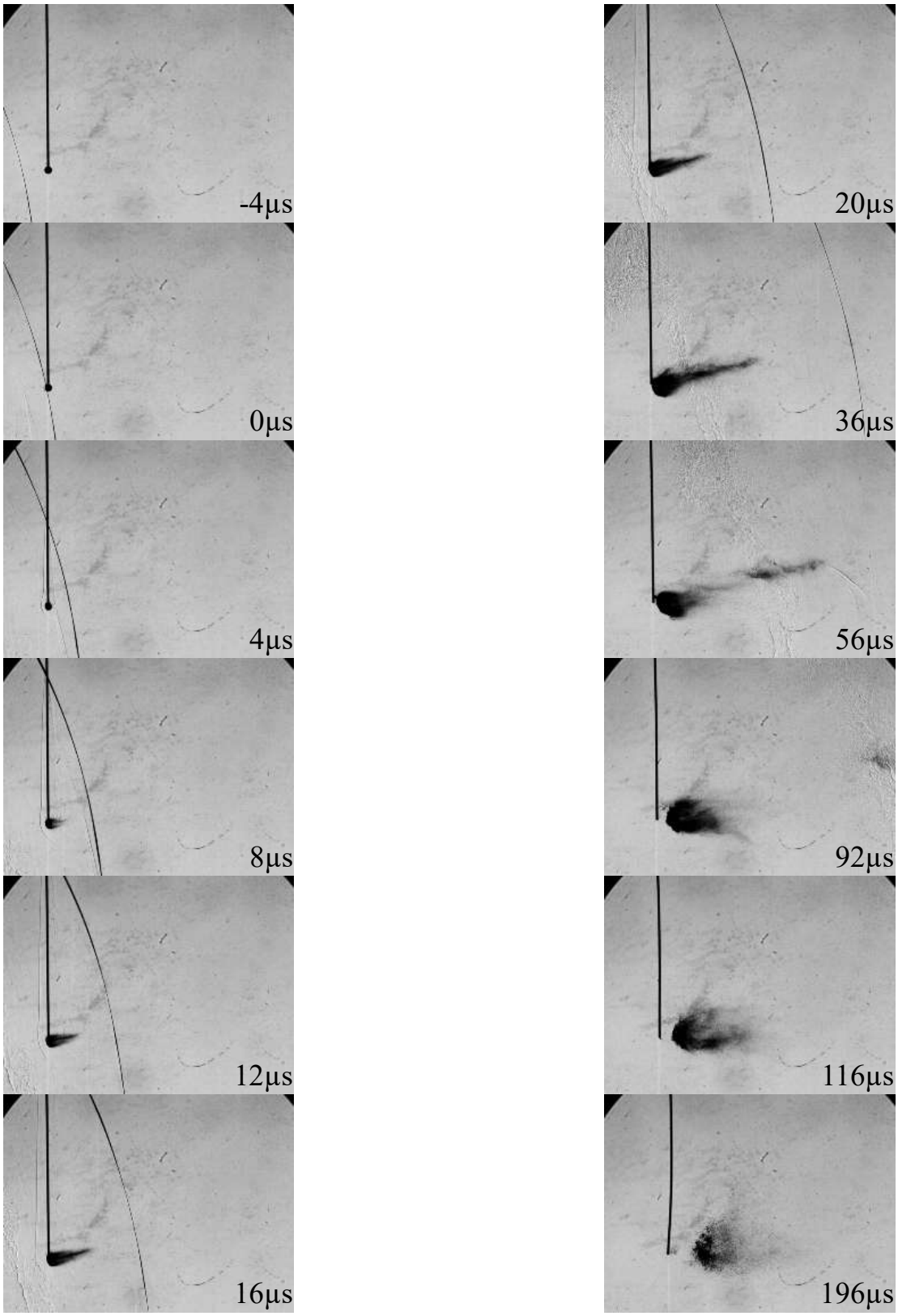

Figure 5.7.2 Water droplet exposed to the decoupled shock-flame wave

Chapter 6: Conclusions

6.1 Concluding Remarks

Interest of utilizing the rotating detonation engine have grown significantly in the past couple decades. Various experimental and computational studies have been conducted to enhance the understanding of the physical phenomena inside the rotating detonation engine. This study is one of them, specifically aiming to understand and provide insights into interaction of wave with injector flowfield inside a rotating detonation engine combustor. It mainly focuses on the wave-refresh jet, wave-wave, and wave-liquid droplet interaction in a partially confined boundary condition like RDEs.

eLMDE facility allows to study the fundamental phenomena inside the combustor by giving visual access. Design of the eLMDE was to unwarp the closed loop shape of RDE to linear model. Because it is open looped design, it cannot create continuous or “steady” flowfield of detonation propagating. However, this enabled the eLMDE to have two pre-detonators from two open end and create counter propagating detonation wave, which frequently found as slapping mode of RDE operation.

Having the ability to have single or counter propagating detonation wave inside the combustor, refresh jet from the injector after the wave passes by was studied. Stable and controlled refresh jet is crucial for stable operation of a rotating detonation engine since it is feeding reactants for the next cycle. Refresh jet would recover when its stagnation pressure overcome the combustor pressure. Hence, being able to generate different pressure inside the combustor from propagating different strength of wave or

to collide two waves heading at each other allowed to investigate how the injector response to the various combustor pressure. Furthermore, studying the effect of different stagnation pressure from the injector, by varying the mass flow rate, provide comprehensive understanding of refresh jets.

Lastly, liquid propellant was considered for more practical usage of the rotating detonation engine. Liquid reactant has higher energy density compared to the gaseous reactant. However, injecting liquid reactant directly into the combustor would not operate the rotating detonation engine properly. There are several reasons for this. One could be that the detonation happens in a very short time but when it is in the form of liquid there is not enough time to breakup, pre-vaporization, and atomization into appropriate size. Also, the reactant injected inside the combustor should be detonable mixture in order to sustain the detonation wave to propagate. Thus, the reactant requires additional time to vaporize into fine size and get mixed to detonable mixture, which could not be achieve in the order of time where detonation wave propagate.

It is regarded that liquid droplet require pre-vaporization or atomization process before the injection and spray into the combustor. The size of the liquid droplet would be distributed. Majority of droplets should be small enough, but some large sized droplet could be injected to the combustor. Recalling that the liquid propellant has higher energy density, this could imply that some existence of large sized droplet could hold large energy in terms of energy per mass. Hence this work investigates the interaction between the relatively large sized droplet and detonation wave.

Test was done by propagating a detonation wave to a suspended liquid fuel droplet inside the eLMDE combustor. Two different types of fuels were considered,

ethanol and JP-8. In addition, three different types of detonation waves were considered: detonation wave, weakly-coupled detonation wave, and decoupled shock-flame wave. Schlieren and shadowgraph images were taken using the high-speed camera. The result was somewhat counter-intuitive. Liquid fuel droplet that was exposed to the decoupled shock-flame wave, which is slowest among three types, showed faster initial breakup and ended up faster pre-vaporization and atomization.

The flow condition that liquid droplet was exposed didn't have significant difference in terms of We, Re_D, and Oh, which are common non-dimensional number that is considered in analyzing the liquid droplet breakup. One distinguishing point was the flowfield after the wave passes. When the detonation wave propagates, it creates an induced flow immediately after the wave. Wave induced flow from the detonation wave hold higher slip velocity relative to droplet, but the slip Mach number is in the region of subsonic. On the other hand, decoupled shock-flame wave creates lower slip velocity but supersonic slip Mach number. This could be explained from the existence of a bow shock sitting when the liquid droplet encounters the decoupled shock-flame wave. We or Re_D could not explain this as suggested in the previous studies. Thus, this work claims that different induced Mach number immediately after the wave passage has critical role in the initial breakup process of liquid droplet inside an rotating detonation engine combustor.

6.2 Contribution Summary

Counter propagating detonation wave inside the partially confined boundary condition like rotating detonation engine was visualized for the first time. Using the

eLMDE facility and high-speed Phantom camera, schlieren and shadowgraph images of collision between 1) detonation wave vs. detonation wave, 2) detonation wave vs. decoupled shock-flame wave, 3) decoupled shock-flame wave vs. decoupled shock-flame wave were captured. In addition, dynamic pressure was measured for the wave collision.

This observation enhanced the insight to physical process that occur inside the rotating detonation engine. Result of collision between detonation wave suggests that weaker shock waves could travel inside the RDE combustor and affect the next cycle. Also, collision between detonation wave and decoupled shock-flame wave provides the evidence of how the counter propagating detonation wave could happen. Also, it shows how a decoupled shock-flame or shock wave inside the combustor could affect the following cycle.

At the same time, behavior of the refresh jet after the wave collision was studied. Understanding the interaction of injector with detonation wave is crucial for operating the rotating detonation engine. Observation made from counter propagating waves was that the injector adjacent from the location of collision would inject the refresh jest the fastest creating uneven height of refresh jets. This was true for all collision cases that was tested. Different timing of the refresh jet and uneven refresh jets would also influence the later cycle.

For deeper understanding of how the injector reacts, additional experiments were conducted. Test was done by evaluating the refresh time, characteristic delay time, when different amount of mass flow rates was injected into the combustor and single detonation wave is propagating along the eLMDE channel. Results indicate that the

refresh jets may recover sooner if its stagnation pressure can overcome the combustor pressure. Hence, the higher mass flow rate could shorten the refresh time delay by overcoming the injector exit pressure.

Another branch of this work explains the breakup process of a relatively large sized liquid droplet encounter different types of detonation waves for the first time. This work has its uniqueness due to boundary condition that rotating detonation engine have. Schlieren and shadowgraph images were taken using the high-speed camera and could observe the breakup, pre-vaporization, and atomization process of liquid droplet exposed to the detonation wave, weakly-coupled detonation wave, and decoupled shock-flame wave. This work found that liquid droplets break up faster when exposed to slower decoupled shock-flame waves compared to faster detonation waves. This work was able to identify that this unexpected difference is attributed to the initial slip flow Mach number around the droplet, which is subsonic for detonation waves but supersonic for decoupled waves. Research findings suggest that the slip flow Mach number, along with the Weber number, plays a crucial role in RDE fuel droplet initial breakup process.

6.3 Future Work

Various research topics could be extended from the work done in this dissertation. As this work has done, the flexibility of the eLMDE facility allows numerous studies to be worked in further investigating the fundamental physics of detonation waves inside the partially confined rotating detonation engine like condition.

Furthermore, considering different diagnostics could lead to further understanding of different aspect of the rotating detonation engine.

As demonstrated in this work, thanks to the optical accessibility of the eLMDE facility qualitative analysis provided valuable data of characteristics of detonation wave behavior inside the rotating detonation engine combustor. Although it brings great insight, few additional quantitative data such as velocity information of the flowfield created by the propagated detonation wave could be helpful. Various instruments could be utilized to measure the velocity. The flowfield, wake of the detonation wave, would decay rapidly due to partially opened boundary condition, and requires highly sensitive and frequency of measurement. Thus, it is not easy to find an instrument that is suitable for using in a severe condition like the combustor of rotating detonation engine.

One possible instrument that could be proposed could be focused laser differential interferometry (FLDI). FLDI is a non-intrusive equipment that uses optical technique. It was first introduced in the 1970s but received attention in recent days taking advantage of advancement of modern lasers and data acquisition systems. Several studies have shown its capability of measuring high velocity flows in for wind tunnel applications. Enable to measure the velocity inside the rotating detonation engine could allow further investigation of both refresh jet and liquid droplet breakup interaction with the detonation wave.

Measuring the refresh jet velocity would provide 1) more accurate refresh time after the wave passage 2) estimation of the height of injected pre-mixed reactant on the next cycle 3) provide useful information when determining the combustion instability caused by acoustic response of the injector.

Additionally, assessment of the flowfield created by the wave could 1) determine the slip velocity immediately after the wave for better understanding the initial breakup 2) better estimate on how fast the flowfield decays for enhanced understanding of the later breakup process of the liquid droplet 3) provide helpful data for accurate numerical analysis.

Recent studies on rotating detonation engine applications expands to utilize the RDE and combine to various propulsion systems to enhance the performance. One idea could be using the rotating detonation engine as the secondary combustion source of a scramjet. Exhaust of a rotating detonation engine holds high temperature and velocity, and this could be injected into the cavity flame holder of a scramjet. This would allow to redistribute heat release which is expected to have positive effect on the operability of the scramjet. To investigate the effeteness of a RDE on the scramjet, eLMDE could be connected to a vitiated heater creating a supersonic jet. In this configuration, detonation wave propagating along the eLMDE, which is perpendicular to the direction of supersonic jet could simulate a simplified case where observation of detonation wave propagating into the supersonic jet could be conduct. This kind of study could do effortlessly due to flexibility and simplicity design of the eLMDE.

Lastly, further study on finding the relationship between the size of a liquid droplet and breakup from the detonation wave could be suggested. One could expect when the size of a liquid droplet is in the order of μm, the breakup process would behave differently from what is presented in this work from estimating Stokes number. Pre-vaporization/atomization of a liquid propellant is considered before injecting into the rotating detonation engine combustor. It is inevitable that the liquid droplet would

be entering the combustor in a range of a distribution in terms of its size. Thus, determining the size effect on the breakup process could help estimate the critical size required for the liquid droplet to react on current cycle. Also, this could assess how much of the fuel is expected to affect the next cycle from the range of distribution.

Appendix A: Experimental Facility

A.1 eLMDE for Counter Propagating Wave Experiment

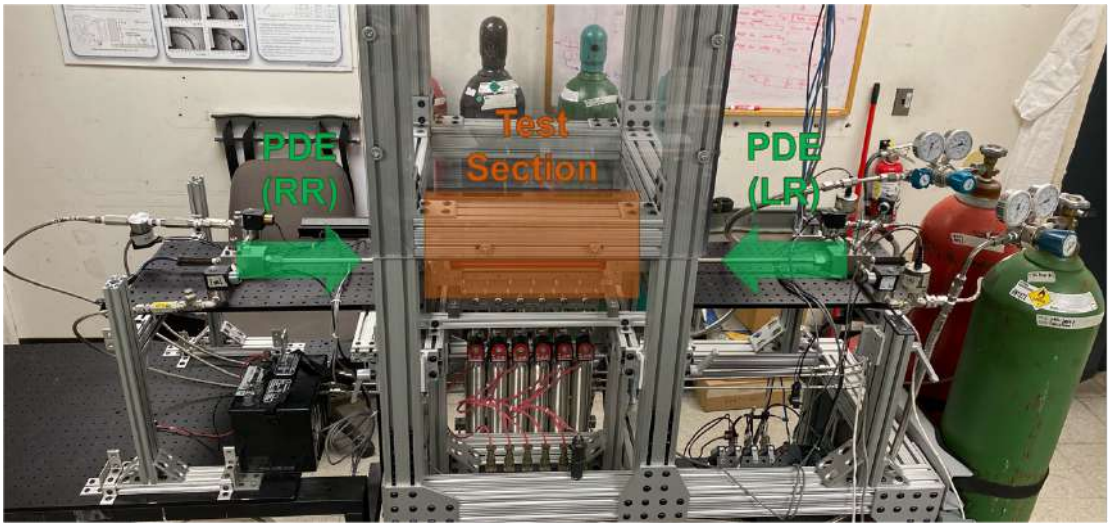

Figure A.1.1: eLMDE connected with both left running (LR) and right running (RR) pre-detonator

Figure A.1.2: Close up view of the eLMDE test section

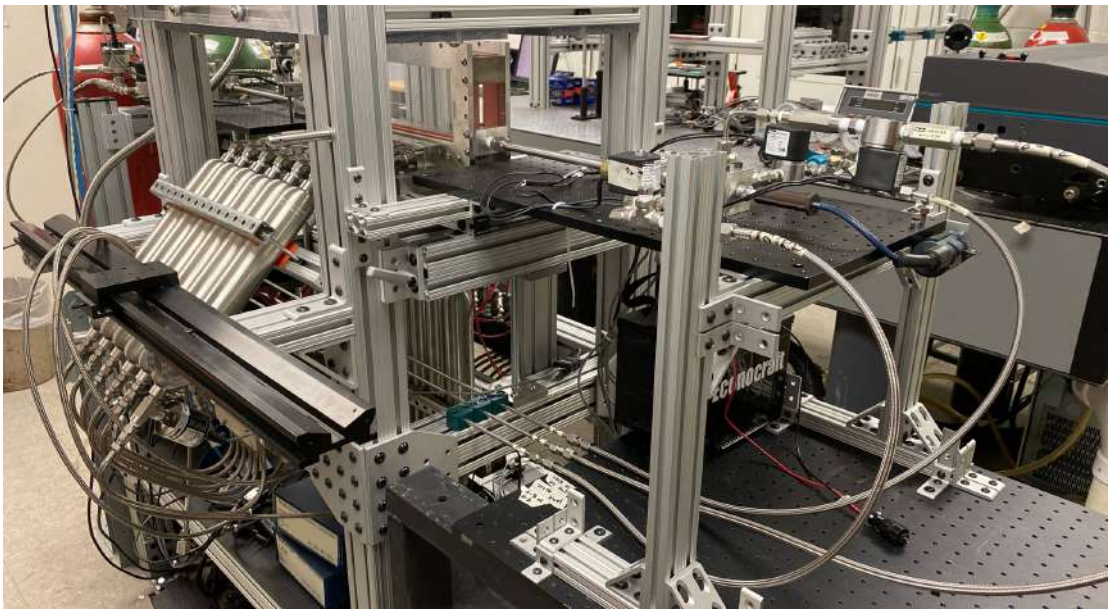

Figure A.1.3: Left running (LR) pre-detonator attached to eLMDE for counter wave propagation test

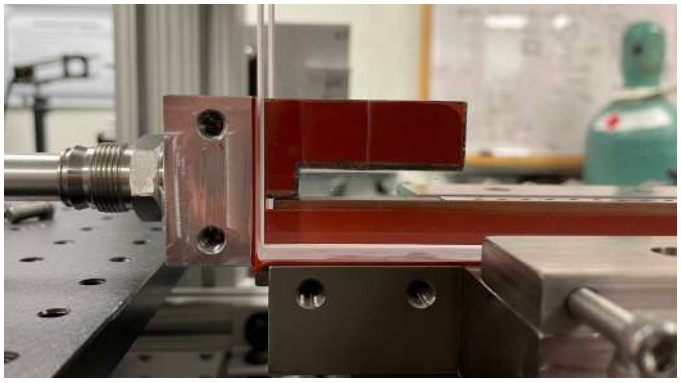

(a)

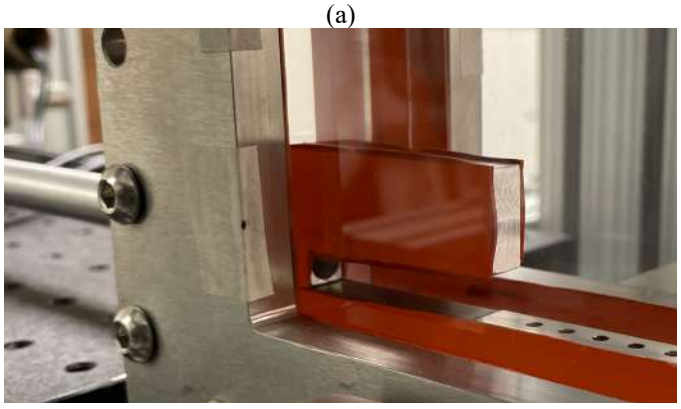

(b)

Figure A.1.4: Transition component installed (a) without window frame and (b) with window frame

A.2 Visualization Setup for Schlieren and Shadowgraph Image

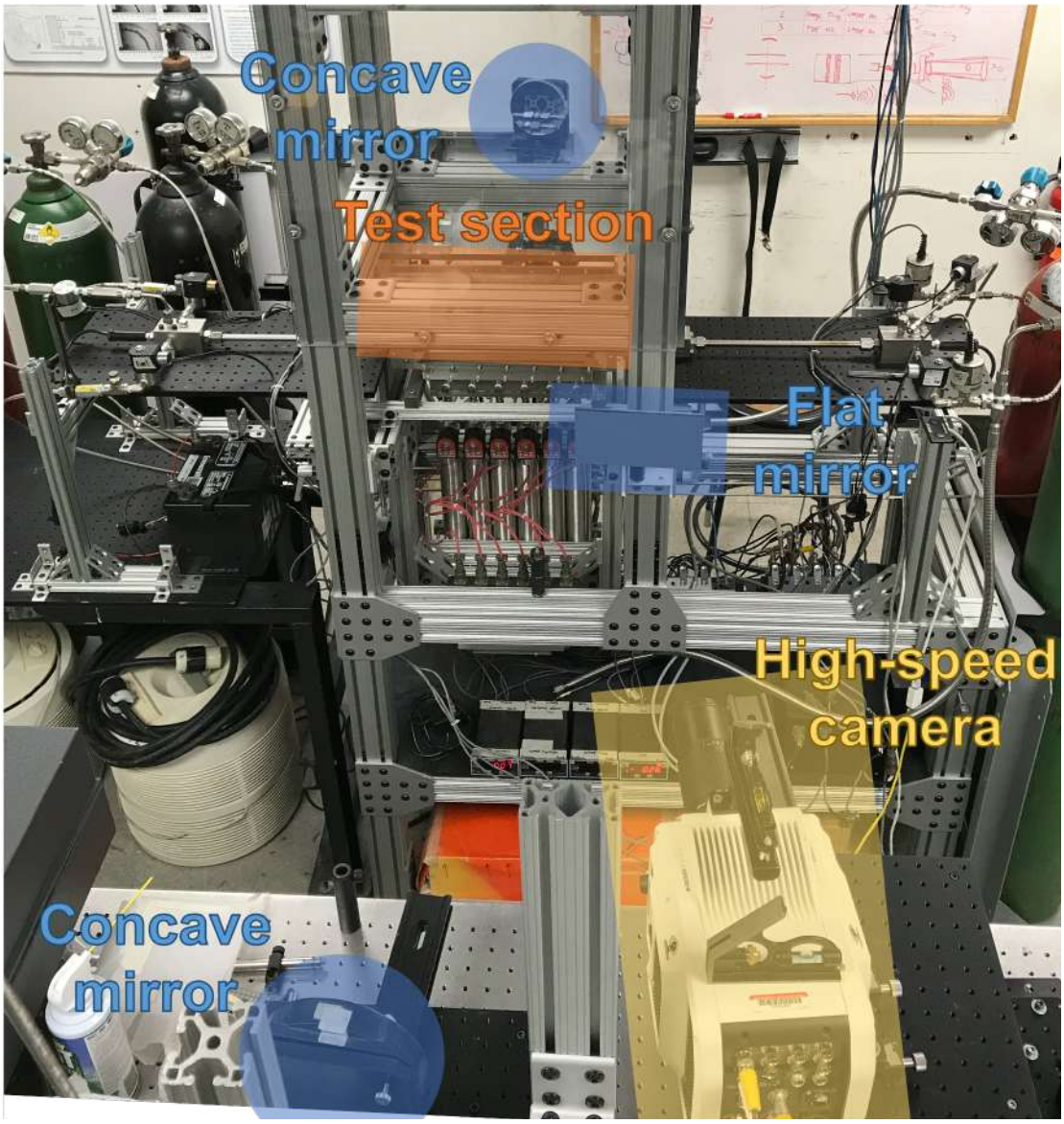

Figure A.2.1: z-type setup using concave and flat mirrors

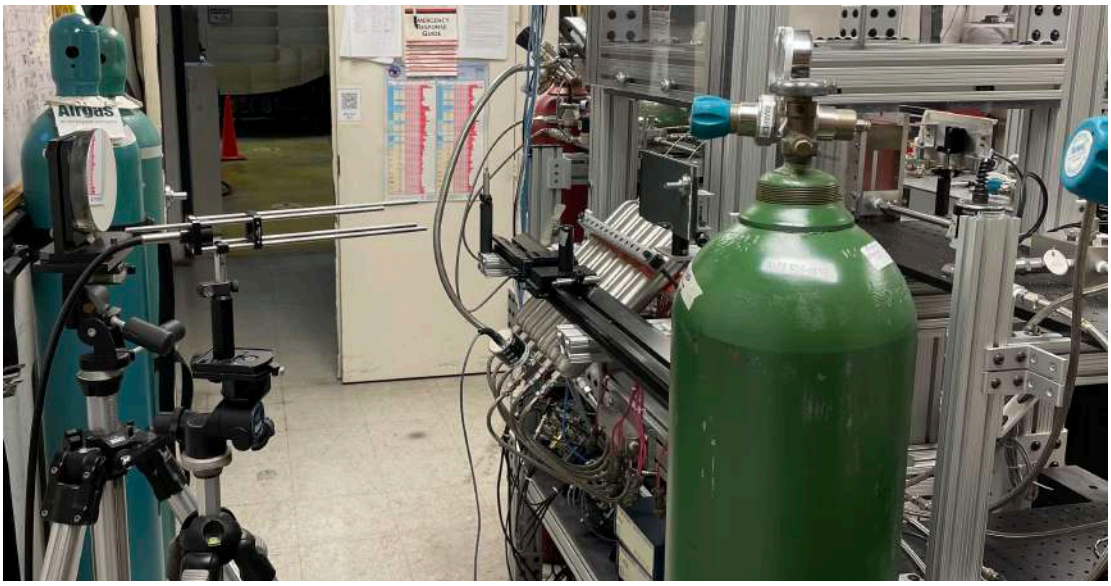

(a)

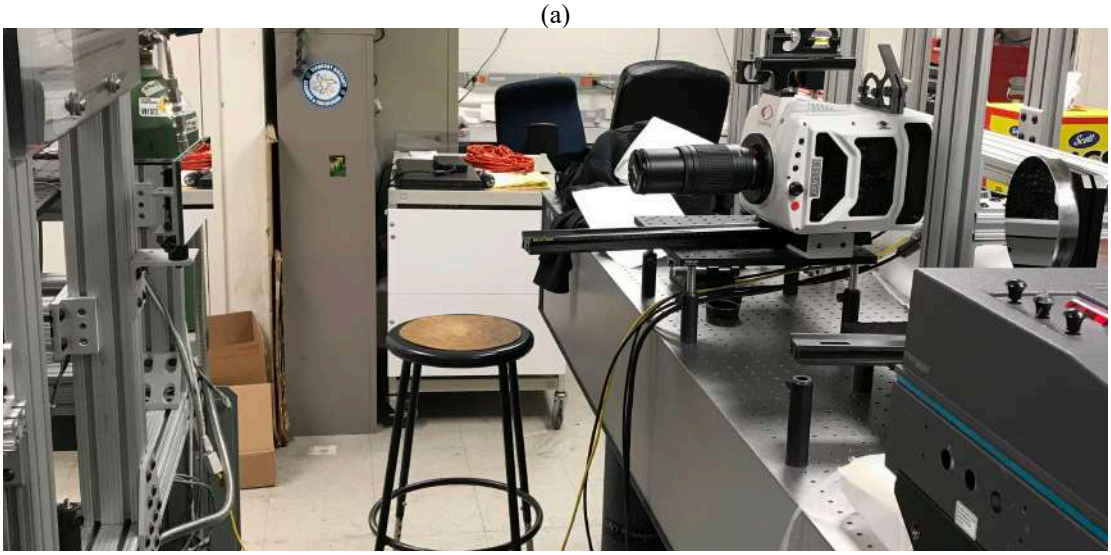

(b)

Figure A.2.2: z-type setup (a) light source side and (b) camera side

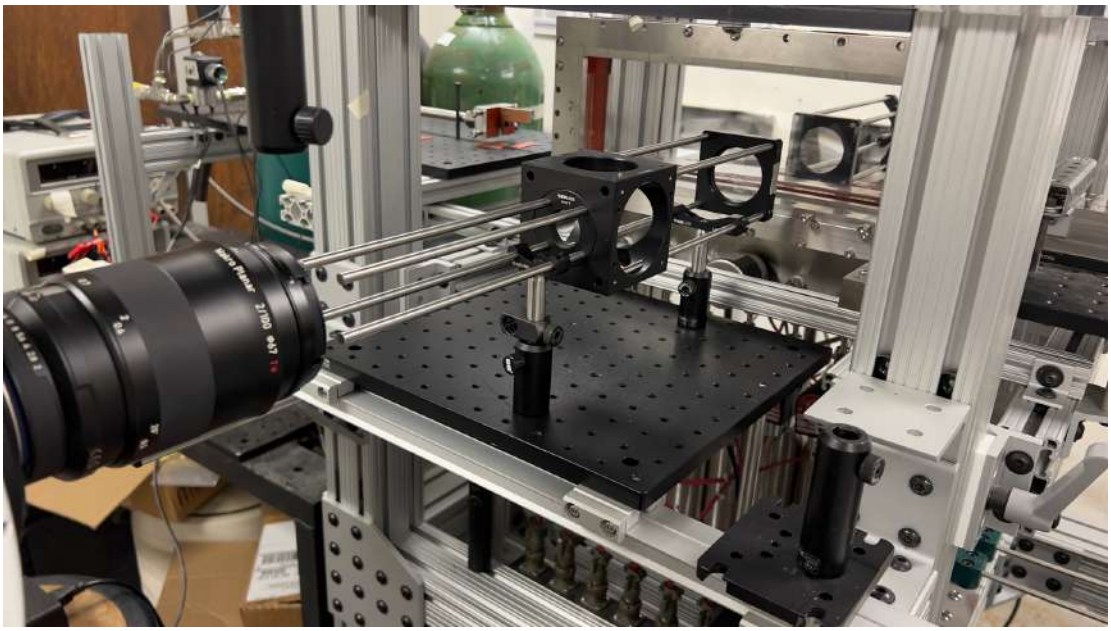

(a)

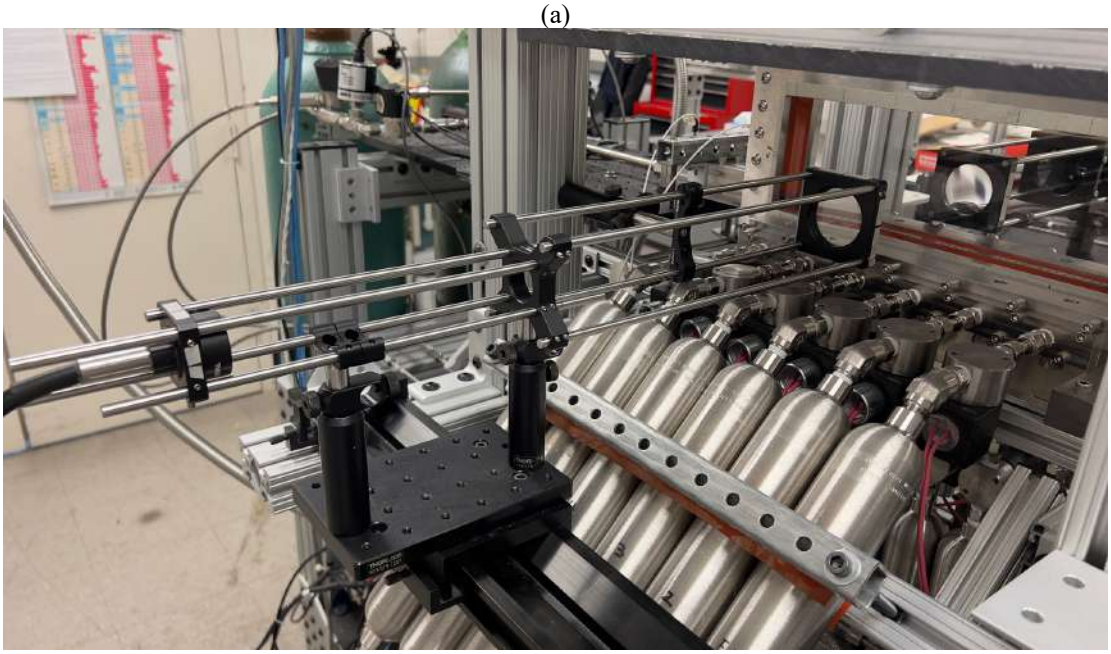

(b)

Figure A.2.3: Toepler's lens-type arrangement (a) light source side and (b) camera side

A.3 Metal Windows for Pressure Measurement Inside the eLMDE Combustor

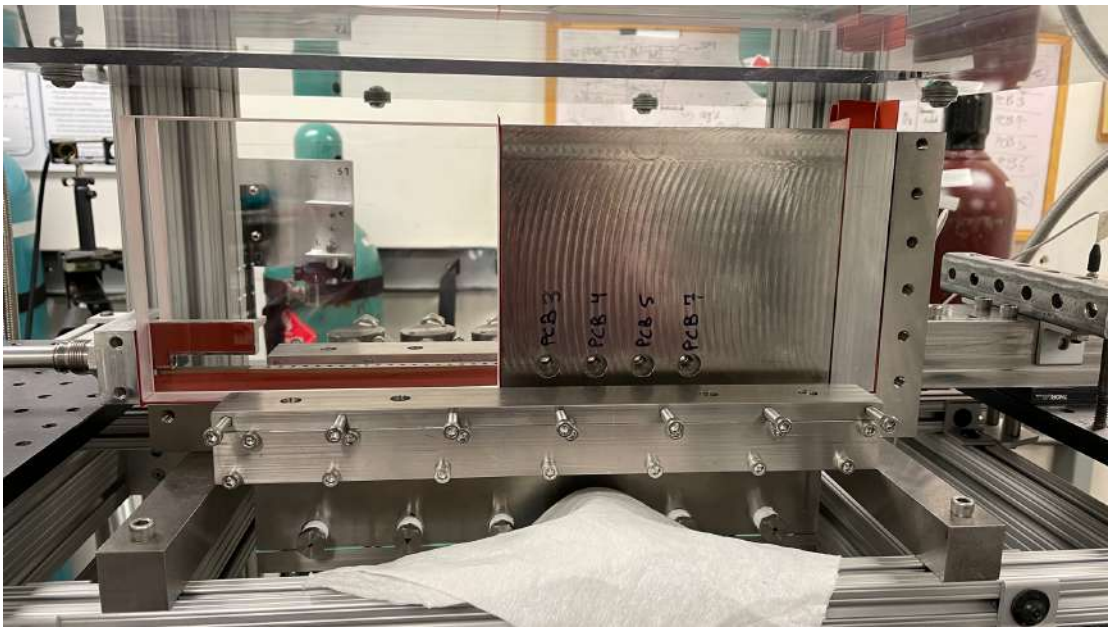

Figure A.3.1: Horizontal array of pressure measurement taps on the metal window

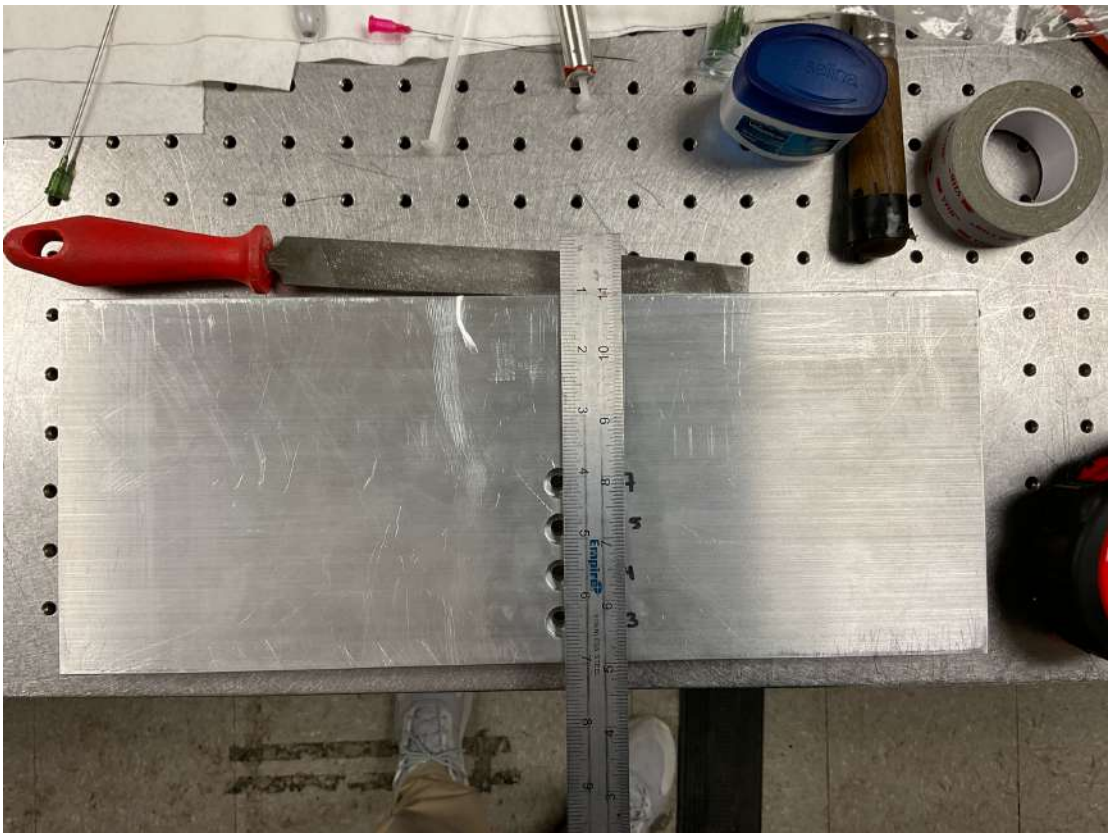

Figure A.3.2: Vertical array of pressure measurement taps on the metal window

A.4 Photomultiplier Tube

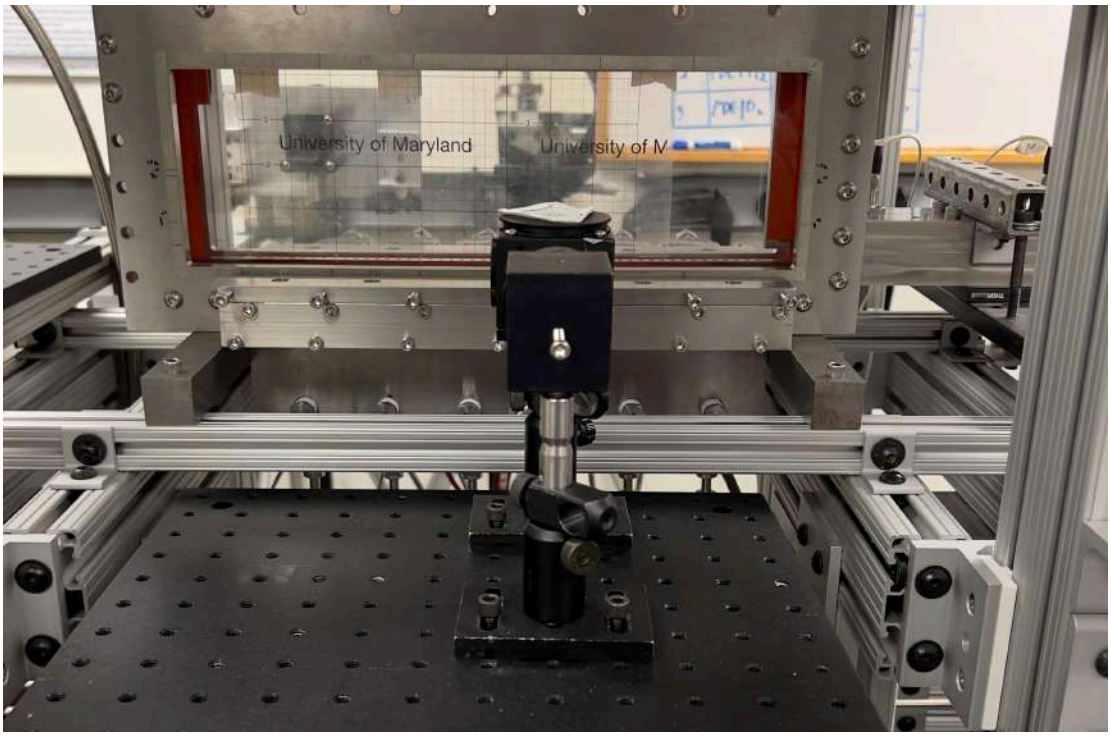

(a)

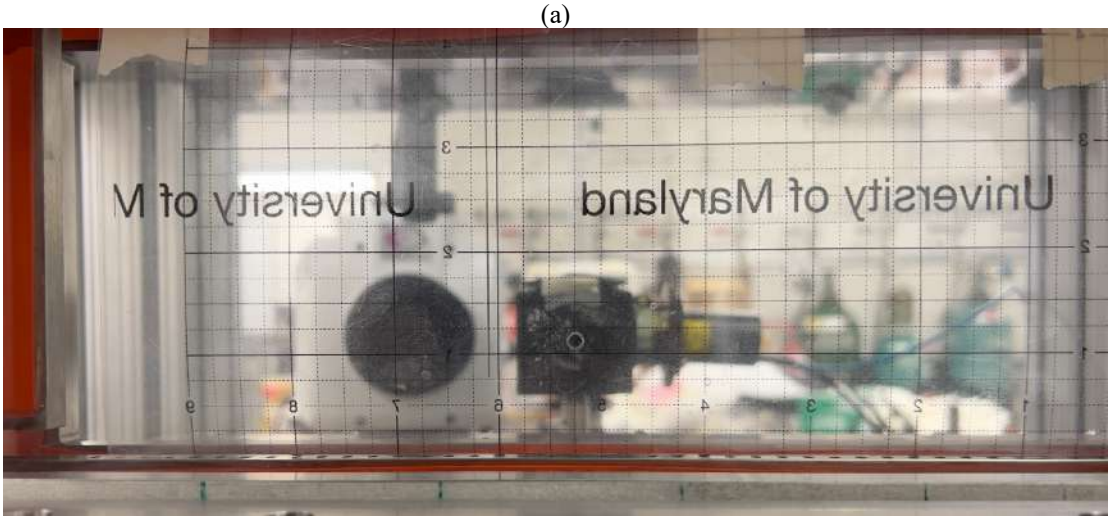

(b)

Figure A.4.1: Photomultiplier tube (a) setup and (b) installed location with the dispensing needle

Appendix B: Standard Operating Procedure (SOP)

Linear Detonation Rig Experiment

Advanced Propulsion Research Laboratory, University of Maryland

I. Safety Precautions:

1. This experiment involves volatile flammable gases at detonable mixture ratios, which can lead to an explosive rise in the local pressure (i.e., 13~55 times). Everyone participating in the experiment must be aware of the danger of detonation testing. Review both the test procedure and the emergency shutdown procedure.
2. All participants are required to wear safety glasses and hearing protection. Also, everyone must be outside of the test bay, safe distance away from the detonation test rig, when detonation experiment is initiated.
3. Prior to starting the experiment, all relevant valves and connections should be checked thoroughly for proper functioning and for any possible leaks. Inspect the supply line for each gas, carefully noting various components involved.

II. Test Procedure:

1. Carefully inspect all test equipment and instrumentations. Make sure the test control and data acquisition programs are ready and functioning properly. Verify the accuracy of pre-test calculations, with special attention to the length of the total test duration and the amount of detonable reactants to be involved.
2. Set the pressure values in the gas supply lines for proper flow rates, including oxidizer, fuel, and purge gases.

3. Check the test section for proper boundary conditions, including any droplet placement if any.
4. Make sure everyone is outside of the test bay and/or safely away. Start the test programs, which control the sequence of solenoid valves openings and closings as well as the timing of the ignition, the automatic stop and the flow of purge gas.
5. Each detonation test should start and end when the pre-programmed sequence is completed from the test control software. If the test continues after it was supposed to stop, employ the EMERGENCY SHUTDOWN PROCEDURE described below. Also, in case of uncontrolled reaction or unplanned disruptive event, employ the EMERGENCY SHUTDOWN PROCEDURE.
6. After each test ends, turn off the solenoid valves for fuel(s) and oxidizer(s) from the switch box. Turn on the purge gas. Close immediately the manual valves for the fuels and the oxidizer lines.
7. At the completion of the tests, purge all gas lines, remove the spark plug wire, and close all the supply gas bottles.

EMERGENCY SHUTDOWN PROCEDURE (PANIC STOP):

T**urn off all fuel and oxidizer solenoid valves and turn on the purge gas solenoid valve.** Close the manual valves for all fuels and oxidizers.

IN CASE OF EMERGENCY:

Fire extinguishers are posted around the laboratory space. The easiest way to eliminate combustor-related fire is to shut off all fuel supply. If any undesirable flow conditions are encountered that needs to be abandoned immediately, turn off or close all fuel solenoid valves and fuel manual valves. Call for help if necessary.

Appendix C: Engineering Drawings

C.1 Transition Component

This appendix contains the engineering drawings for the transition component of the Extended Linear Model Detonation Engine (eLMDE) used for the counter propagation detonation wave experiments. The dimension in the drawing is provided in inches and the scale is 1:2.5.

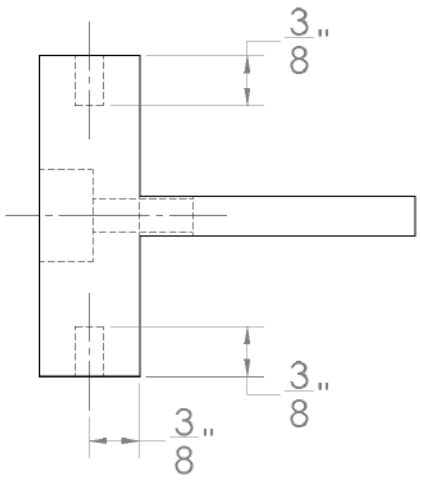
3/8"
3/8"
3/8"

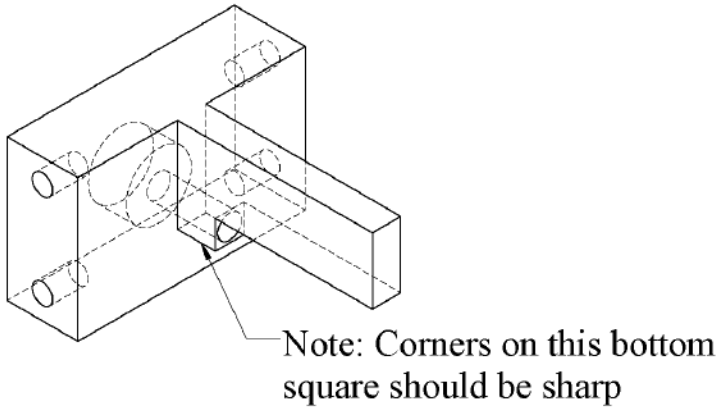
Note: Corners on this bottom square should be sharp

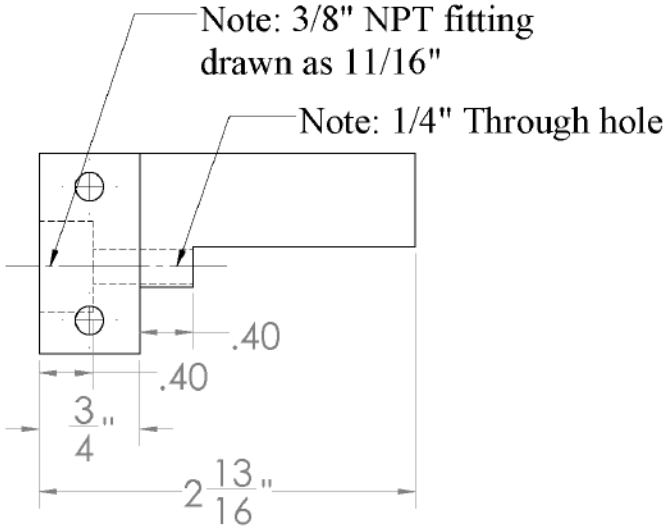
Note: 3/8" NPT fitting drawn as 11/16"
Note: 1/4" Through hole
.40
.40
3/4"
2 13/16"

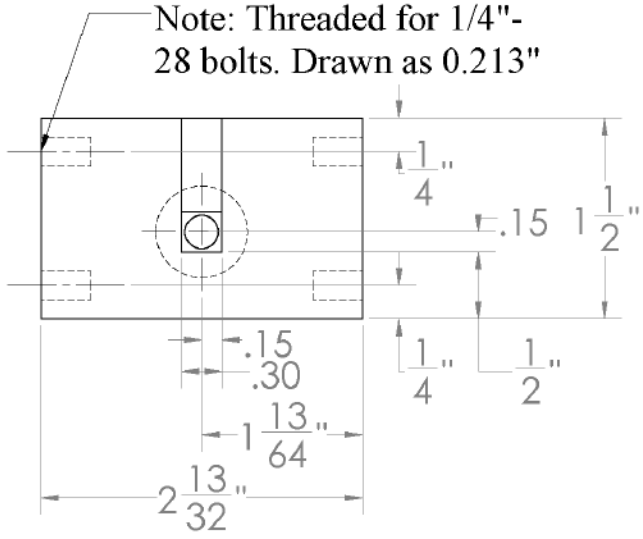
Note: Threaded for 1/4"-28 bolts. Drawn as 0.213"
1/4"
.15
1 1/2"
.15
.30
1/4"
1/2"
1 13/64"
2 13/32"

C.2 Smooth Injector Rail

This appendix contains the engineering drawings for the smooth injector rail component of the Extended Linear Model Detonation Engine (eLMDE) used for the liquid droplet interacting with detonation wave experiments. The dimension in the drawing is provided in inches and the scale is 1:2.5.

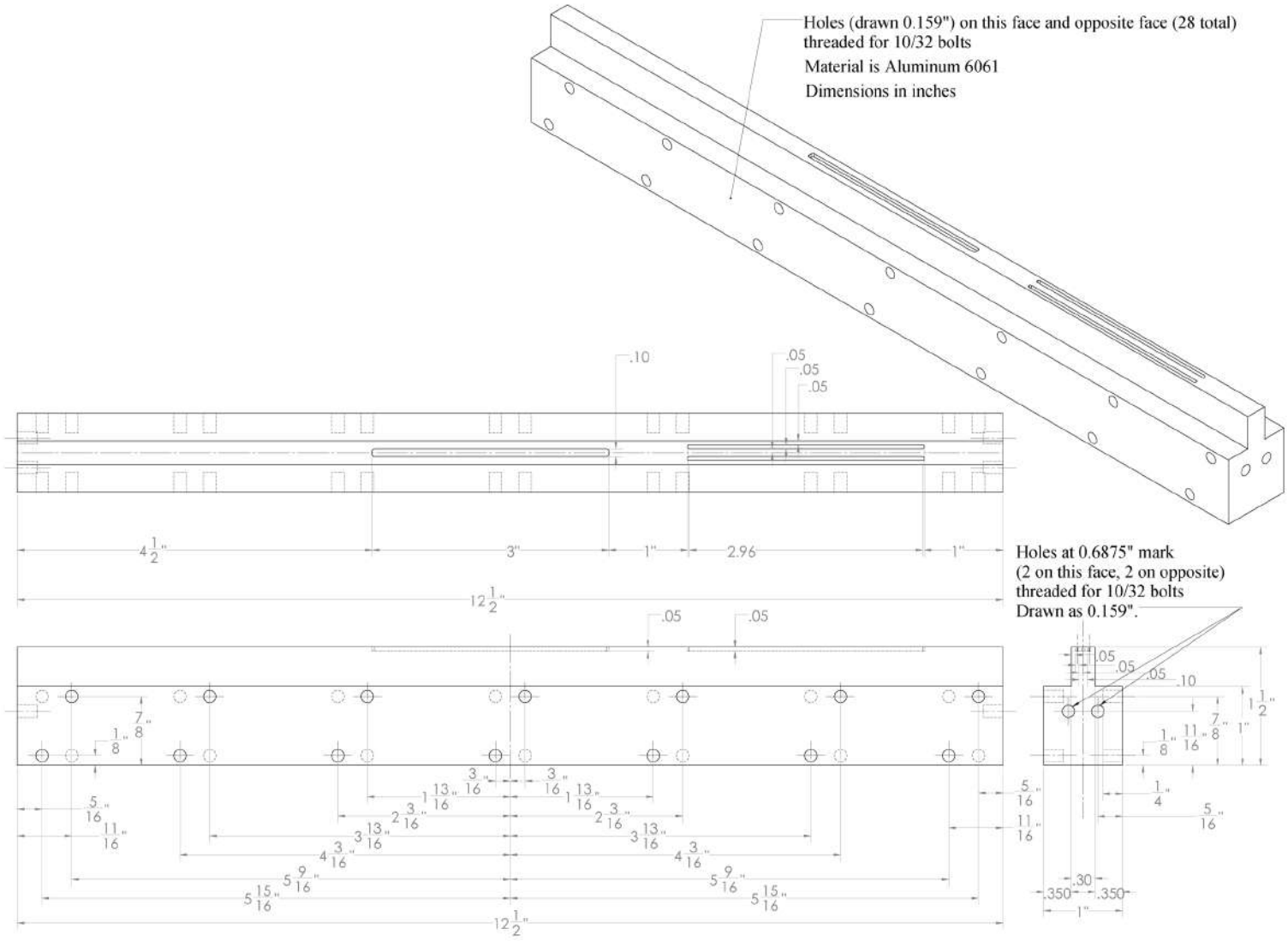
Holes (drawn 0.159") on this face and opposite face (28 total)
threaded for 10/32 bolts
Material is Aluminum 6061
Dimensions in inches
Holes at 0.6875" mark
(2 on this face, 2 on opposite)
threaded for 10/32 bolts
Drawn as 0.159".

Appendix D: Additional Results of Counter Propagating Waves

This appendix is a record of additional results of counter propagating waves that is not presented in the chapter 4. Here, Figure D.1 and D.2 shows the sequence of left running and right running decoupled shock-flame wave collision. t=0μs is define when the collision occurs. Both waves are clearly decoupled and shock front and flame front is apart. In each region behind the shock wave and before the flame front, reactant is shocked/compressed. Thus, when two waves collide, it creates another region shocked/compressed from the wave coming toward. However, it is not enough for the reactant to reignite.

Another feature that is noticed is the interaction between the shock wave propagating to the counter propagating flame front. It shows that the shock disappear behind the flame front and the shock front interacts with the flame front. Shock wave confronting the flame front creates reflected shock and eventually develop forming a Mach stem from t=90μs. This was one reason to add this result in the appendix.

Last, some spillage from the injector is observed even from the first image. This is considered reflected shock bounced back from the bottom end of the injector. Next, clearly distinct refresh jet is observed when t=75μs, yet no refresh jet is observed adjacent to the collision location. This could be regarded as opposite from what we concluded previously refresh jet is injected from injector closest to the injector for the collision of counter propagating wave. Refresh jet is noticed from t=135μs where the two waves collided even in this case. This implies that injector far enough from the

collision could refresh earlier than the collision adjacent injector. However, considering the wave propagation speed is much slower, shown in Figure D.3, comparing to the detonation waves usually seen inside the rotating detonation engine this observation should be consider exceptional case when the wave is decoupled and propagating relatively slow.

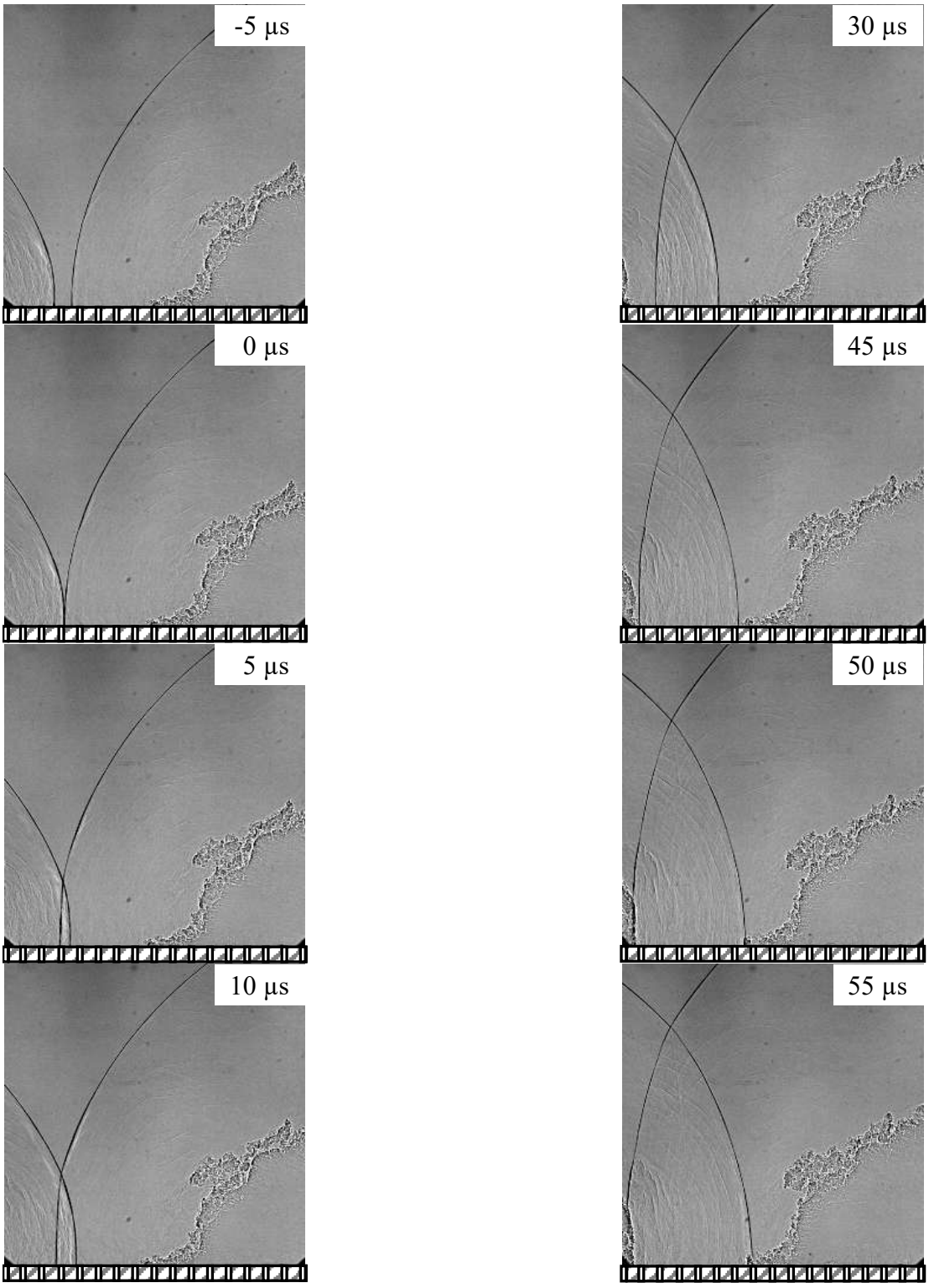

Figure D.1: Sequence of counter propagating decoupled shock-flame wave from t=-5µs to t=55µs

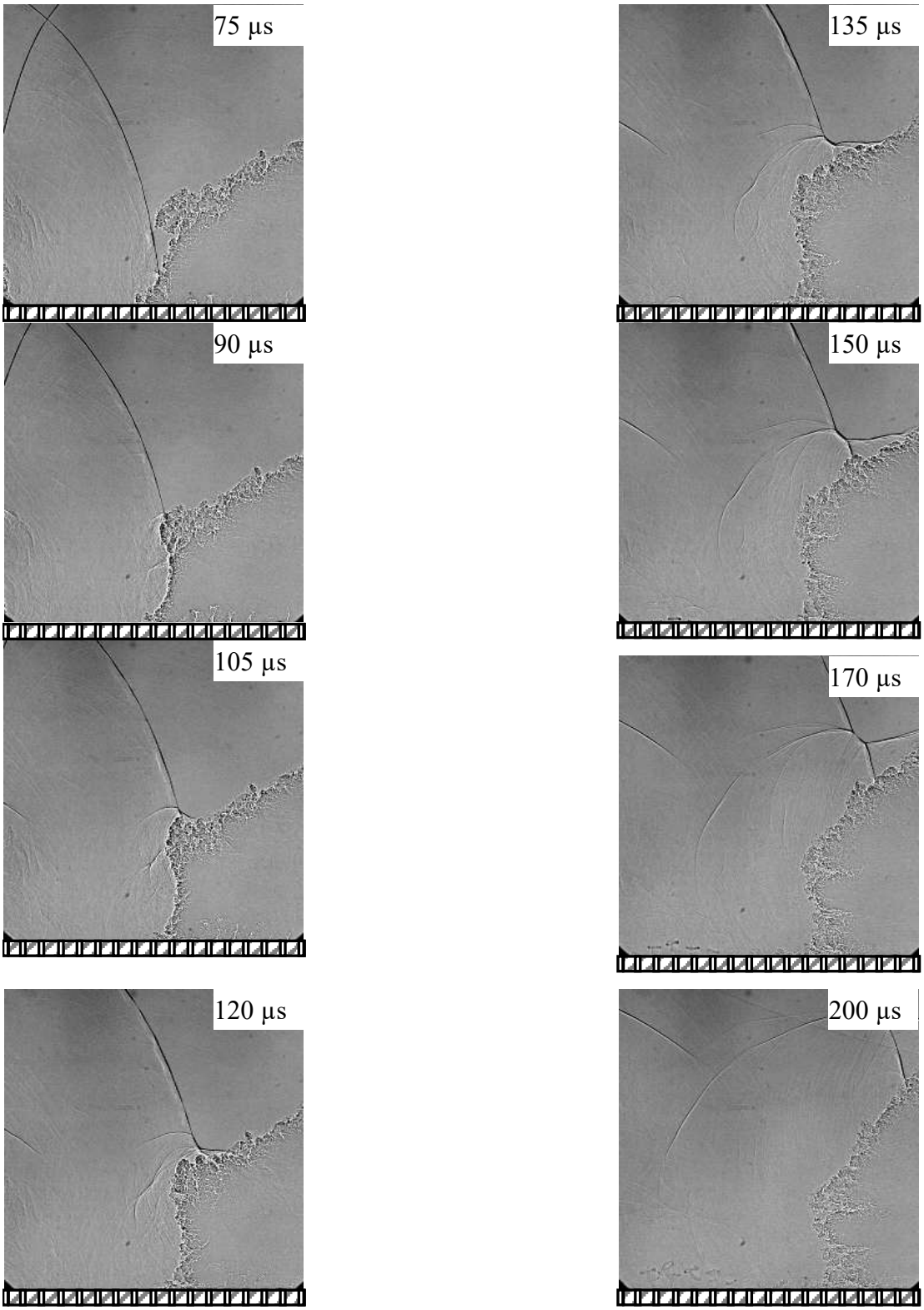

Figure D.2: Sequence of counter propagating decoupled shock-flame wave from t=75µs to t=200µs

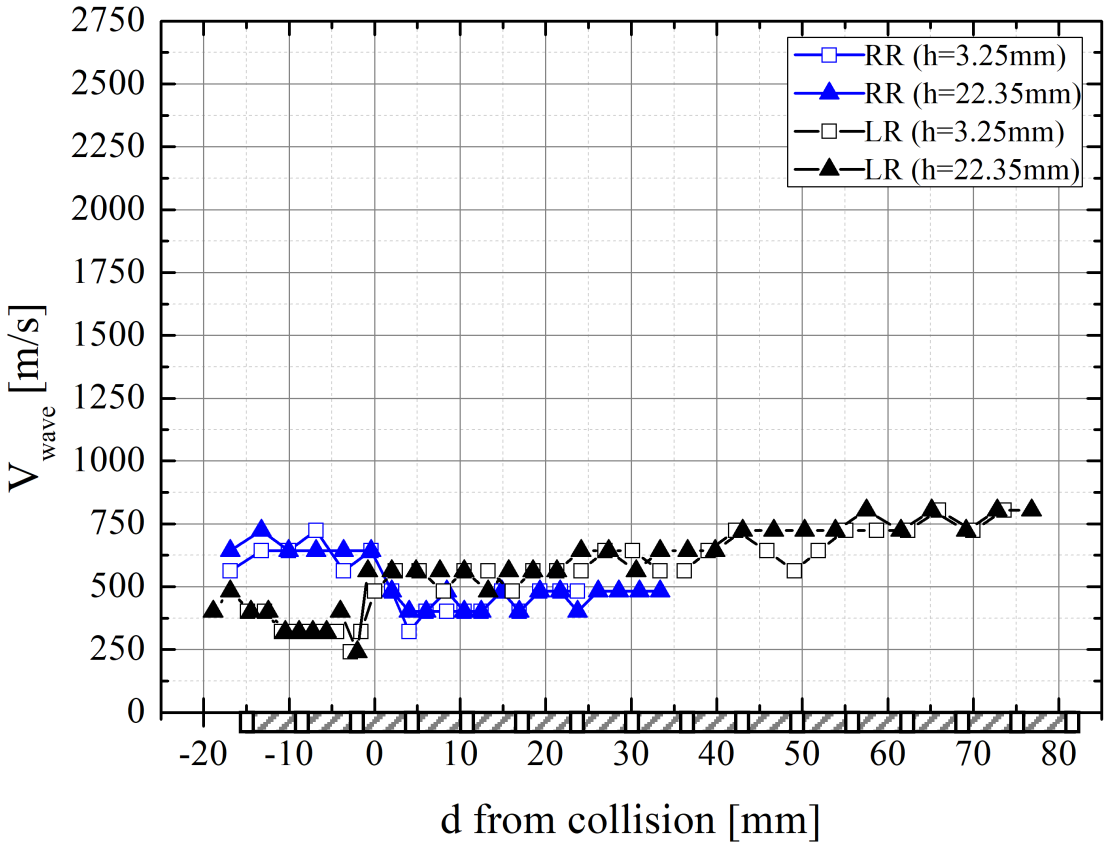

Figure D.3: Velocity of right running (RR) and left running (LR) wave along the channel of eLMDE, showing distance with respect to the collision location

Appendix E: Edge Detection Code for Tracking the Detonation Wave

Appendix E includes the MATLAB code written specifically for detecting the edge of the propagating detonation wave and liquid droplet from taken high-speed schlieren or shadowgraph images. This allows to estimate the wave propagating speed, propagating angle, and angle between the detonation wave and liquid droplet at impact in stationary observer's frame of reference. The work frame of this code is explained in the previous chapter 3.3.4.

The code is partially automated tracking code since its ability to detect the edge of the liquid droplet is not perfect. Thus, it needs additional manual input of edge pixel location information when some pixel of liquid droplet's edge is missing. Also, user needs to input frame number of when the detonation wave is closest to the liquid droplet and before the detonation wave collides to the liquid droplet. This is because the code calculates the shortest distance between the detonation wave and liquid droplet using the normal direction of the wave front, which the normal direction is obtain from the estimated wave front at the frame where the detonation wave and liquid droplet is closest and before the collision.

Although this code needs manual input of liquid droplet information and frame information for the accuracy, it was able to successfully capture the wave front and estimate the wave angle throughout the entire sequence indeed after the collision using polynomial fit using the RANSAC algorithm.

```
% Edge Detection
% Use edge() function
% Could try use different edge detection method such as
% 'canny', 'prewitt', 'roberts', 'log', 'Sobel'
% Here 'sobel' is used.
% Finds edges at those points where the gradient of the image I is maximum,
using the Sobel approximation to the derivative.
%
% ------------------------------------------------------------------------
% First Image (before wave arrive)
I = tempimg{testnn,1};
% Edge Detect
BW51 = edge(I,'sobel');
%
% ------------------------------------------------------------------------
% Droplet edge detection modification
% Manually include pixel info. of edge missed from edge function
switch testnn
    case 1
        BW51(67,101) = 1;
        BW51(66,102) = 1;
end
%
% ------------------------------------------------------------------------
% Find Interest window
windowsize = 21;
find_dw = 5;
[imgh, imgw] = size(I);
img_height = imgh;
img_width = imgw;
imgnn = 1;
searchimage = BW51;
originalimage = tempimg{testnn,imgnn};
threshold = 5;
prewavexy = [0,0];
tttt = findedgewindow(windowsize, find_dw, img_height, img_width, ...
    searchimage,imgnn,originalimage,prewavexy,threshold);
ww{testnn,imgnn} = tttt;
ww{testnn,imgnn}.BW51 = BW51;
% ww{testnn,imgnn}.BW52 = BW52;
%
% ------------------------------------------------------------------------
% Color the boundary to RED
fnn = fnn + 1;
figure(fnn)
imshow(I)
hold on;
scatter(ww{testnn,1}.dropxy(:,1),ww{testnn,1}.dropxy(:,2),'MarkerFaceColor',
'r')
xlim([77 123]);
ylim([44 78]);
set(gcf,'units','pixels','pos',[0 0 800 600])
hold off;
%
% ------------------------------------------------------------------------
% Find Background Edge
ww{testnn,1}.x0 = find(BW51);
[ww{testnn,1}.indx(:,1),ww{testnn,1}.indx(:,2)] = find(BW51);
dpn = length(ww{testnn,1}.indx);
%
% ------------------------------------------------------------------------
```

```
% Find Wave Edge
order = [velcalimg,2:velcalimg-1,velcalimg+1:endimgn];
for imgnn = order
    clear I BW51 tttt
    I = tempimg{testnn,imgnn};
    % Detect edge
    % BW51 => Edge detection / BW52 => Wave only detection
    BW51 = edge(I,'sobel');
    % Fill Initial Edges
    BW52 = BW51;
    BW52(ww{testnn,1}.x0) = 0;
    %
    % Show Interset Area
    windowsize = 15;
    find_dw = 5;
    [imgh, imgw] = size(I);
    img_height = imgh;
    img_width = imgw;
    searchimage = BW52;
    originalimage = tempimg{testnn,imgnn};
    threshold = 3;
    if imgnn <= velcalimg
        prewavexy = [0,0];
        tttt = findedgewindow(windowsize, find_dw, img_height,
img_width, ...
            searchimage,imgnn,originalimage,prewavexy,threshold);
    else
        prewavexy = ww{testnn,imgnn-1}.wavexy(1,:);
        tttt = findedgewindow(windowsize, find_dw, img_height,
img_width, ...
            searchimage,imgnn,originalimage,prewavexy,threshold);
    end
    ww{testnn,imgnn} = tttt;
    ww{testnn,imgnn}.BW51 = BW51;
    ww{testnn,imgnn}.BW52 = BW52;
    % Find edge for wave only
    [ww{testnn,imgnn}.indx(:,1),ww{testnn,imgnn}.indx(:,2)] = find(BW52);
    clear BW52 tttt
    %     %
    % Find closest point between Wave front and droplet boundary
    % Points from wave front
    wavepoint = ww{testnn,imgnn}.wavexy;
    % Points from droplet boundary
    if imgnn == velcalimg
        dropletpoint = ww{testnn,1}.dropxy;
    else
        dropletpoint = ww{testnn,velcalimg}.droppt;
    end
    % Find closeest
    ll = findclosest(dropletpoint,wavepoint,imgnn);
    % Distance
    ww{testnn,imgnn}.droptowave = ll.droptowave;
    % Min distance
    ww{testnn,imgnn}.dlmin = ll.dl_min;
    % Droplet point at min. distance
    ww{testnn,imgnn}.droploc = ll.droploc;
    % Wave point at min. distance
    ww{testnn,imgnn}.waveloc= ll.waveloc;
    clear ll
    ww{testnn,imgnn}.droppt =
ww{testnn,1}.dropxy(ww{testnn,imgnn}.droploc,:);
```

```
    ww{testnn,imgnn}.wavept =
ww{testnn,imgnn}.wavexy(ww{testnn,imgnn}.waveloc,:);
    %
    % ------------------------------------------------------------------------
    % Show droplet(blue) & wave boundary(green)
    fnn = fnn + 1;
    figure(fnn)
    imshow(I);
    hold on;

scatter(ww{testnn,1}.dropxy(:,1),ww{testnn,1}.dropxy(:,2),'MarkerEdgeColor',
'b','MarkerFaceColor','b')

scatter(ww{testnn,imgnn}.wavexy(:,1),ww{testnn,imgnn}.wavexy(:,2),'MarkerEdg
eColor','g','MarkerFaceColor','g')
    xloc = 10;
    yloc = 10;
    width = 900;
    height = 700;
    set(gcf,'position',[xloc,yloc,width,height])
    %
    % ------------------------------------------------------------------------
    % Show shortest line3
    if imgnn == velcalimg
        dxy = ww{testnn,imgnn}.droppt;
    else
        dxy = ww{testnn,velcalimg}.droppt;
    end
    [dxyn,~] = size(dxy);
    wxyn = length(ww{testnn,imgnn}.waveloc);
    if dxyn > 1 && wxyn > 1 % Multiple Set of closest point
        msg = compose("Choose lowest cloese set @ img# %d",imgnn);
        warning(msg);
        clear msg
        dxyind = 1;
        scatter(dxy(dxyind,1),dxy(dxyind,2),'Filled','MarkerFaceColor','r');
        wxy = ww{testnn,imgnn}.wavexy(ww{testnn,imgnn}.waveloc(dxyind),:);
        scatter(wxy(1),wxy(2),'Filled','MarkerFaceColor','r');
        line([dxy(dxyind,1),wxy(1)],[dxy(dxyind,2),wxy(2)],'Color','red');
    elseif dxyn == 1 && wxyn > 1
        msg = compose("One droplet point & Multiple wave point @
img# %d",imgnn);
        warning(msg);
        clear msg
        dxyind = 1;
        scatter(dxy(dxyind,1),dxy(dxyind,2),'Filled','MarkerFaceColor','r');
        for ii = 1 : wxyn
            wxy = ww{testnn,imgnn}.wavexy(ww{testnn,imgnn}.waveloc(ii),:);
            scatter(wxy(1),wxy(2),'Filled','MarkerFaceColor','r');
            line([dxy(1),wxy(1)],[dxy(2),wxy(2)],'Color','red');
        end
    elseif dxyn == 1 && wxyn == 1
        msg = compose("Only one set @ img# %d",imgnn);
        warning(msg);
        clear msg
        dxyind = 1;
        scatter(dxy(dxyind,1),dxy(dxyind,2),'Filled','MarkerFaceColor','r');
        wxy = ww{testnn,imgnn}.wavexy(ww{testnn,imgnn}.waveloc(dxyind),:);
        scatter(wxy(1),wxy(2),'Filled','MarkerFaceColor','r');
        line([dxy(dxyind,1),wxy(1)],[dxy(dxyind,2),wxy(2)],'Color','red');
    end
```

```
    if  imgnn == velcalimg
        wavexy = ww{testnn,velcalimg}.wavexy;
        wavept = ww{testnn,velcalimg}.wavept(dxyind,:);
        droppt = ww{testnn,velcalimg}.droppt(dxyind,:);
        [img_height,img_width] = size(ww{testnn,velcalimg}.BW51);
        numofpoint = 10;
        wwfit = findnormal(wavexy, wavept,
numofpoint,img_height,droppt,resolution(testnn,:),testnn);
        figure(fnn-1)
    else
        figure(fnn)
        [img_height,img_width] = size(ww{testnn,imgnn}.BW51);
    end
    %
    % ------------------------------------------------------------------------
    % Draw Wave front
    xx = wwfit.wavefront(:,1);
    yy = img_height - wwfit.Ycal;
    plot(xx, yy,'--k','linewidth',3)
    clear xx yy
    %
    % ------------------------------------------------------------------------
    % Draw normal line
    xx = 1 : img_width;
    yy = wwfit.findB(2) * xx + wwfit.findB(1);
    yy = img_height - yy;
    plot(xx,yy,':m','LineWidth',1);
    clear xx yy
    %
    % ------------------------------------------------------------------------
    % Draw arrow for wave direction
    xx = [wwfit.findx,wwfit.dropxy(1)];
    yy = [img_height - wwfit.findy,img_height - wwfit.dropxy(2)];
    drawArrow = @(x,y,varargin) quiver( x(1),y(1),x(2)-x(1),y(2)-y(1),0,
varargin{:} );
    drawArrow(xx,yy,'linewidth',3,'color','r','maxheadsize',0.9)
    clear xx yy
    %
    % ------------------------------------------------------------------------
    % Find Closest point on the normal line
    solB = wwfit.findB;
    wavefront = ww{testnn,imgnn}.wavexy;
    dropfront = wwfit.droppt;
    wwnorm =
findclosestnormal(solB,wavefront,dropfront,img_height,resolution(testnn,:));
    ww{testnn,imgnn}.diffdroptowave = wwnorm.diff;
    ww{testnn,imgnn}.closewavexy = wwnorm.closewavexy;
    ww{testnn,imgnn}.closewavept = wwnorm.closewavept;
    ww{testnn,imgnn}.normlengthmm = wwnorm.normlengthmm;
    clear wwnorm
    %
    % ------------------------------------------------------------------------
    % Plot Normal point2

scatter(ww{testnn,imgnn}.closewavept(1),ww{testnn,imgnn}.closewavept(2),'Fil
led','MarkerFaceColor','m');
    normdisttext = num2str(ww{testnn,imgnn}.normlengthmm);

text(ww{testnn,imgnn}.closewavept(1),ww{testnn,imgnn}.closewavept(2),normdis
ttext);
    clear normdisttext
```

```
    hold off;
    % 3Save length, wave beta, normal to beta, droplet point, wave point
    reduceddata(1,1) = ww{testnn,imgnn}.normlengthmm;    % Normal direction
Length
    reduceddata = [reduceddata,wwfit.wbeta];    % Wave beta angle
    reduceddata = [reduceddata,wwfit.normtobeta];   % Normal to beta angle
    reduceddata = [reduceddata, wwfit.dropxy];    % Droplet location in xy
coordinate
    reduceddata = [reduceddata, ww{testnn,imgnn}.closewavexy];   % Wave
front location in xy coordinate
    data(imgnn,:) = reduceddata;
    clear reduceddata
    %
end
%
% ------------------------------------------------------------------------
%% function findedgewindow
function ww = findedgewindow(windowsize, find_dw, img_height, ...
    img_width,searchimage,imgnn,originalimage,previouswavexy,threshold)
% ------------------------------------------------------------------------
% Search
searchsize = windowsize;
hl = round(searchsize/2);
searchdouble = double(searchimage);
dw = find_dw;
cc = 1;
for ii = [hl:dw:img_width-searchsize, img_width-hl+1]
    for jj = [hl:dw:img_height-searchsize, img_height-hl+1]
        findww = searchdouble(jj-hl+1:jj+hl-1,ii-hl+1:ii+hl-1);
        wwnum = sum(findww,'all');
        if wwnum > windowsize^2*threshold/100 % threshold
            loc(cc,:) = [jj,ii];
            wwsearch{jj,ii} = findww;
            wwsearchn(jj,ii) = length(wwnum);
            cc = cc + 1;
        end
    end
end
%
% ------------------------------------------------------------------------
% Plot Search Windows
plotyn = input('Plot side by side?  y = 1 n = 0   ');
% plotyn = 0;
global fnn
if plotyn == 1
    fnn = fnn + 1;
    figure(fnn)
    imshowpair(originalimage,searchimage,'falsecolor')
    hold on;
    for ii = 1:length(loc)
        xx = loc(ii,2)-hl+1;
        yy = loc(ii,1)-hl+1;
        rectangle('Position',[xx,yy,searchsize,searchsize], 'EdgeColor','b')
        clear xx yy
    end
    %     hold off;
elseif plotyn == 0
    %
end
%
% ------------------------------------------------------------------------
```

```
% For First Image
% Filter for bottom 10
if imgnn == 1
    [aa,bb] = size(wwsearchn);
    cc = 1;
    for ii = 1:bb
        if wwsearchn(end,ii) > 0
            bottomlr(cc) = ii;
            cc = cc + 1;
            if cc > 2
                break
            end
        end
    end
    bottomlr = [bottomlr(1)-dw,bottomlr,bottomlr(2)+dw];
    for jj = 1:length(bottomlr)
        cc = 1;
        for ii = 1:aa
            if wwsearchn(ii,bottomlr(jj)) > 0
                bottomtb{1,jj}(cc,1) = ii;
                cc = cc + 1;
            end
        end
    end
    %
    % ------------------------------------------------------------------------
    % Finding & Plot for last 5 bottom windows
    nofwindow = 5;
    for ii = 1:length(bottomlr)
        bb = length(bottomtb{1,ii});
        if bb < 6
            for jj = 1:bb
                if plotyn == 1
                    xx = bottomlr(ii)-hl+1;
                    yy = bottomtb{ii}(jj)-hl+1;
                    rectangle('Position',[xx,yy,searchsize,searchsize],
'EdgeColor',[0.8500 0.3250 0.0980])
                    clear xx yy
                end
                mm(jj,ii) = wwsearchn(bottomtb{ii}(jj),bottomlr(ii)-hl+1);
                bottom5{jj,ii} = [bottomlr(ii)-hl+1,bottomtb{ii}(jj)];
            end
        else
            cc = 1;
            for jj = bb-nofwindow+1:bb
                if plotyn == 1
                    xx = bottomlr(ii)-hl+1;
                    yy = bottomtb{ii}(jj)-hl+1;
                    rectangle('Position',[xx,yy,searchsize,searchsize],
'EdgeColor',[0.8500 0.3250 0.0980])
                    clear xx yy
                end
                mm(cc,ii) = wwsearchn(bottomtb{ii}(jj),bottomlr(ii));
                bottom5{cc,ii} = [bottomlr(ii),bottomtb{ii}(jj)];
                cc = cc + 1;

            end
        end
    end
    % Find Droplet Window
    ww.bottom = bottom5;
```

```
    ww.bottomn = mm;
    ww.max = max(mm,[],'all');
    [ww.findmaxloc(:,1),ww.findmaxloc(:,2)] = find(mm == ww.max);
    maxnn = length(ww.findmaxloc(:,1));
    if  maxnn > 1 % If there is more than one max locations
        % Find lowest window
        [aa,~] = find(max(ww.findmaxloc(:,1)) == ww.findmaxloc(:,1));
        if length(aa) > 1 % if multiple max is located in same row
            % Find most right window
            [dd,~] = find(max(ww.findmaxloc(aa(:),2)) ==
ww.findmaxloc(aa(:),2));
            ww.maxloc =
ww.bottom{ww.findmaxloc(aa(dd),1),ww.findmaxloc(aa(dd),2)};
        elseif length(aa) == 1 % Found lowest Window
            ww.maxloc = ww.bottom{ww.findmaxloc(aa,1),ww.findmaxloc(aa,2)};
        end
    elseif maxnn == 1 % Only one MAX Found
        ww.maxloc =
ww.bottom{ww.findmaxloc(maxnn,1),ww.findmaxloc(maxnn,2)};
    elseif isempty(ww.findmaxloc)
        error('Could not find MAX')
    end
    ww.maxloc = flip(ww.maxloc);
    % Fine adjustment
    % Vertical direction
    jj = -hl:hl;
    xx = ww.maxloc(2) + jj;
    cc = 0;
    for ii = 1:hl
        yy = ww.maxloc(1) + hl - 1 + ii;
        if ~isempty( find(searchimage(yy,xx)) )
            cc = cc + 1;
        else
        end
    end
    if cc > 0
        ww.maxloc(1) = ww.maxloc(1) + cc;
    end
    clear xx yy
    % Horizontal direction
    jj = -hl:hl;
    yy = ww.maxloc(1) + jj;
    cc = 0;
    for ii = 1:hl
        xx = ww.maxloc(2) + hl - 1 + ii;
        if ~isempty( find(searchimage(yy,xx)) )
            cc = cc + 1;
        else
        end
    end
    if cc > 0
        ww.maxloc(2) = ww.maxloc(2) + cc;
    end
    clear xx yy
    %
    ww.maxww = searchimage(ww.maxloc(1)-(hl-1):ww.maxloc(1)+(hl-
1),ww.maxloc(2)-(hl-1):ww.maxloc(2)+(hl-1));
    if plotyn == 1
        xx = ww.maxloc(2) - hl + 1;
        yy = ww.maxloc(1) - hl + 1;
```

```
        rectangle('Position',[xx,yy,searchsize,searchsize],
'EdgeColor','r','LineWidth',4)
        hold off;
        clear xx yy
    end
    %
    % Find droplet loc
    cc = 1;
    for ii = 1:searchsize
        for jj = 1:searchsize
            if ww.maxww(ii,jj) == 1
                xy(cc,1) = ww.maxloc(2)-hl+jj;
                xy(cc,2) = ww.maxloc(1)-hl+ii;
                cc = cc + 1;
            end
        end
    end
    ww.dropxy = xy;
    % Find for wave
else
    if sum(previouswavexy==0)   % Wave locate before droplet
        order = img_height:-1:1;
    else % Wave locate after the droplet
        for ee = img_height:-1:1
            if ~isempty(find(searchimage(ee,:) == 1)) % Find first lowest
point
                if ee > img_height-5 || ee >= previouswavexy(1,2)-5 % Found
point
                    if min(find(searchimage(ee,:) == 1)) <
previouswavexy(1,1)  % Wave propagated still in frame
                        order = img_height:-1:1;
                        break
                    else % Wave may have captured weird
                        order = 1:img_height;
                        break
                    end
                else % Found point higher than 5th line
                    order = 1:img_height;
                    break
                end
            else
            end
        end
    end
    cc = 1;
    skipcc = 0;
    for ii = order
        if ~isempty(find(searchimage(ii,:)==1))
            if  skipcc > 1
                skipcc = 0;
            else
            end
            for jj = 1:img_width
                if searchimage(ii,jj) == 1
                    if cc > 1
                        if abs(waveloc(cc-1,1)-jj) < 10
                            waveloc(cc,2) = ii;
                            waveloc(cc,1) = jj;
                            cc = cc + 1;
                            break
                            %                     continue
```

```
                        else
                            break
                        end
                    else
                        waveloc(cc,2) = ii;
                        waveloc(cc,1) = jj;
                        cc = cc + 1;
                        break
                    end
                else
                end
            end
        else
            skipcc = skipcc + 1;
            if skipcc > 11 % && cc > 10
                break
            else
            end
        end
    end
    A = exist('waveloc','var');
    if A==1
    ww.wavexy = waveloc;
    else
        ww.wavexy = [];
    end
    clear A
end
%
% ------------------------------------------------------------------------
% Save output
A = exist('loc','var');
if A==1
    ww.initialwindow_loc = loc;
    ww.search_window = wwsearch;
    ww.searched_n = wwsearchn;
else
    msg = compose("No points found @ img# %d ",imgnn);
    warning(msg);
    ww.initialwindow_loc = [];
    ww.search_window = [];
    ww.searched_n = [];

end
%
% ------------------------------------------------------------------------
%% function findclosest
function ll = findclosest(dropletpoint,wavepoint,imgnn)
% Find closest points
[dpn,~] = size(dropletpoint);
wpn = length(wavepoint);
wavetodrop = zeros(dpn,wpn);
if dpn == 1
    for ii = 1
        for jj = 1:wpn
            wavetodrop(ii,jj) = sqrt( (dropletpoint(ii,1) -
wavepoint(jj,1))^2 + (dropletpoint(ii,2) - wavepoint(jj,2))^2 );
        end
    end
else
    for ii = 1:dpn
```

```
        for jj = 1:wpn
            wavetodrop(ii,jj) = sqrt( (dropletpoint(ii,1) -
wavepoint(jj,1))^2 + (dropletpoint(ii,2) - wavepoint(jj,2))^2 );
        end
    end
end
%
dlmin = min(wavetodrop,[],'all');
[row,col] = find(wavetodrop == dlmin);
if length(row) > 1
    msg = compose("Multiple Points at Droplet @ img# %d",imgnn);
    warning(msg);
    clear msg
     if length(row) == sum(row==row(1))
         msg = "All same point ";
         warning(msg);
         clear msg
         ll.droploc = row(1);
         ll.waveloc = col(1);
     else
         multipointnn = length(row) - sum(row==row(1));
         msg = compose("Different Droplet point captured require attention @
img# %d, Number of points %d ",[imgnn,multipointnn]);
         warning(msg);
         clear msg
         ll.droploc = row;
         ll.waveloc = col;
     end
else
    msg = compose("One Point at Droplet @ img# %d ",imgnn);
    warning(msg);
    clear msg
    ll.droploc = row;
    ll.waveloc = col;
end
ll.droptowave = wavetodrop;
ll.dl_min = dlmin;
%
% ------------------------------------------------------------------------
%% function findnormal
function wwfit = findnormal(wavexy, wavept,
numofpoint,img_h,droppt,res,testnn)
% numofpoint = number of points on one way
% Linear fit to the wave front
% Data set ready
[row,~] = find(wavexy(:,2) == wavept(2));
[wavefrontn,~] = size(wavexy);
if row-numofpoint < 1
    startpt = 1;
else
    startpt = row - numofpoint;
end
if row + numofpoint > wavefrontn
    endpt = wavefrontn;
else
    endpt = row + numofpoint;
end
rangeofpoints = startpt : endpt;
wavefront = wavexy(rangeofpoints,:);
Y = wavefront(:,2);
Y = img_h-Y;
```

```
% RANSAC
maxdist = 1.5;
N = 1; % Order of polyfit
X = wavefront(:,1);
[P, inlierIdx] = fitPolynomialRANSAC([X,Y], N, maxdist);
Ycal = polyval(P,wavefront(:,1));
B = flip(P);
%
% Plot
global fnn
fnn = fnn + 1;
figure(fnn)
plot(X,Ycal,'-g','LineWidth',3)
hold on;
plot(X(inlierIdx),Y(inlierIdx), '.', X(~inlierIdx,1),Y(~inlierIdx),'ro')
legend('Fit line', 'Inlier Point', 'Outlier Point')
%
% Find normal line
dropxy = droppt;
dropxy(2) = img_h - dropxy(2);
solB(2) = -1/B(2); % Normal Slope
solB(1) = -solB(2)*dropxy(1) + dropxy(2);   % x intercept
% Find the point on the wave front
syms findx findy
% findy = B(2)*findx + B(1);
% two eqns
eqns = [solB(2)*findx+solB(1)==findy, B(2)*findx+B(1)==findy];
sol = solve(eqns,[findx,findy]);
solx = double(sol.findx);
soly = double(sol.findy);
%
xx = [solx,dropxy(1)];
yy = [soly,dropxy(2)];
dxsq = ( (solx - dropxy(1)) * res(1) )^2;
dysq = ( (soly - dropxy(2)) * res(2) )^2;
normlengthmm = sqrt( dxsq + dysq ); % length in [mm]
% plot(xx, yy, 'r','LineWidth',3);
drawArrow = @(x,y,varargin) quiver( x(1),y(1),x(2)-x(1),y(2)-y(1),0,
varargin{:} );
drawArrow(xx,yy,'linewidth',3,'color','r','maxheadsize',0.7)
% xlim([90,120])
% ylim([15,45])
grid on;
daspect([1 1 1])
figname = compose('Wavefront Normalvect T%03d',testnn);
title(figname);
f = gcf;
figname = compose('Wavefront_Normalvect_T%03d.png',testnn);
exportgraphics(f,figname{1},'Resolution',300);
hold off;
%
% Wave angle
wbeta = rad2deg(atan(B(2)));
normtobeta = rad2deg(atan(solB(2)))+180;
%
% Save
wwfit.B = B;
wwfit.X = X;
wwfit.Y = Y;
wwfit.Ycal = Ycal;
wwfit.wavefront = wavefront;
```

```
wwfit.rangeofpoints = rangeofpoints;
wwfit.sol = sol;
wwfit.findx = solx;
wwfit.findy = soly;
wwfit.findB = solB;
wwfit.droppt = droppt;
wwfit.dropxy = dropxy;
wwfit.normlength = normlengthmm;
wwfit.P = P;
wwfit.inlierindx = inlierIdx;
wwfit.wbeta = wbeta;
wwfit.normtobeta = normtobeta;
%
% ------------------------------------------------------------------------
%% function findclosestnormal
function wwnorm = findclosestnormal(solB,wavefront,dropfront,img_h,res)
% Find closest wave front point from normal line
xx = wavefront(:,1);
yy = solB(2) * xx + solB(1);
wavefrontxy = wavefront;
wavefrontxy(:,2) = img_h - wavefront(:,2);
diff = abs(yy - wavefrontxy(:,2));
[row,~] = find(min(diff)==diff);
closewavexy = wavefrontxy(row,:);
closewavept = wavefront(row,:);
resx = res(1);
resy = res(2);
dropfrontxy = dropfront;
dropfrontxy(:,2) = img_h - dropfrontxy(:,2);
% Calculate the lenth in [mm]
dxsq = ( (dropfrontxy(1) - closewavexy(1)) * resx )^2;
dysq = ( (dropfrontxy(2) - closewavexy(2)) * resy )^2;
normlengthmm = sqrt( dxsq + dysq ); % length in [mm]
%
wwnorm.diff = diff;
wwnorm.closewavexy = closewavexy;
wwnorm.closewavept = closewavept;
wwnorm.normlengthmm = normlengthmm;
%
% ------------------------------------------------------------------------
```

Bibliography

[1] D.M. Davidenko, I. Gökalp, A.N. Kudryavtsev, Numerical simulation of the continuous rotating hydrogen-oxygen detonation with a detailed chemical mechanism, in: West-East High Speed Flow Field Conference, 2007.

[2] W. Fickett, W.C. Davis, Detonation : theory and experiment, Dover Publications, Mineola, N.Y. :, 2000.

[3] T.R. Bussing, G. Pappas, An Introduction to Pulse Detonation Engines, 32nd Aerospace Sciences Meeting and Exhibit (1994). https://doi.org/10.2514/6.1994-263.

[4] K. Kailasanath, Applications of detonations to propulsion: A review, 37th Aerospace Sciences Meeting and Exhibit (1999). https://doi.org/10.2514/6.1999-1067.

[5] K. Kailasanath, N. Reno, Recent developments in the research on pulse detonation engines, 40th AIAA Aerospace Sciences Meeting and Exhibit (2002). https://doi.org/10.2514/6.2002-470.

[6] G.D. Roy, S.M. Frolov, A.A. Borisov, D.W. Netzer, Pulse detonation propulsion: challenges, current status, and future perspective, Prog Energy Combust Sci 30 (2004) 545–672. https://doi.org/10.1016/J.PECS.2004.05.001.

[7] P. Wolański, Detonative propulsion, Proceedings of the Combustion Institute 34 (2013) 125–158. https://doi.org/10.1016/J.PROCI.2012.10.005.

[8] R.T. Fievisohn, K.H. Yu, Steady-State analysis of rotating detonation engine flowfields with the method of characteristics, J Propuls Power 33 (2017) 89–99. https://doi.org/10.2514/1.B36103.

[9] T. Bussing, G.P. Exhibit, An introduction to pulse detonation engines, 32nd Aerospace Sciences Meeting and Exhibit (1994). https://doi.org/10.2514/6.1994-263.

[10] G.D. Roy, S.M. Frolov, A.A. Borisov, D.W. Netzer, Pulse detonation propulsion: Challenges, current status, and future perspective, Prog Energy Combust Sci 30 (2004) 545–672. https://doi.org/10.1016/J.PECS.2004.05.001.

[11] F.A. Bykovskii, S.A. Zhdan, E.F. Vedernikov, Continuous spin detonations, J Propuls Power 22 (2006) 1204–1216. https://doi.org/10.2514/1.17656.

[12] F.R. Schauer, PULSE DETONATION PHYSIOCHEMICAL AND EXHAUST RELAXATION PROCESSES, AFOSR-ARO Basic Combustion Research Review Meeting (2006). http://www.dtic.mil (accessed November 1, 2023).

[13] F.K. Lu, E.M. Braun, J. Powers, Rotating detonation wave propulsion: Experimental challenges, modeling, and engine concepts, J Propuls Power 30 (2014) 1125–1142. https://doi.org/10.2514/1.B34802.

[14] J.R. Burr, K.H. Yu, Experimental characterization of RDE combustor flowfield using linear channel, Proceedings of the Combustion Institute 37 (2019) 3471–3478. https://doi.org/10.1016/J.PROCI.2018.09.001.

[15] J.C. Shank, Development and testing of a rotating detonation engine run on hydrogen and air, Air Force Institute of Technology, 2012. https://scholar.afit.edu/etd/1065/ (accessed November 1, 2023).

[16] W. Hargus, S. Schumaker, E. Paulson, Air force research laboratory rotating detonation rocket engine development, AIAA Joint Propulsion Conference (2018). https://doi.org/10.2514/6.2018-4876.

[17] P. Wolański, Detonation engines, Journal of KONES 18 (2011) 515–521. https://bibliotekanauki.pl/articles/950134.pdf (accessed November 1, 2023).

[18] Q. Xie, Z. Ji, H. Wen, Z. Ren, P. Wolanski, B. Wang, Review on the Rotating Detonation Engine and It's Typical Problems, Transactions on Aerospace Research 2020 (2020) 107–163. https://doi.org/10.2478/TAR-2020-0024.

[19] M. Hishida, T. Fujiwara, P.W.-S. waves, undefined 2009, Fundamentals of rotating detonations, SpringerM Hishida, T Fujiwara, P WolanskiShock Waves, 2009•Springer 19 (2009) 1–10. https://doi.org/10.1007/s00193-008-0178-2.

[20] D. Schwer, K. Kailasanath, Numerical investigation of the physics of rotating-detonation-engines, Proceedings of the Combustion Institute 33 (2011) 2195–2202. https://doi.org/10.1016/J.PROCI.2010.07.050.

[21] F.A. Bykovskii, E.F. Vedernikov, Continuous detonation combustion of an annular gas-mixture layer, Combust Explos Shock Waves 32 (1996) 489–491. https://doi.org/10.1007/BF01998570.

[22] R.M. Clayton, R.S. Rogero, D. Dipprey, Experimental measurements on a rotating detonation-like wave observed during liquid rocket resonant combustion, (1965). https://ntrs.nasa.gov/api/citations/19650025518/downloads/19650025518.pdf (accessed November 3, 2023).

[23] J.A. Nicholls, R.E. Cullen, K.W. Ragland, Feasibility studies of a rotating detonation wave rocket motor., Https://Doi.Org/10.2514/3.28557 3 (2012) 893–898. https://doi.org/10.2514/3.28557.

[24] J. Kindracki, P. Wolański, Z.G.-S. waves, undefined 2011, Experimental research on the rotating detonation in gaseous fuels–oxygen mixtures, SpringerJ Kindracki, P Wolański, Z GutShock Waves, 2011•Springer 21 (2011) 75–84. https://doi.org/10.1007/s00193-011-0298-y.

[25] J. Humble, S. Heister, Heterogeneous detonation physics as applied to high pressure rotating detonation engines, AIAA Scitech 2021 Forum (2021) 1–23. https://doi.org/10.2514/6.2021-1027.

[26] J. Bennewitz, B. Bigler, W. Hargus, S. Danczyk, R. Smith, Characterization of detonation wave propagation in a rotating detonation rocket engine using direct high-speed imaging, 2018 Joint Propulsion Conference (2018). https://doi.org/10.2514/6.2018-4688.

[27] F.A. Bykovskii, S.A. Zhdan, E.F. Vedernikov, Continuous spin detonation of hydrogen-oxygen mixtures. 1. Annular cylindrical combustors, Combust Explos Shock Waves 44 (2008) 150–162. https://doi.org/10.1007/S10573-008-0021-1.

[28] J.W. Bennewitz, B.R. Bigler, S.A. Danczyk, W.A. Hargus, R.D. Smith, Performance of a rotating detonation rocket engine with various convergent Nozzles, AIAA Propulsion and Energy 2019 Forum (2019). https://doi.org/10.2514/6.2019-4299.

[29] B. Bigler, J. Bennewitz, S. Schumaker, S. Danczyk, W. Hargus, Injector alignment study for variable mixing in rotating detonation rocket engines, AIAA Scitech 2019 Forum (2019). https://doi.org/10.2514/6.2019-2019.

[30] B. Bigler, J. Bennewitz, S. Danczyk, W. Hargus, Injector mixing effects in rotating detonation rocket engines, AIAA Propulsion and Energy 2019 Forum (2019) 3869. https://doi.org/10.2514/6.2019-3869.

[31] S. Kubicki, W. Anderson, S. Heister, Further experimental study of a hypergolically-ignited liquid-liquid rotating detonation rocket engine, AIAA Scitech 2020 Forum (2020). https://doi.org/10.2514/6.2020-0196.

[32] W.A. Stoddard, E.J. Gutmark, Comparative numerical study of RDE injection designs, 52nd Aerospace Sciences Meeting (2014). https://doi.org/10.2514/6.2014-0285.

[33] A.K. Hayashi, Y. Kimura, T. Yamada, E. Yamada, J. Kindracki, E. Dzieminska, P. Wolanski, N. Tsuboi, V.E. Tangirala, T. Fujiwara, Sensitivity Analysis of Rotating Detonation Engine with a Detailed Reaction Model, Aerospace Sciences Meeting AIAA (2009). https://doi.org/10.2514/6.2009-633.

[34] P. Wolański, Rotating detonation wave stability, 23rd International Colloquium On The Dynamics of Explosions and Reactive Systems (2011). http://www.icders.org/ICDERS2011/abstracts/ICDERS2011-0211.pdf (accessed November 3, 2023).

[35] B.A. Rankin, D.R. Richardson, A.W. Caswell, A. Naples, J.L. Hoke, F.R. Schauer, Imaging of OH* chemiluminescence in an optically accessible nonpremixed rotating detonation engine, 53rd AIAA Aerospace Sciences Meeting (2015). https://doi.org/10.2514/6.2015-1604.

[36] C. Wang, W. Liu, S. Liu, L. Jiang, Z. Lin, Experimental investigation on detonation combustion patterns of hydrogen/vitiated air within annular combustor, Exp Therm Fluid Sci 66 (2015) 269–278. https://doi.org/10.1016/J.EXPTHERMFLUSCI.2015.02.024.

[37] A. Roy, D. Ferguson, T. Sidwell, B. O'meara, P. Strakey, C. Bedick, Experimental study of rotating detonation combustor performance under preheat and back pressure operation, 55th AIAA Aerospace Sciences Meeting (2017). https://doi.org/10.2514/6.2017-1065.

[38] Q. Xie, H. Wen, W. Li, Z. Ji, B. Wang, P. Wolanski, Analysis of operating diagram for H2/Air rotating detonation combustors under lean fuel condition, Energy 151 (2018) 408–419. https://doi.org/10.1016/J.ENERGY.2018.03.062.

[39] J. Duvall, F. Chacon, C. Harvey, M. Gamba, Study of the effects of various injection geomteries on the operation of a rotating detonation engine, AIAA Aerospace Sciences Meeting, 2018 (2018). https://doi.org/10.2514/6.2018-0631.

[40] L. Deng, H. Ma, C. Xu, X. Liu, C. Zhou, The feasibility of mode control in rotating detonation engine, Appl Therm Eng 129 (2018) 1538–1550. https://doi.org/10.1016/J.APPLTHERMALENG.2017.10.146.

[41] J.A. Suchocki, S.T.J. Yu, J.L. Hoke, A.G. Naples, F.R. Schauer, R. Russo, Rotating detonation engine operation, 50th AIAA Aerospace Sciences Meeting Including the New Horizons Forum and Aerospace Exposition (2012). https://doi.org/10.2514/6.2012-119.

[42] V. Raman, S. Prakash, M. Gamba, Nonidealities in Rotating Detonation Engines, Annu Rev Fluid Mech 55 (2023) 639–674. https://doi.org/10.1146/ANNUREV-FLUID-120720-032612.

[43] J. Kindracki, A. Kobiera, P. Wolański, Z. Gut, M. Folusiak, K. Swiderski, Experimental and numerical study of the rotating detonation engine in hydrogen-air mixtures, Progress in Propulsion Physics 2 (2011) 555–582. https://doi.org/10.1051/eucass/201102555.

[44] V. Anand, A. St. George, R. Driscoll, E. Gutmark, Characterization of instabilities in a Rotating Detonation Combustor, Int J Hydrogen Energy 40 (2015) 16649–16659. https://doi.org/10.1016/J.IJHYDENE.2015.09.046.

[45] J. Kindracki, Experimental research on rotating detonation in liquid fuel-gaseous air mixtures, Aerosp Sci Technol 43 (2015) 445–453. https://doi.org/10.1016/J.AST.2015.04.006.

[46] Y. Ma, S. Zhou, H. Ma, G. Ge, D. Yu, G. Zou, Z. Liang, T. Zhang, Experimental investigation on propagation characteristics of liquid-fuel/preheated-air rotating detonation wave, Int J Hydrogen Energy 47 (2022) 24080–24092. https://doi.org/10.1016/J.IJHYDENE.2022.05.186.

[47] F. Bykovskii, S. Zhdan, E.V.- Combustion, undefined Explosion, undefined and, undefined 2019, Continuous detonation of the liquid kerosene—air mixture with addition of hydrogen or syngas, SpringerFA Bykovskii, SA Zhdan, EF VedernikovCombustion, Explosion, and Shock Waves, 2019•Springer 55 (2019) 83–92. https://doi.org/10.1134/S0010508219050101.

[48] Q. Zheng, H. long Meng, C. sheng Weng, Y. wen Wu, W. kang Feng, M. liang Wu, Experimental research on the instability propagation characteristics of liquid kerosene rotating detonation wave, Defence Technology 16 (2020) 1106–1115. https://doi.org/10.1016/J.DT.2020.06.028.

[49] S.M. Frolov, V.S. Aksenov, V.S. Ivanov, I.O. Shamshin, Continuous detonation combustion of ternary “hydrogen–liquid propane–air” mixture in annular combustor, Int J Hydrogen Energy 42 (2017) 16808–16820. https://doi.org/10.1016/J.IJHYDENE.2017.05.138.

[50] E.K. Dabora, K.W. Ragland, J.A. Nicholls, Drop-size effects in spray detonations, Symposium (International) on Combustion 12 (1969) 19–26. https://doi.org/10.1016/S0082-0784(69)80388-7.

[51] K.W. Ragland, E.K. Dabora, J.A. Nicholls, Observed structure of spray detonations, Physics of Fluids 11 (1968) 2377–2388. https://doi.org/10.1063/1.1691827.

[52] F.B. Cramer, The onset of detonation in a droplet combustion field, Symposium (International) on Combustion 9 (1963) 482–487. https://doi.org/10.1016/S0082-0784(63)80058-2.

[53] J.R. Bowen, K.W. Ragland, F.J. Steffes, T.G. Loflin, Heterogeneous detonation supported by fuel fogs or films, Symposium (International) on Combustion 13 (1971) 1131–1139. https://doi.org/10.1016/S0082-0784(71)80110-8.

[54] E.K. Dabora, L.P. Weinberger, Present status of detonations in two-phase systems, Acta Astronaut 1 (1974) 361–372. https://doi.org/10.1016/0094-5765(74)90103-9.

[55] W.T. Webber, Spray combustion in the presence of a travelling wave, Symposium (International) on Combustion 8 (1961) 1129–1140. https://doi.org/10.1016/S0082-0784(06)80611-9.

[56] A.A. Ranger, J.A. Nicnolls, Aerodynamic shattering of liquid drops, AIAA Journal 7 (1969) 285–290. https://doi.org/10.2514/3.5087.

[57] C. Kauffman, J. Nicholls, Shock-wave ignition of liquid fuel drops, AIAA Journal 9 (1971) 880–885. https://doi.org/10.2514/3.6290.

[58] O.G. Engel, Fragmentation of Waterdrops in the Zone Behind an Air Shock *, J Res Natl Bur Stand (1934) 60 (1958).

[59] J. Nicholson, J. Hill, Rain Erosion on Spike Protected Supersonic Radomes, 1965. https://apps.dtic.mil/sti/citations/AD0363299 (accessed November 1, 2023).

[60] W.G. Reinecke, W.L. McKay, EXPERIMENTS ON WATER DROP BREAKUP BEHIND MACH 3 TO 12 SHOCKS, 1969. https://doi.org/10.2172/4160011.

[61] W. Reinecke, G. Waldman, A study of drop breakup behind strong shocks with applications to flight, 1970. https://apps.dtic.mil/sti/citations/AD0871218 (accessed November 1, 2023).

[62] M. Pilch, C.A. Erdman, Use of breakup time data and velocity history data to predict the maximum size of stable fragments for acceleration-induced breakup of a liquid drop, Int. J. Multiphase Flow 13 (1987) 741–757.

[63] T.G. Theofanous, G.J. Li, T.N. Dinh, Aerobreakup in rarefied supersonic gas flows, Journal of Fluids Engineering, Transactions of the ASME 126 (2004) 516–527. https://doi.org/10.1115/1.1777234.

[64] D.R. Guildenbecher, C. López-Rivera, P.E. Sojka, Secondary atomization, Exp Fluids 46 (2009) 371–402. https://doi.org/10.1007/S00348-008-0593-2.

[65] J.C. Meng, T. Colonius, Numerical simulations of the early stages of high-speed droplet breakup, Shock Waves 25 (2015) 399–414. https://doi.org/10.1007/S00193-014-0546-Z.

[66] S. V. Poplavski, A. V. Minakov, A.A. Shebeleva, An early stage of the drop interaction with shock wave: airflow, deformation, destruction, J Phys Conf Ser 1359 (2019) 012032. https://doi.org/10.1088/1742-6596/1359/1/012032.

[67] A. Martinez, S. Heister, Wave structure of heterogeneous detonations in rotating detonation rocket engines, AIAA Science and Technology Forum and Exposition, AIAA SciTech Forum 2022 (2022). https://doi.org/10.2514/6.2022-0091.

[68] S. Prakash, R. Fiévet, V. Raman, J. Burr, K.H. Yu, Analysis of the detonation wave structure in a linearized rotating detonation engine, AIAA Journal 58 (2020) 5063–5077. https://doi.org/10.2514/1.J058156/ASSET/IMAGES/LARGE/FIGURE25.JPEG.

[69] J.R. Burr, K.H. Yu, Characterization of CH4-O2 detonation in unwrapped RDE channel combustor, AIAA Propulsion and Energy Forum and Exposition, 2019 (2019). https://doi.org/10.2514/6.2019-4215.

[70] S.C. Redhal, J.R. Burr, K.H. Yu, Injector flowfield-detonation wave interaction in unwrapped RDE channel, AIAA Propulsion and Energy Forum and Exposition, 2019 (2019). https://doi.org/10.2514/6.2019-4216.

[71] S. Redhal, J. Burr, K. Yu, Fuel Injection, Mixing, and Detonative Combustion in Model Detonation Engine, 24th International Society of Air Breathing Engines Conference (2019).

[72] J. Burr, K.H. Yu, Mixing in linear detonation channel with discrete injectors and side relief, AIAA Scitech 2019 Forum (2019). https://doi.org/10.2514/6.2019-1014.

[73] S.C. Redhal, J.R. Burr, K.H. Yu, Fuel injection, mixing and combustion in model rotating detonation engine, 22nd AIAA International Space Planes and Hypersonics Systems and Technologies Conference (2018). https://doi.org/10.2514/6.2018-5200.

[74] J. Burr, K.H. Yu, Impulsively started ethylene-oxygen injection in linear channel following detonation wave passage, 2018 Joint Propulsion Conference (2018). https://doi.org/10.2514/6.2018-4570.

[75] J. Burr, K.H. Yu, Detonation wave propagation in discretely spaced hydrocarbon cross-flow, AIAA Aerospace Sciences Meeting, 2018 (2018). https://doi.org/10.2514/6.2018-1420.

[76] J.R. Burr, K. Yu, Detonation Wave Propagation in Cross-Flow of Discretely Spaced Reactant Jets, 53rd AIAA/SAE/ASEE Joint Propulsion Conference (2017). https://doi.org/10.2514/6.2017-4908.

[77] D.A. Schwer, K. Kailasanath, Feedback into mixture plenums in rotating detonation engines, 50th AIAA Aerospace Sciences Meeting Including the New

Horizons Forum and Aerospace Exposition (2012). https://doi.org/10.2514/6.2012-617.

[78] A. Braeuer, Shadowgraph and Schlieren Techniques, Supercritical Fluid Science and Technology 7 (2015) 283–312. https://doi.org/10.1016/B978-0-444-63422-1.00004-3.

[79] G. Settles, M.H.-M.S. and, undefined 2017, A review of recent developments in schlieren and shadowgraph techniques, Iopscience.Iop.OrgGS Settles, MJ HargatherMeasurement Science and Technology, 2017•iopscience.Iop.Org 28 (2017) 42001. https://doi.org/10.1088/1361-6501/aa5748.

[80] V.N. Nori, J.M. Scitzman, CH* chemiluminescence modeling for combustion diagnostics, Proceedings of the Combustion Institute 32 I (2009) 895–903. https://doi.org/10.1016/J.PROCI.2008.05.050.

[81] M. Bozkurt, M. Fikri, C. Schulz, Experimental and Numerical Investigation of CH* and OH* Chemiluminescence in Acetylene Combustion behind Reflected Shock Waves, 28th International Symposium on Shock Waves (2012) 421–426. https://doi.org/10.1007/978-3-642-25688-2_65.

[82] S.C. Redhal, M. Chang, J.R. Burr, K.H. Yu, Effects of Partial Mixing and Confinement on Detonation Wave Characteristics and RDE Mode of Operation, Icders.OrgSC Redhal, M Chang, JR Burr, KH Yuicders.Org (n.d.). http://www.icders.org/ICDERS2022/abstracts/ICDERS2022-231.pdf (accessed November 1, 2023).

[83] M. Chang, S.C. Redhal, J.R. Burr, K.H. Yu, Detonation wave-refresh jet interaction in unwrapped rde combustor, AIAA Scitech 2021 Forum (2021) 1–9. https://doi.org/10.2514/6.2021-1379.

[84] J.R. Burr, K.H. Yu, DETONATION STRUCTURE IN AN "UNWRAPPED" ROTATING DETONATION ENGINE, 22nd International Society of Air Breathing Engines Conference (2015).